DISCRIMINATING CLEAR-SKY FROM CLOUD WITH MODIS
ALGORITHM THEORETICAL BASIS DOCUMENT (MOD35)

MODIS Cloud Mask Team

Steve Ackerman, Richard Frey, Kathleen Strabala, Yinghui Liu, Liam Gumley, Bryan Baum, Paul Menzel

Cooperative Institute for Meteorological Satellite Studies, University of Wisconsin - Madison

Version 6.1

October 2010

TABLE OF CONTENTS

1.0 Introduction

Clouds are generally characterized by higher reflectance and lower temperature than the underlying earth surface. As such, simple visible and infrared window threshold approaches offer considerable skill in cloud detection. However, there are many surface conditions when this characterization of clouds is inappropriate, most notably over snow and ice. Additionally, some cloud types such as thin cirrus, fog and low-level stratus at night, and small-scale cumulus are difficult to detect because of insufficient contrast with the surface radiance. Cloud edges increase difficulty since the instrument field of view is not completely cloudy or clear.

The 36 channel Moderate Resolution Imaging Spectroradiometer (MODIS) offers the opportunity for multispectral approaches to cloud detection so that many of these concerns can be mitigated; additionally, spatial uniformity measures add textural information that is useful in discriminating cloudy from clear-sky conditions. This document describes the approach and algorithms for detecting clouds (commonly called a cloud mask) using MODIS observations, developed in collaboration with members of the MODIS Science Teams (Ackerman et al., 1998). The MODIS cloud screening approach includes new spectral techniques and incorporates many existing techniques to detect obstructed fields of view. Section 2 gives an overview of the masking approach. Individual spectral and textural cloud detection tests are discussed in Section 3. Examples of results and how to interpret the cloud mask output are included in Section 4 along with validation activities. Appendix A includes an example FORTRAN, Matlab and IDL code for reading the cloud mask.

2.0 Overview

2.1 Objective

The MODIS cloud mask indicates whether a given view of the earth surface is unobstructed by clouds or optically thick aerosol. The cloud mask is generated at 250 and 1000-meter resolutions. Input to the cloud mask algorithm is assumed to be calibrated and navigated level 1B ra-

diance data. The cloud mask may use any of bands 1, 2, 3, 4, 5, 6, 7, 8, 9, 17, 18, 20, 21, 22, 26, 27, 28, 29, 31, 32, 33, and 35. Missing or bad radiometric data may create missing or lowered quality cloud mask output. A cloud mask result is not attempted in the case of missing or invalid geolocation data.

Several points need to be made regarding the approach to the MODIS cloud mask presented in this Algorithm Theoretical Basis Document (ATBD).

1) The cloud mask is not the final cloud product from MODIS; several principal investigators have the responsibility to deliver algorithms for various additional cloud parameters, such as water phase and altitude.
2) The cloud mask ATBD assumes that calibrated, quality controlled data are the input and a cloud mask is the output. The overall template for the MODIS data processing was planned at the project level and coordinated with activities that produced calibrated level 1B data.
3) The snow/ice processing path flag (bit #5) in the cloud mask output indicates a processing path through the algorithm and should not be considered as confirmation of snow or ice in the scene. Bit #10 (added for Collection 6) indicates surface snow/ice according to ancillary information.
4) In certain heavy aerosol loading situations (e.g., dust storms, volcanic eruptions and forest fires), some tests may flag the aerosol-laden atmosphere as cloudy. Two aerosol flags are included in the mask to indicate fields-of-view that are potentially contaminated with optically thick aerosol. Bit #8 indicates smoke for daytime land and water surfaces. Bit #28 indicates airborne dust for all non-snow/ice scenes. *Note that cloud vs. aerosol discrimination from spectral tests alone is problematic, and these flags cannot be used as a substitute for complete aerosol detection algorithms such as MOD04.*
5) Thin cirrus detection is conveyed through two separate thin cirrus flags. These are designed to caution the user that thin cirrus may be present, though the cloud mask final result may indicate no obstruction. These are defined in Section 3.2.4.

There are operational constraints to consider in the cloud mask algorithm for MODIS. These constraints are driven by the need to process MODIS data in a timely fashion.

1) CPU Constraint: Many algorithms must first determine if the pixel is cloudy or clear. Thus, the cloud mask algorithm lies at the top of the data processing chain and must be versatile enough to satisfy the needs of many applications. The clear-sky determination algorithm must run in near-real time, limiting the use of CPU-intensive algorithms.
2) Output File Size Constraint: Storage requirements are also a concern. The cloud mask is more than a yes/no decision. The 48 bits of the mask include an indication of the likelihood that the pixel is contaminated with cloud. It also includes ancillary information regarding the processing path and results from individual tests. In processing applications, one need not process all the bits of the mask. An algorithm can make use of only the first 8 bits of the mask if that is appropriate.
3) Comprehension: Because there are many users of the cloud mask, it is important that the mask provide enough information to be widely used and that it may be easily understood. To intelligently interpret the output from this algorithm, it is important to have the algorithm simple in concept but effective in its application.

Our approach to MODIS cloudy vs. clear-sky discrimination is, in its simplest form, to provide a confidence flag indicating the certainty of clear sky for each pixel; beyond that, to provide additional information designed to help users interpret the result for his or her particular application. In addition, the algorithm must operate in near-real time with limited computer storage for the final product.

2.2 Background

Development of the MODIS cloud mask algorithm benefits from previous work to characterize global cloud cover using satellite observations. The International Satellite Cloud Climatology Project (ISCCP) has developed cloud detection schemes using visible and infrared window radiances. The AVHRR (Advanced Very High Resolution Radiometer) Processing scheme

Over cLoud Land and Ocean (APOLLO) cloud detection algorithm uses the five visible and infrared channels of the AVHRR. The Cloud Advanced Very High Resolution Radiometer (CLAVR) and the Cloud and Surface Parameter Retrieval (CASPR) systems also use a series of spectral and spatial variability tests to detect clouds with CASPR focusing on polar areas. CO_2 slicing characterizes global high cloud cover, including thin cirrus, using infrared radiances in the carbon dioxide sensitive portion of the spectrum. Additionally, spatial coherence of infrared radiances in cloudy and clear skies has been used successfully in regional cloud studies. The following paragraphs briefly summarize some of these prior approaches to cloud detection.

The ISCCP cloud masking algorithm described by Rossow (1989), Rossow et al. (1989), Sèze and Rossow (1991a) and Rossow and Garder (1993) utilizes the narrowband visible (0.6 μm) and the infrared window (11 μm) channels on geostationary platforms. Each observed radiance value is compared with its corresponding clear-sky composite value. Clouds are detected only when they alter the clear-sky radiances by more than the uncertainty in the clear values. In this way the "threshold" for cloud detection is the magnitude of the uncertainty in the clear radiance estimates.

The ISCCP algorithm is based on the premise that the observed visible and infrared radiances are caused by only two types of conditions, *cloudy* and *clear*, and that the ranges of radiances and their variability associated with these two conditions do not overlap (Rossow and Garder 1993). As a result, the algorithm is based upon thresholds; a pixel is classified as cloudy only if at least one radiance value is distinct from the inferred clear value by an amount larger than the uncertainty in that clear threshold value. The uncertainty can be caused both by measurement errors and by natural variability. This algorithm is constructed to be cloud-conservative, minimizing false cloud detections but missing clouds that resemble clear conditions.

APOLLO is discussed in detail by Saunders and Kriebel (1988), Kriebel et al. (1989) and Gesell (1989). The scheme uses AVHRR channels 1 through 5 at full spatial resolution, nominally 1.1 km at nadir. The 5 spectral band passes are approximately 0.58-0.68 μm, 0.72-1.10

μm, 3.55-3.93 μm, 10.3-11.3 μm, and 11.5-12.5 μm. The technique is based on 5 threshold tests. A pixel is called cloudy if it is brighter or colder than a threshold, if the reflectance ratio of channels 2 to 1 is between 0.7 and 1.1, if the temperature difference between channels 4 and 5 is above a certain threshold, and if the spatial uniformity over ocean is greater than a threshold (Kriebel and Saunders 1988). A pixel is defined as cloud free if all spectral measures fall on the "clear-sky" sides of the various thresholds. A pixel is defined as cloud contaminated if it fails any single test, thus this algorithm is clear-sky conservative.

CLAVR-x is an operational cloud processing system run by NESDIS on data from AVHRR instruments (Stowe et al. 1991, 1994). CLAVR-x consists of four main cloud algorithms that perform cloud detection, cloud typing, cloud height estimation and cloud optical/microphysical property retrievals. The cloud mask consists of a set of multispectral sequential tests that may be divided into contrast, spectral, and spatial signature types. Contrast tests compare measurements against thresholds selected to discriminate cloudy from clear scenes. Spectral tests utilize ratios or differences of two AVHRR spectral bands in an effort to compensate for atmospheric effects that sometimes lead to false cloud detection by the simple contrast tests. Spatial tests are applied on 2x2 pixel arrays in a "moving window" algorithm that characterize the variability of scenes and make use of the fact that uniform scenes are less likely to contain partial or sub-pixel clouds that the other tests fail to detect.

The Cloud and Surface Parameter Retrieval (CASPR) system is a toolkit for the analysis of data from the AVHRR satellite sensors carried on NOAA polar-orbiting satellites (Key 2002). The cloud masking procedure consists of thresholding operations that are based on modeled sensor radiances. The AVHRR radiances are simulated for a wide variety of surface and atmospheric conditions, and values that approximately divide clear from cloudy scenes are determined. The single image cloud mask uses four primary spectral tests and an optional secondary test. Many of the cloud test concepts can be found in the Support of Environmental Requirements for Cloud Analysis and Archive (SERCAA) procedures (Gustafson et al., 1994); some appear in the NOAA CLAVR algorithm (Stowe et al., 1991); most were developed and/or used elsewhere but

refined and extended for use in polar regions. The cloud detection procedure incorporates separate spectral tests to identify cirrus, warm clouds, water clouds, low stratus-thin cirrus, and very cold clouds. To account for potential problems with the cloud tests, tests that confidently identify clear pixels are also used.

CO_2 slicing (Menzel et al., 2008) has been used to distinguish transmissive clouds from opaque clouds and clear-sky using High resolution Infrared Radiation Sounder (HIRS) multispectral observations. Using radiances within the broad CO_2 absorption band centered at 15 μm, clouds at various levels of the atmosphere can be detected. Radiances near the center of the absorption band are sensitive to the upper troposphere while radiances from the wings of the band (away from the band center) see successively lower into the atmosphere. The CO_2 slicing algorithm determines both cloud level and effective cloud amount from radiative transfer principles. It is especially effective for detecting thin cirrus clouds that are often missed by simple infrared window and visible broad-based approaches. Difficulties arise when the clear minus cloudy radiance for a spectral band is less than the instrument noise. Li et al (2001) use a 1DVAR method to retrieve the cloud top height and effective cloud amount using the CO2-slicing technique as a first guess.

Many algorithms have also been developed for cloud clearing of the Advanced TIROS Operational Vertical Sounder (ATOVS) that uses HIRS/3 observations. An integral part of the temperature and moisture retrieval algorithm is the detection of clouds. A number of cloud detection schemes developed for the earlier HIRS/2 processing system (Smith and Platt, 1978; McMillin and Dean 1982; Li et al. 2001) are also applied to the HIRS/3 data. In addition, AMSU-A measurements from channels 4–14 are used to predict HIRS/3 brightness temperatures. The differences between observed and AMSU-A predicted HIRS/3 brightness temperatures are used for cloud detection.

The operational GOES (Geostationary Operational Environmental Satellite) sounder algorithms use visible reflectances along with 11, 12, 3.7, and 13.3 μm BTs to define cloudy FOVs. For example, the cloud top pressure algorithm uses simple thresholds, BTDs, regression relation-

ships to estimate skin temperatures, and measurements in neighboring pixels to determine clear, cloudy, or unknown conditions (Schreiner et. al., 2001).

The above algorithms are noted as they have been incorporated into existing global cloud climatologies or have been executed in an operational mode over long time periods. The MODIS cloud mask algorithm builds on this work, as well as on others not mentioned here (see the reference list). MODIS cloud detection benefits from extended spectral coverage coupled with high spatial resolution and high radiometric accuracy. MODIS has 250-meter resolution in the 0.65 and 0.87 μm bands, 500-meter resolution in five other visible and near-infrared bands, and 1000-meter resolution in the remaining bands. Aggregated 1-km radiance data from 22 out of 36 bands available in the visible, near-infrared, and infrared spectral regions are used in an attempt to create a high quality cloud mask that incorporates preexisting experience while mitigating some of the difficulties experienced by previous algorithms.

Table 1 lists many of the spectral threshold tests used by legacy cloud detection algorithms for various cloud and scene types. Many of these tests were included in the MODIS cloud mask algorithm. Some comments associated with these tests are given in the last column of the table. The MODIS bands used in the cloud mask algorithm are identified in Table 2. The uses of each band are listed in the last column.

Table 1. General approaches to cloud detection over different land types using satellite observations that rely on thresholds for reflected and emitted energy.

Scene	Solar/Reflectance	Thermal	Comments
Low cloud over water	$R_{0.87}$, $R_{0.67}/R_{0.87}$, BT_{11}-$BT_{3.7}$	Difficult. Compare BT_{11} to daytime mean clear-sky values of BT_{11}; BT_{11} in combination with brightness temperature difference tests; Over oceans, expect a relationship between BT_{11}-$BT_{8.6}$, BT_{11}-BT_{12} due to water vapor amount being correlated to SST	Spatial and temporal uniformity tests sometimes used over water scenes; Sun-glint regions over water present a problem.
High Thick cloud over water	$R_{1.38}$, $R_{0.87}$, $R_{0.67}/R_{0.87}$,	BT_{11} ; $BT_{13.9}$; $BT_{6.7}$ BT_{11}-$BT_{8.6}$, BT_{11}-BT_{12}	
High Thin cloud over water	$R_{1.38}$	$BT_{6.7}$; $BT_{13.9}$ BT_{11}-BT_{12}, $BT_{3.7}$-BT_{12}	For $R_{1.38}$, surface reflectance for atmospheres with low total water vapor amounts can be a problem.
Low cloud over snow	($R_{0.55}$ – $R_{1.6}$) / ($R_{0.55}$ + $R_{1.6}$); BT_{11}-$BT_{3.7}$	BT_{11} -$BT_{6.7}$, BT_{13} - BT_{11} Difficult, look for inversions	Ratio test is called, NDSI (Normalized Difference Snow Index). $R_{2.1}$ is also dark over snow and bright for low cloud.
High thick cloud over snow	$R_{1.38}$; ($R_{0.55}$ – $R_{1.6}$) / ($R_{0.55}$ + $R_{1.6}$);	$BT_{13.6}$; BT_{11} -$BT_{6.7}$, BT_{13} - BT_{11} Look for inversions, suggesting cloud-free.	
High thin cloud over snow	$R_{1.38}$; ($R_{0.55}$ – $R_{1.6}$) / ($R_{0.55}$ + $R_{1.6}$);	$BT_{13.6}$; BT_{11} -$BT_{6.7}$, BT_{13} - BT_{11}	Look for inversions, suggesting cloud-free region.

Table 1. Continued

Scene	Solar/Reflectance	Thermal	Comments
Low cloud over vegetation	$R_{0.87}$, $R_{0.67}/R_{0.87}$, BT_{11}-$BT_{3.7}$; ($R_{0.87} - R_{0.65}$) / ($R_{0.87} + R_{0.65}$);	Difficult. BT_{11} in combination with brightness temperature difference tests.	Ratio test is called, NDVI (Normalized Difference Vegetation Index). Other ratio tests have also been developed.
High Thick cloud over vegetation	$R_{1.38}$, $R_{0.87}$, $R_{0.67}/R_{0.87}$, ($R_{0.87} - R_{0.65}$) / ($R_{0.87} + R_{0.65}$);	BT_{11} ; $BT_{13.9}$; $BT_{6.7}$ BT_{11}-$BT_{8.6}$, BT_{11}-BT_{12}	
High Thin cloud over vegetation	$R_{1.38}$, $R_{0.87}$, $R_{0.67}/R_{0.87}$, ($R_{0.87} - R_{0.65}$) / ($R_{0.87} + R_{0.65}$);	$BT_{13.9}$; $BT_{6.7}$ BT_{11}-$BT_{8.6}$, BT_{11}-BT_{12}	Tests a function of ecosystem to account for variations in surface emittance and reflectance.
Low cloud over bare soil	$R_{0.87}$, $R_{0.67}/R_{0.87}$, BT_{11}-$BT_{3.7}$; $BT_{3.7}$-$BT_{3.9}$	BT_{11} in combination with brightness temperature difference tests. $BT_{3.7}$-$BT_{3.9}$ BT_{11}-$BT_{3.7}$	Difficult due to brightness and spectral variation in surface emissivity. Surface reflectance at 3.7 and 3.9 μm is similar and therefore thermal test is useful.
High Thick cloud over bare soil	$R_{1.38}$, $R_{0.87}$, $R_{0.67}/R_{0.87}$	$BT_{13.9}$; $BT_{6.7}$ BT_{11} in combination with brightness temperature difference tests.	
High Thin cloud over bare soil	$R_{1.38}$, $R_{0.87}$, $R_{0.67}/R_{0.87}$, BT_{11}-$BT_{3.7}$;	$BT_{13.9}$; $BT_{6.7}$ BT_{11} in combination with brightness temperature difference tests, for example $BT_{3.7}$-$BT_{3.9}$	Difficult for global applications. Surface reflectance at 1.38 μm can sometimes cause a problem for high altitude deserts. For BT difference tests, variations in surface emissivity can cause false cloud screening.

Table 2. MODIS bands used in the MODIS cloud mask algorithm.

Band	Wavelength (μm)		Comment
1 (250 m)	0.659	Y	250-m and 1-km cloud detection
2 (250 m)	0.865	Y	250-m and 1-km cloud detection
3 (500 m)	0.470	Y	Smoke, dust detection
4 (500 m)	0.555	Y	Snow/ice detection (NDSI)
5 (500 m)	1.240	Y	Smoke, dust detection
6 (500 m)	1.640	Y	Terra snow/ice detection (NDSI)
7 (500 m)	2.130	Y	Aqua snow/ice detection (NDSI)
8	0.415	Y	Desert cloud detection
9	0.443	Y	Sun-glint clear-sky restoral tests
10	0.490	N	
11	0.531	N	
12	0.565	N	
13	0.653	N	
14	0.681	N	
15	0.750	N	
16	0.865	N	
17	0.905	Y	Sun-glint clear-sky restoral tests
18	0.936	Y	Sun-glint clear-sky restoral tests
19	0.940	N	
26	1.375	Y	Thin cirrus, high cloud detection
20	3.750	Y	Land, sun-glint clear-sky restoral tests Snow/ice, dust detection
21/22	3.959	Y(21)/Y(22)	smoke detection (21)/Cloud detection (22)
23	4.050	N	
24	4.465	N	
25	4.515	N	
27	6.715	Y	High cloud, inversion detection
28	7.325	Y	Cloud, inversion detection
29	8.550	Y	Cloud, dust, snow detection
30	9.730	N	
31	11.030	Y	Cloud, dust, snow detection, Land, sun-glint clear-sky restoral tests Inversion detection Thin cirrus detection
32	12.020	Y	Cloud, dust detection
33	13.335	Y	Inversion detection
34	13.635	N	
35	13.935	Y	High cloud detection
36	14.235	N	

2.3 Cloud Mask Inputs and Outputs

The following paragraphs summarize the input and output of the MODIS cloud algorithm. Details on the multispectral single field-of-view (FOV) and spatial variability algorithms are found in the algorithm description section. As indicated earlier, input to the cloud mask algorithm is assumed to be calibrated and navigated level 1B radiance data in bands 1, 2, 3, 4, 5, 6, 7, 8, 9, 17, 18, 20, 21, 22, 26, 27, 28, 29, 31, 32, 33, and 35. Additionally, the cloud mask requires several ancillary data inputs:

1) sun, relative azimuth, viewing angles: obtained/derived from MOD03 (MODIS geolocation fields);
2) land/water map at 1-km resolution: obtained from MOD03;
3) topography: elevation above mean sea level from MOD03;
4) ecosystems: global 1-km map of ecosystems based on the Olson classification system;
5) daily NISE snow/ice map provided by NSIDC (National Snow and Ice Data Center);
6) weekly sea-surface temperature map from NOAA;
7) 5-year mean NDVI (Normalized Difference Vegetation Index) maps for 16-day periods;
8) surface temperature, total precipitable water maps from Global Data Assimilation System (GDAS);

The output of the MODIS cloud mask algorithm is a 48-bit (6 byte) data segment associated with each 1-km pixel (Table 3). The mask includes information about the processing path the algorithm followed (e.g., land or ocean) and whether or not a view of the surface is obstructed. We recognize that a potentially large number of applications use the cloud mask. Some algorithms are more tolerant of cloud contamination than others. For example, some algorithms may apply a correction to account for the radiative effects of a thin cloud, while other applications will avoid all cloud contaminated scenes. In addition, certain algorithms may use spectral channels that are more sensitive to the presence of clouds than others. For this reason, the cloud mask output also includes results from particular cloud detection tests.

The boundary between defining a pixel as cloudy or clear is sometimes ambiguous. For example, a pixel may be partly cloudy, or a pixel may appear as cloudy in one spectral channel and appear cloud-free at a different wavelength. Figure 1 shows three images of subvisual contrails and thin cirrus taken from Terra MODIS over Europe in June 2001. The top-left panel is a MODIS image in the 0.86 μm band, found on many satellites and commonly used for land surface classifications such as the NDVI. The contrails are not discernible in this image and scattering effects of the radiation may be accounted for in an appropriate atmospheric correction algorithm. The top-right panel shows the corresponding image of the MODIS 1.38 μm band. The 1.38 μm spectral channel is near a strong water vapor absorption band and, during the day, is extremely sensitive to the presence of high-level clouds. While the contrail seems to have little impact on visible reflectances, it is very apparent in the 1.38 μm channel. In this type of scene, the cloud mask needs to provide enough information to be useful for a variety of applications.

To accommodate a wide variety of applications, the mask contains more than a simple yes/no decision (though bit 2 alone could be used to represent a single bit cloud mask). The cloud mask includes 4 levels of 'confidence' with regard to whether a pixel is thought to be clear (bits 1 and 2)[1] as well as the results from different spectral tests. The bit structure of the cloud mask is:

[1] In this document, representations of bit fields are ordered from right to left. Bit 0, or the right-most bit, is the least significant.

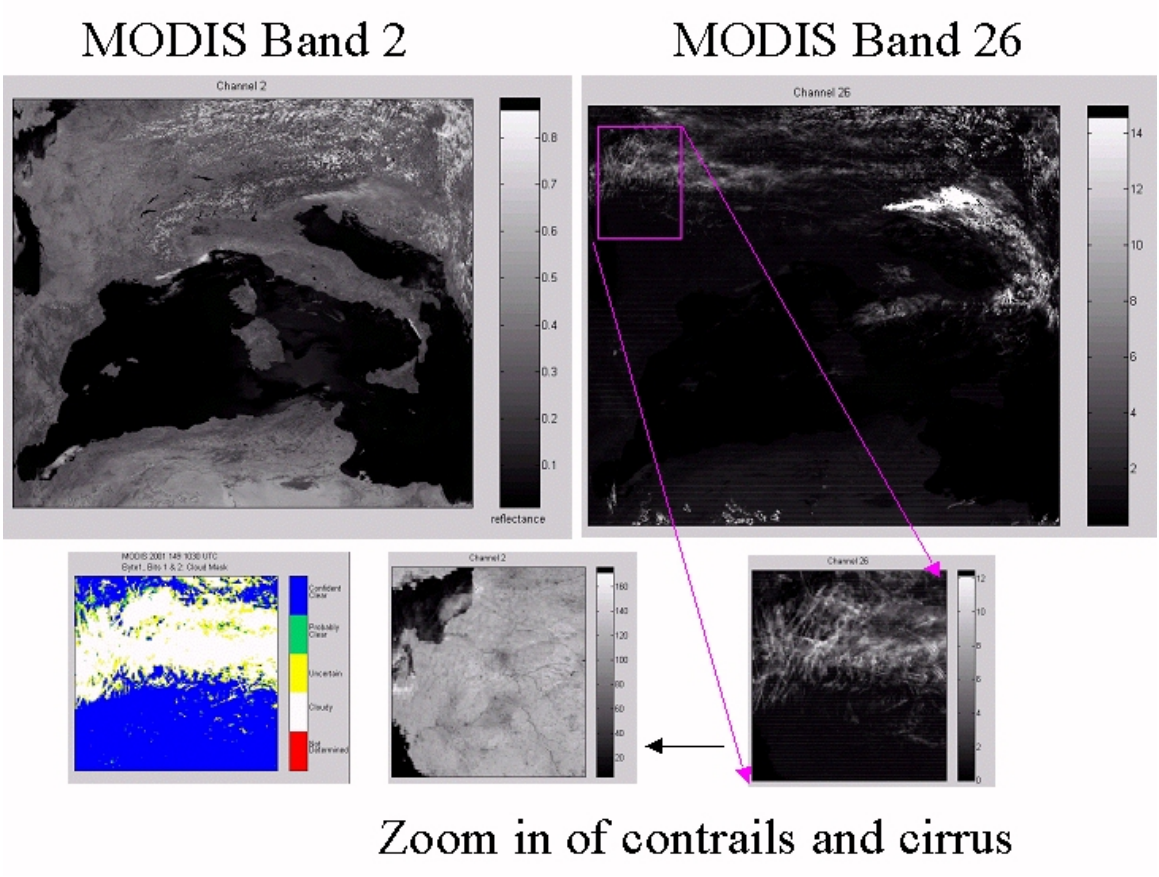

Figure 1. Two MODIS spectral images (0.86, 1.38) taken over Europe in June 2001. The lower image to the left represents the results of the MODIS cloud mask algorithm.

Table 3. File specification for the 48-bit MODIS cloud mask. A '0' for tests 13-47 may indicate that the test was not run.

BIT FIELD	DESCRIPTION KEY	RESULT
0	Cloud Mask Flag	0 = not determined 1 = determined
1-2	Unobstructed FOV Confidence Flag	00 = cloudy 01 = probably cloudy 10 = probably clear 11 = confident clear
	PROCESSING PATH FLAGS	
3	Day / Night Flag	0 = Night / 1 = Day
4	Sun glint Flag	0 = Yes / 1 = No
5	Snow / Ice Background Flag	0 = Yes/ 1 = No
6-7	Land / Water Flag	00 = Water 01 = Coastal 10 = Desert 11 = Land
	1-km FLAGS	
8	Non-Cloud Obstruction: day land thick smoke, day water thick smoke, other thick non-dust aerosol	0 = Yes / 1 = No
9	Thin Cirrus Detected (solar)	0 = Yes / 1 = No
10	Snow cover from ancillary map	0 = Yes / 1 = No
11	Thin Cirrus Detected (infrared)	0 = Yes / 1 = No
12	Cloud Adjacency (cloudy, prob. cloudy, plus 1-pixel adjacent)	0 = Yes / 1 = No
13	Cloud Flag – Ocean IR Threshold Test	0 = Yes / 1 = No
14	High Cloud Flag - CO_2 Threshold Test	0 = Yes / 1 = No
15	High Cloud Flag – 6.7 μm Test	0 = Yes / 1 = No
16	High Cloud Flag – 1.38 μm Test	0 = Yes / 1 = No
17	High Cloud Flag – 3.9-12 μm Test (night only)	0 = Yes / 1 = No
18	Cloud Flag - IR Temperature Difference Tests	0 = Yes / 1 = No
19	Cloud Flag - 3.9-11 μm Test	0 = Yes / 1 = No
20	Cloud Flag – Visible Reflectance Test	0 = Yes / 1 = No

21	Cloud Flag – Visible Ratio Test	0 = Yes / 1 = No
22	Clear-sky Restoral Test- NDVI in Coastal Areas	0 = Yes / 1 = No
23	Cloud Flag – Land, Polar Night 7.3-11μm Test	0 = Yes / 1 = No
24	Cloud Flag – Water 8.6-11 μm Test	0 = Yes / 1 = No
25	Clear-sky Restoral Test – Spatial Consistency (ocean)	0 = Yes / 1 = No
26	Clear-sky Restoral Tests (polar night, land, sun-glint)	0 = Yes / 1 = No
27	Cloud Flag – Surface Temperature Tests (water, night land)	0 = Yes / 1 = No
28	Suspended Dust Flag	0 = Yes / 1 = No
29	Cloud Flag - Night Ocean 8.6 - 7.3 μm Test	0 = Yes / 1 = No
30	Cloud Flag – Night Ocean 11 μm Variability Test	0 = Yes / 1 = No
31	Cloud Flag – Night Ocean "Low-Emissivity" 3.9-11 μm Test	0 = Yes / 1 = No
	250-m CLOUD FLAG	
32	Element(1,1)	0 = Yes / 1 = No
33	Element(1,2)	0 = Yes / 1 = No
34	Element(1,3)	0 = Yes / 1 = No
35	Element(1,4)	0 = Yes / 1 = No
36	Element(2,1)	0 = Yes / 1 = No
37	Element(2,2)	0 = Yes / 1 = No
38	Element(2,3)	0 = Yes / 1 = No
39	Element(2,4)	0 = Yes / 1 = No
40	Element(3,1)	0 = Yes / 1 = No
41	Element(3,2)	0 = Yes / 1 = No
42	Element(3,3)	0 = Yes / 1 = No
43	Element(3,4)	0 = Yes / 1 = No
44	Element(4,1)	0 = Yes / 1 = No
45	Element(4,2)	0 = Yes / 1 = No
46	Element(4,3)	0 = Yes / 1 = No
47	Element(4,4)	0 = Yes / 1 = No

2.3.1 PROCESSING PATH (BITS 3-7 PLUS BIT 10)

These bits describe the processing path taken by the cloud mask algorithm. The number and type of tests executed, and the test thresholds are a function of the processing path.

BIT 3: DAY / NIGHT FLAG

A combination of solar zenith angle and instrument mode (day or night mode) at the pixel latitude and longitude at the time of the observation is used to determine if a daytime or night-time cloud masking algorithm should be applied. Daytime algorithms, which include solar reflectance data, are constrained to solar zenith angles less than 85°. If this bit is set to 1, daytime algorithms were executed.

BIT 4: SUN GLINT FLAG

The sun glint processing path is taken when the reflected sun angle, θ_r, lies between 0° and 36°, where

$$\cos\theta_r = \sin\theta \sin\theta_0 \cos\phi + \cos\theta \cos\theta_0 . \quad (1)$$

Solar zenith angel is indicated by θ_0, θ is the viewing zenith angle, and ϕ is the azimuthal angle. Sun glint is also a function of surface wind and sea state, though that dependence is not directly included in the algorithm. Certain tests (e.g. visible reflectance over water) consist of thresholds that are a function of this sun glint angle. Bit 4 = 0 indicates that algorithms and thresholds specific to sun glint conditions will be applied.

BIT 5: SNOW / ICE PROCESSING FLAG

Certain cloud detection tests (e.g., visible reflectance tests) are applied differently in the presence of snow or ice. This bit is set to a value of 0 when the cloud mask algorithm finds that snow is present. The bit is set based on an abbreviated normalized difference snow index (NDSI, Hall et al. 1995) incorporated into the cloud mask. The NDSI uses MODIS 0.55 and 1.6

μm reflectances to form a ratio where values greater than a predetermined threshold are deemed snow or ice covered. The NDSI is defined as:

$$NDSI = (R_{0.55} - R_{NIR}) / (R_{0.55} + R_{NIR}), \quad (2)$$

where NIR denotes $R_{1.6}$ for Terra and $R_{2.1}$ for Aqua. In warmer parts of the globe, the NSIDC ancillary snow and ice data set is used as a check on the NDSI algorithm. At night, only the ancillary data are used to indicate the presence of surface snow or ice.

Note that bit 5 indicates a *processing path* and does not necessarily indicate that surface ice was detected, implying clear skies. Users interested in snow detection should access MODIS Level 2 Product MOD10.

BITS 6-7: LAND / WATER BACKGROUND FLAG

Bits 6 and 7 of the cloud mask output file contain additional information concerning the processing path taken through the algorithm. In addition to snow/ice mentioned above, there are four possible surface-type processing paths: land, water, desert, or coast. Naturally, there are times when more than one of these flags could apply to a pixel. For example, the northwest coast of the African continent could be simultaneously characterized as coast, land, and desert. In such cases, we choose to output the flag that indicates the most important characteristic for the cloud masking process. The flag precedence is as follows: coast, desert, land or water. These two bits have the following values: 00 = water, 01=coast, 10=desert, 11=land.

BIT 10: ANCILLARY SURFACE SNOW / ICE FLAG

Beginning with Collection 6, a flag is included in Bit 10 that indicates whether or not snow/ice was indicated by ancillary data (e.g., snow/ice map from NSIDC).

2.3.2 OUTPUT (BITS 0, 1, 2 AND 8-47)

This section contains a brief description of the output bit flags. More discussion is given in

the following sections.

BIT 0: EXECUTION FLAG

There are conditions for which the cloud mask algorithm will not be executed. For example, if all the radiance values used in the cloud mask are deemed bad, then masking cannot be undertaken. If bit 0 is set to 0, then the cloud mask algorithm was not executed. Conditions for which the cloud mask algorithm will not be executed include: no valid radiance data, no valid geolocation data, or any missing or invalid required radiance data when processing in sun-glint regions.

BITS 1-2: UNOBSTRUCTED (CLEAR SKY) CONFIDENCE FLAG

Confidence flags convey certainty in the outcome of the cloud mask algorithm tests for a given FOV. When performing spectral tests, as one approaches a threshold limit, the certainty or confidence in the outcome is reduced. Therefore, a confidence flag for each individual test, based upon proximity to the threshold value, is assigned and used to work towards a final confidence flag determination for the FOV. For most tests, linear interpolation is applied between a low confidence clear threshold (0% confidence of clear) and high a confidence clear threshold (100% confidence clear) to define a confidence. Sigmoid ("S-curves") curves may also be used.

The final cloud mask determination is one of four possible confidence levels calculated from a combination of clear-sky confidences from all tests performed (see section 3 for more detail). These are: confident clear (confidence > 0.99), probably clear ($0.99 \geq$ confidence > 0.95), probably cloudy ($0.95 \geq$ confidence > 0.66), and confident cloudy (confidence ≤ 0.66). The values of bits 1-2 are 3, 2, 1, and 0, respectively, for the above confidence ranges. This approach quantifies our confidence in the derived cloud mask for a given pixel. In the cloud mask algorithm, spatial consistency and/or additional spectral tests (called "clear-sky restoral" tests) are invoked as a final check for some scene types. If some or all clear-sky restoral tests pass, the final output clear-sky confidence is increased.

BIT 8: NON-CLOUD OBSTRUCTION

Smoke from forest fires, dust storms over deserts, and other aerosols between the surface and the satellite that result in obstruction of the FOV may be flagged as "cloud." The non-cloud obstruction bit is set to 0 if spectral tests indicate the possible presence of aerosols. *This bit is not an aerosol product*; rather, if the bit is set to zero, then the instrument may be viewing an aerosol-laden atmosphere. Bit 8 records potential smoke-filled pixels for daytime land and water scenes. See bit 28 for suspended dust.

BIT 9: THIN CIRRUS (NEAR-INFRARED)

MODIS includes a unique spectral band—1.38 μm—specifically included for the detection of thin cirrus. Land and sea surface retrieval algorithms may attempt to correct the observed radiances for the effects of thin cirrus. This test is discussed in Section 3.2.4. If this bit is set to 0, thin cirrus was detected using this band.

BIT 11: THIN CIRRUS (INFRARED)

This second thin cirrus bit indicates that IR tests detect a thin cirrus cloud. The results are independent of the results of bit 9, which makes use of the 1.38 μm band. This test is discussed in Section 3.2.5. If this bit is set to 0, thin cirrus was detected using infrared channels.

BIT 12: CLOUD ADJACENCY BIT

A one-pixel boundary around probably cloudy and/or confident cloudy pixels is defined as "cloud adjacent". A bit value of 0 indicates a given pixel is either confident cloudy, probably cloudy, or cloud adjacent.

BITS 13-21, 23-24, 27, 29-31: 1 KM CLOUD MASK

These bits represent the results of tests performed specifically to detect the presence of clouds using MODIS 1-km observations or smaller-scale MODIS observations that are aggregated to 1-km. Each test is discussed in the next section. The number of spectral tests applied is

a function of the processing path. Table 4 lists the tests applied for each path where snow and/or ice cover is assumed for the polar categories. It is important to refer to this table (or the associated Quality Assurance data) when interpreting the meaning of these flags, as a value of 0 can mean either the pixel was determined to be cloudy by a certain test, or that the test was not performed. Note that the table cannot list all complicating factors such as surface elevation, extremely dry atmospheres, etc., where some tests my not be applied. The Quality Assurance (QA) data is definitive for which tests are applied.

BITS 22, 25-26: CLEAR-SKY RESTORAL TESTS

These bits represent results from spatial consistency and other spectral clear-sky restoral tests.

Bits 32-47: 250-Meter Resolution Cloud Mask

The 250-m cloud mask is collocated within the 1000-m cloud mask in a fixed way; of the twenty-eight 250-m pixels that can be considered located within a 1000-m pixel, the most centered sixteen are processed for the cloud mask. The relationship between the sixteen 250-m FOVs and the 1-km footprint in the cloud mask is defined as:

250-m beginning element number = (1-km element number - 1) * 4 + 1

250-m beginning line number = (1-km line number - 1) * 4 + 1

where the first line and element are 1,1. From this beginning location, a 4×4 array of lines and elements can be identified. The indexing order of the sixteen 250-m pixels in the cloud mask file (i.e., bits 32-47) is lines, elements. Bit 3 must be set to 1 for the 250-m mask to have any meaning (e.g., ignore these 16 bits in night conditions).

It is possible to infer cloud fraction in the 1000-m field of view from the 16 visible pixels within the 1-km footprint. The cloud fraction would be the number of zeros divided by 16.

In creating the 250-m mask, results from the 1-km cloud mask are first copied into the 16 250-m flags, where a confidence ≤ 0.95 is considered cloudy. The final result for a particular

250-m pixel may then be changed based on tests described in sections 3.2.7 and 3.2.8.

Table 4. MODIS cloud mask tests executed for a given processing path.

Test/Bit #		Day Ocean	Night Ocean	Day Land	Night Land	Day Snow/ice	Night Snow/ice	Day Coast	Day Desert	Polar Day	Polar Night
BT_{11}	13	✓	✓								
$BT_{13.9}$	14	✓	✓	✓	✓	✓	✓	✓	✓		
$BT_{6.7}$	15	✓	✓	✓	✓	✓	✓	✓	✓	✓	✓
$R_{1.38}$	16	✓		✓		✓		✓	✓	✓	
$BT_{3.9}$-BT_{12}	17				✓		✓				✓
BT_{11}-BT_{12}	18	✓	✓	✓	✓	✓	✓	✓	✓	✓	✓
BT_{11}-$BT_{3.9}$	19	✓	✓	✓	✓	✓	✓	✓	✓	✓	✓
$R_{0.66}$, $R_{0.87}$	20	✓		✓				✓	✓		
$R_{0.48}$	20								✓		
$R_{0.87}/R_{0.66}$	21	✓							✓		
$BT_{7.3}$-BT_{11}	23				✓		✓				✓
$BT_{8.6}$-BT_{11}	24	✓	✓								
Sfc. Temp.	27	✓	✓		✓						
$BT_{8.6}$-$BT_{7.3}$	29		✓								
BT_{11} Var.	30		✓								

3.0 Algorithm Description

The strategy for clear vs. cloudy discrimination in a given MODIS FOV is as follows:

1) Perform various spectral and/or spatial variability tests appropriate to the given scene and illumination characteristics to detect the presence or absence of cloud
2) Calculate clear-sky confidences for each test applied
3) Combine individual test confidences into a preliminary overall confidence of clear sky for the FOV
4) If necessary, apply clear-sky restoral tests appropriate for the given scene type, illumination, and preliminary confidence value
5) Determine final output confidence as one of four categories: confident clear, probably clear, probably cloud, or confident cloud

The details of this process are discussed in Sections 3.1 and 3.2 below. The physical bases for the various spectral tests are detailed in Section 3.1. Test thresholds have been determined using several methods: 1) from heritage algorithms mentioned above, 2) manual inspection of MODIS imagery, 3) statistics derived from collocated CALIOP (Cloud-Aerosol Lidar with Orthogonal Polarization) cloud products and MODIS radiance data, and 4) statistics compiled from carefully selected and quality controlled MODIS radiance data and MOD35 cloud mask results. The method for combining results of individual cloud tests to determine a final confidence of clear sky is detailed in Section 3.2.

3.1 Theoretical Description of Cloud Detection

The theoretical basis of the spectral cloud tests and practical considerations are contained in this section. For nomenclature, we shall denote the satellite measured solar reflectance as R, and refer to the infrared radiance as brightness temperature (equivalent blackbody temperature determined using the Planck function) denoted as BT. Subscripts refer to the wavelength at which the measurement is made.

3.1.1 INFRARED BRIGHTNESS TEMPERATURE THRESHOLDS AND DIFFERENCE (BTD) TESTS

The azimuthally averaged form of the infrared radiative transfer equation is given by

$$\mu \frac{\mathrm{d}\, I(\delta,\mu)}{\mathrm{d}\,\delta} = I(\delta,\,\mu) - (1-\omega_0)B(T) - \frac{\omega_0}{2}\int_{-1}^{1} P(\delta,\mu,\mu')\, I(\delta,\mu')\,\mathrm{d}\,\mu'. \tag{3}$$

In addition to atmospheric structure, which determines *B(T)*, the parameters describing the transfer of radiation through the atmosphere are the single scattering albedo, $\omega_0 = \sigma_{sca}/\sigma_{ext}$, which ranges between 1 for a non-absorbing medium and 0 for a medium that absorbs and does not scatter energy, the optical depth, δ, and the Phase function, $P(\mu, \mu')$, which describes the direction of the scattered energy.

To gain insight on the issue of detecting clouds using IR observations from satellites, it is useful to first consider the two-stream solution to Eq. (3). Using the discrete-ordinates approach (Liou 1973; Stamnes and Swanson 1981), the solution for the upward radiance from the top of a uniform single cloud layer is:

$$I_{\mathrm{obs}} = M\_L\_\exp(-k\delta) + M_+L_+ + B(T_{\mathrm{c}}), \tag{4}$$

where

$$L_+ = \frac{1}{2}\left[\frac{I\downarrow + I\uparrow - 2B(T_{\mathrm{c}})}{M_+ \mathrm{e}^{-k\delta} + M_-} + \frac{I\downarrow + I\uparrow}{M_+ \mathrm{e}^{-k\delta} + M_-}\right], \tag{5}$$

$$L_- = \frac{1}{2}\left[\frac{I\downarrow + I\uparrow - 2B(T_{\mathrm{c}})}{M_+ \mathrm{e}^{-k\delta} + M_-} + \frac{I\downarrow - I\uparrow}{M_+ \mathrm{e}^{-k\delta} - M_-}\right], \tag{6}$$

$$M_\pm = \frac{1}{1\pm k}\left(\omega_0 \mp \omega_0 g(1-\omega_0)\frac{1}{k}\right), \tag{7}$$

$$k = \left[(1-\omega_\circ)(1-\omega_\circ g)\right]^{\frac{1}{2}}. \tag{8}$$

$I\downarrow$ is the downward radiance (assumed isotropic) incident on the top of the cloud layer, $I\uparrow$ the upward radiance at the base of the layer, and g the asymmetry parameter. T_{c} is a representative temperature of the cloud layer.

A challenge in cloud masking is detecting thin clouds. Assuming a thin cloud layer, the effective transmittance (ratio of the radiance exiting the layer to that incident on the base) is de-

rived from equation (4) by expanding the exponential. The effective transmittance is a function of the ratio of $I\downarrow/I\uparrow$ and $B(T_c)/I\uparrow$. Using atmospheric window regions for cloud detection minimizes the $I\downarrow/I\uparrow$ term and maximizes the $B(T_c)/I\uparrow$ term. Figure 2 is a simulation of differences in brightness temperature between clear and cloudy sky conditions using the simplified set of equations (4)-(8). In these simulations, there is no atmosphere, the surface is emitting at a blackbody temperature of 290 K, and cloud particles are ice spheres with a gamma size distribution assuming an effective radius of 10 μm, and the cloud optical depth $\delta = 0.1$. Two cloud temperatures are simulated (210 K and 250 K). Brightness temperature differences between the clear and cloudy sky are caused by non-linearity of the Planck function and spectral variation in the single scattering properties of the cloud. This figure does not include the absorption and emission of atmospheric gases, which would also contribute to brightness temperature differences. Observations of brightness temperature differences at two or more wavelengths can help separate the atmospheric signal from the cloud effect.

The infrared threshold technique is sensitive to thin clouds given the appropriate characterization of surface emissivity and temperature. For example, with a surface at 300 K and a cloud

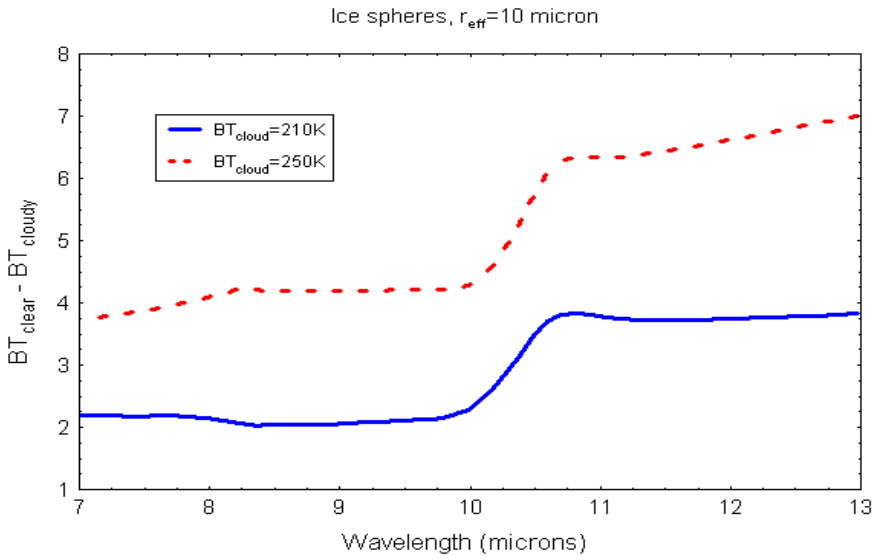

Figure 2. A simple simulation of the brightness temperature differences between a "clear" and cloudy sky as a function of wavelength. The underlying temperature is 290 K and the cloud optical depth is 0.1. All computations assume ice spheres with $r_e = 10$ μm.

at 220 K, a cloud with an emissivity of 0.01 affects the top-of-atmosphere brightness temperature by 0.5 K. Since the expected noise equivalent temperature of MODIS infrared window channel 31 is 0.05 K, the cloud detecting potential of MODIS is obviously very good. The presence of a cloud modifies the spectral structure of the radiance of a clear-sky scene depending on cloud microphysical properties (e.g., particle size distribution and shape). This spectral signature, as demonstrated in Figure 2, is the physical basis behind the brightness temperature difference tests.

BT_{11} THRESHOLD ("FREEZING") TEST (BIT 13)

Several infrared window threshold and temperature difference techniques have been developed. These algorithms are most effective for cold clouds over water and must be used with caution in other situations. Over (liquid) water when the brightness temperature in the 11 μm (BT_{11}) channel (band 31) is less than 270 K, we assume the pixel to fail the clear-sky condition. The three thresholds over ocean are 267, 270, and 273 K, for low, middle, and high confidence of clear sky thresholds, respectively. Note that "high confidence clear" in this case means that *BTs* warmer than 273 K cannot indicate cloud *according to this test*. Obviously, clouds may exist at warmer temperatures and may be detected by other cloud tests. See Section 3.2 for a full description of the thresholding and confidence-setting process.

Cloud masking over land surface from thermal infrared bands is more difficult than over ocean due to potentially larger variations in surface emittance. Nonetheless, simple thresholds are useful over certain land features. Over land, the BT_{11} is used as a clear-sky restoral test. If the initial determination for a pixel is cloudy, that pixel may be "restored" to clear if the observed BT_{11} exceeds a threshold defined as a function of elevation and ecosystem. Table 5 lists the "freezing test" and clear sky restoral test thresholds. Unless otherwise indicated, all thresholds listed in this document apply to the Aqua instrument. Though most thresholds are identical between Aqua and Terra, there are some small differences due to variations in instrument age and other characteristics.

BT_{11} - BT_{12} AND $BT_{8.6}$ - BT_{11} TEST (BITS 18 AND 24)

As a result of the relative spectral uniformity of surface emittance in the IR, spectral tests within various atmospheric windows (such as MODIS bands 29, 31, 32 at 8.6, 11, and 12 μm, respectively) can be used to detect the presence of cloud. Differences between BT_{11} and BT_{12} are widely used for cloud screening with AVHRR and GOES measurements, and this technique is often referred to as the split window technique. Saunders and Kriebel (1988) used BT_{11} - BT_{12} differences to detect cirrus clouds—brightness temperature differences are larger over thin clouds than over clear or overcast conditions. Cloud thresholds were set as a function of satellite zenith angle and the BT_{11} brightness temperature. Inoue (1987) also used BT_{11} - BT_{12} versus BT_{11} to separate clear from cloudy conditions.

Table 5. Thresholds used for BT_{11} threshold test in the MODIS cloud mask algorithm.

Scene Type	Threshold	High confidence clear	Low confidence clear
Day ocean	270 K	273 K	267 K
Night ocean	270 K	273 K	267 K
Day land*	300.0 K	305.0	NA
Night land*	292.5 K	297.5	NA
Night desert*	292.5K	297.5	NA
Day Desert*	295.0K	305.0	NA

* Restoral test at sea level

In difference techniques, the measured radiances at two wavelengths are converted to brightness temperatures and subtracted. Because of the wavelength dependence of optical thickness and the non-linear nature of the Planck function (B_λ), the two brightness temperatures are often different. Figure 3 is an example of a theoretical simulation of the brightness temperature difference between 11 and 12 μm versus the brightness temperature at 11 μm, assuming a standard tropical atmosphere. The difference is a function of cloud optical thickness, the cloud temperature, and the cloud particle size distribution.

The basis of the split window and 8.6-11 μm BTD for cloud detection lies in the differential water vapor absorption that exists between different window channel (8.6 and 11 μm and 11 and 12 μm) bands. These spectral regions are considered to be part of the atmospheric window where absorption is relatively weak. Most of the absorption lines are a result of water vapor molecules, with a minimum occurring around 11 μm.

In the MODIS cloud mask, we follow Saunders and Kriebel (1988) in the use of 11-12 μm BTDs to detect transmissive cirrus cloud, with small corrections to the thresholds for nighttime

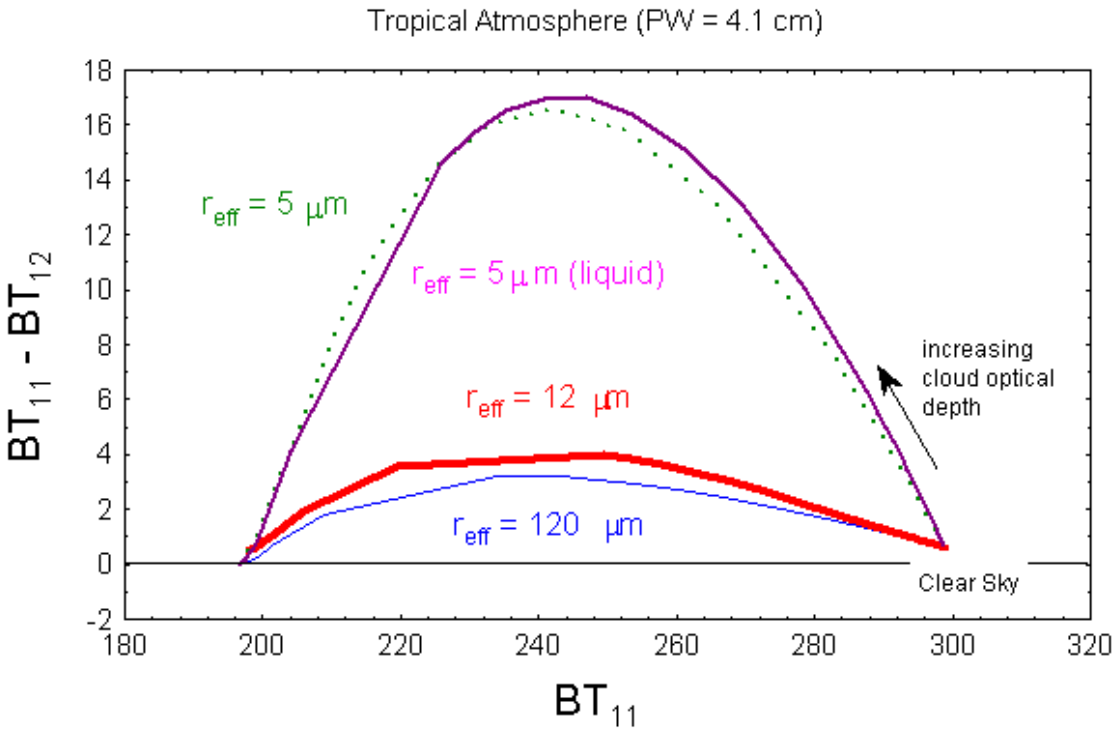

Figure 3. Theoretical simulations of the brightness temperature difference as a function of BT_{11} for a cirrus cloud of varying cloud microphysical properties.

scenes where surface temperature inversions are possible, and in scenes with surface ice and snow. Previous versions of the cloud mask algorithm made use of this test only over surfaces not covered by snow or ice. Beginning with the Collection 5 algorithm, this test makes use of thresholds taken from Key (2002) who extended the Saunders and Kriebel values to very low temperatures. The 11-12 μm test is performed in all processing paths for both day and night except for Antarctica. For 8.6-11 μm BTDs, we use thresholds of 0.0, -0.5, and -1.0 K for low, middle, and high confidence of clear sky, respectively. The 8.6-11 μm BTD test is only performed over liquid water surfaces as land surface emittance at 8.6 μm is quite variable.

SURFACE TEMPERATURE TESTS (BIT 27)

Building on the discussion above, BT_{11} can be corrected for moisture absorption by adding the scaled brightness temperature difference of two spectrally close channels with different water vapor absorption coefficients; the scaling coefficient is a function of the differential water vapor absorption between the two channels. The surface temperature, T_s, can be determined using remote sensing instruments if observations are corrected for water vapor absorption effects,

$$T_s = BT_{11} + \Delta BT, \tag{9}$$

where BT_{11} is a window channel brightness temperature. To begin, the radiative transfer equation for a clear atmosphere can be written

$$I_{\lambda,\mathrm{clr}} = B_\lambda(T(p_s))\tau_\lambda(p_s) + \int_{p_s}^{p_0} B_\lambda(T(p))\frac{\mathrm{d}\,\tau_\lambda(p)}{\mathrm{d}\,p}\mathrm{d}\,p\,. \tag{10}$$

As noted above, absorption is relatively weak across the window region so that a linear approximation is made to the transmittance

$$\tau \approx 1 - k_\lambda u, \tag{11}$$

Here k_λ is the absorption coefficient of water vapor and u is the path length. The differential transmittance then becomes

$$\mathrm{d}\tau_\lambda = -k_\lambda \mathrm{d}u. \tag{12}$$

Inserting this approximation into the window region radiative transfer equation will lead to

$$I_{\lambda,\mathrm{clr}} = B_{\lambda,\mathrm{s}}(1 - k_\lambda u) + k_\lambda \int_0^{u_\mathrm{s}} \overline{B}_\lambda \, \mathrm{d}\, u \,. \tag{13}$$

Here, $\overline{B_\lambda}$ is the atmospheric mean Planck radiance. Since $B_{\lambda,\mathrm{s}}$ will be close to both $I_{\lambda,\mathrm{clr}}$ and $\overline{B_\lambda}$, we can linearize the radiative transfer equation with respect to T_s

$$BT_{\mathrm{b}\lambda} = T_\mathrm{s}(1 - k_\lambda u_\mathrm{s}) + k_\lambda u_\mathrm{s} \overline{BT_\lambda}\,, \tag{14}$$

where $\overline{BT_\lambda}$ is the mean atmospheric temperature corresponding to $\overline{B_\lambda}$. Using observations from two window channels, one may ratio this equation, cancel out common factors and rearrange to end up with the following approximation

$$\frac{T_\mathrm{s} - BT_{\lambda,1}}{T_\mathrm{s} - BT_{\lambda,2}} = \frac{k_{\lambda,1}}{k_{\lambda,2}} \,. \tag{15}$$

Solving the equation for T_s yields

$$T_\mathrm{s} = BT_{\lambda,1} + \frac{k_{\lambda,1}}{k_{\lambda,2} - k_{\lambda,1}} (BT_{\lambda,1} - BT_{\lambda,2}). \tag{16}$$

Thus, with a reasonable estimate of the sea surface temperature and total precipitable water (on which k_λ is dependent), one can develop appropriate thresholds for cloudy sky detection. For example,

$$BT_{11} + a_{\mathrm{PW}}(BT_{11} - BT_{12}) < \mathrm{SST}. \tag{17}$$

Using a formulation from the MODIS Ocean Science Team, we compute an estimate of the bulk sea-surface temperature (SST),

$$\mathrm{SST} = \mathrm{k}_0 + \mathrm{k}_1 BT_{31} + \mathrm{k}_2(BT_{11}\text{-}BT_{12})\ \mathrm{T}_{\mathrm{env}} + \mathrm{k}_3(BT_{11}\text{-}BT_{12})(1/\mu\text{-}1), \tag{18}$$

where $\mathrm{k}_0 =$ 1.886, $\mathrm{k}_1 = 0.938$, $\mathrm{k}_2 = 0.128$, $\mathrm{k}_3 = 1.094$, $\mathrm{T}_{\mathrm{env}}$ is a first guess SST from GDAS data, and μ is the cosine of the viewing zenith angle (Brown et al., 1999). Use of these coefficients approximates the expected decrease in clear-sky observed BT_{11} due to water vapor absorption as a function of viewing zenith angle. The surface temperature test for ocean surfaces compares (SST - BT_{11}) against threshold values to detect cloud: 3.0, 2.5, and 2.0 K for low, middle, and

high confidence of clear sky, respectively.

For land surfaces, the situation is complicated by varying surface emittances, vegetation types and amounts, temperature inversions at night, and snow cover. For night scenes, differences between surface temperatures from GDAS data (SFCT) and BT_{11} (SFCT - BT_{11}) are compared to empirically derived thresholds. The thresholds are computed as follows:

$$\text{MIDPT} = \text{TH}_0 + \text{b}(BT_{11}\text{-}BT_{12}) + \text{c}(\phi/\phi_{max})^4, \quad (19)$$

where MIDPT is the mid-confidence value (0.5 confidence of clear sky), TH_0 is either 12 K or 20 K depending on expected atmospheric moisture content (e.g., desert=20 K, vegetated land=12 K), b = 2.0, c = 3.0, ϕ is viewing zenith angle, and ϕ_{max} is the MODIS maximum viewing zenith angle (65.49). High and low confidence thresholds are -2.0 K and +2 K, respectively. A surface temperature test is not performed for daytime or snow/ice covered scenes.

BT_{11} - $BT_{3.9}$ TEST (BITS 19 AND 31)

MODIS band 22 (3.9 μm) measures radiances in the window region near 3.5-4 μm. The BTD between BT_{11} and $BT_{3.9}$ can be used to detect the presence of clouds. During daylight hours the difference between BT_{11} and $BT_{3.9}$ is large and negative because of reflected solar energy at 3.9 μm. This technique is very successful at detecting low-level water clouds in most scenes; however, the application of $BT_{11} - BT_{3.9}$ is difficult in deserts during daytime. Bright desert regions with highly variable surface emissivities can be incorrectly classified as cloudy with this test. The problem is mitigated somewhat in the MODIS cloud mask by making use of a double-sided test where brightness temperature differences greater than a "low" threshold but less than a "high" threshold are labeled clear while values outside this range are called cloudy. This threshold strategy along with the use of clear-sky restoral tests is effective in detecting most low-level clouds over deserts.

At night, $BT_{11} - BT_{3.9}$ can be used to detect partial cloud or thin cloud within MODIS FOVs. Small negative or positive differences are observed only for cases where an opaque scene (such as thick cloud or the surface) fills the field of view of the sensor. Larger negative differ-

ences between BT_{11} and $BT_{3.9}$ result when a non-uniform scene (e.g., broken cloud) is observed. This is a result of Planck's law. The brightness temperature dependence on the warmer portion of the scene increases with decreasing wavelength. The shortwave window Planck radiance is proportional to temperature to the thirteenth power, while the long wave dependence is only to the fourth power. Differences in the brightness temperatures of the long wave and shortwave channels are small when viewing mostly clear or mostly cloudy scenes; however, for intermediate situations the differences become large (< -3°C). Positive $BT_{11} - BT_{3.9}$ differences occur over some stratus clouds due to lower cloud emissivities at 3.9 μm than at 11 μm. Table 6 lists some simple thresholds used in the MODIS Collection 6 algorithm. More tests and thresholds using 3.9 and 11 μm are detailed below.

Detecting clouds at high latitudes using infrared window radiance data is a challenging problem due to very cold surface temperatures. The nighttime BTD may be either negative or positive depending on cloud optical depth and particle size (Liu et. al., 2004). The situation becomes more complex in temperature inversions that are frequent in polar night conditions. For a complete discussion of the problem, see Liu et al. (2004). Early versions of MOD35 used 11-3.9 μm cloud test thresholds that did not take temperature inversions into account and were most appropriate for non-polar, thick water clouds. Beginning with Collection 5, polar night confident cloud thresholds vary linearly from –0.8K to +0.6K as BT_{11} varies between 235K and 265K. The threshold is constant below 235K and above 265K. This assumes that more inversions are found as surface temperatures decrease. Thresholds for polar day scenes with snow or ice surfaces vary from 7K to 14.5K as BT_{11} moves from 230K to 245K.

Nighttime land and ocean scenes have BT_{11} - $BT_{3.9}$ test thresholds that are functions of TPW because atmospheric moisture loading has a large impact on these BTDs relative to the small expected changes between clear and cloudy skies. Beginning with Collection 6, collocated CALIOP clear vs. cloudy determinations and MODIS radiance data were used to define the following relationship:

$$THR = b0 + (b1 * TPW) + (b2 * TPW^2).$$

THR is the mid-confidence of clear sky (0.5) threshold, b0 = -0.0077 (0.5972), b1 = 1.1234 (-0.2460), and b2 = -0.3403 (0.1501) for land (ocean). An adjustment of -0.5 is made to THR for Terra data, also these thresholds are not used for desert regions. Figure 4 shows a plot of clear (red points) and cloudy (blue points) $BT_{11} - BT_{3.9}$ BTDs for night oceans with the black line defining the relationship above.

Note that a night ocean "low-emissivity" stratus cloud test (see above) result is reported separately in bit 31 beginning with Collection 6. This test is the same as was reported in bit 19 for night oceans in previous versions of the cloud mask.

For nighttime deserts, the Collection 5 test is retained where thresholds are functions of 11-12 µm BTDs.

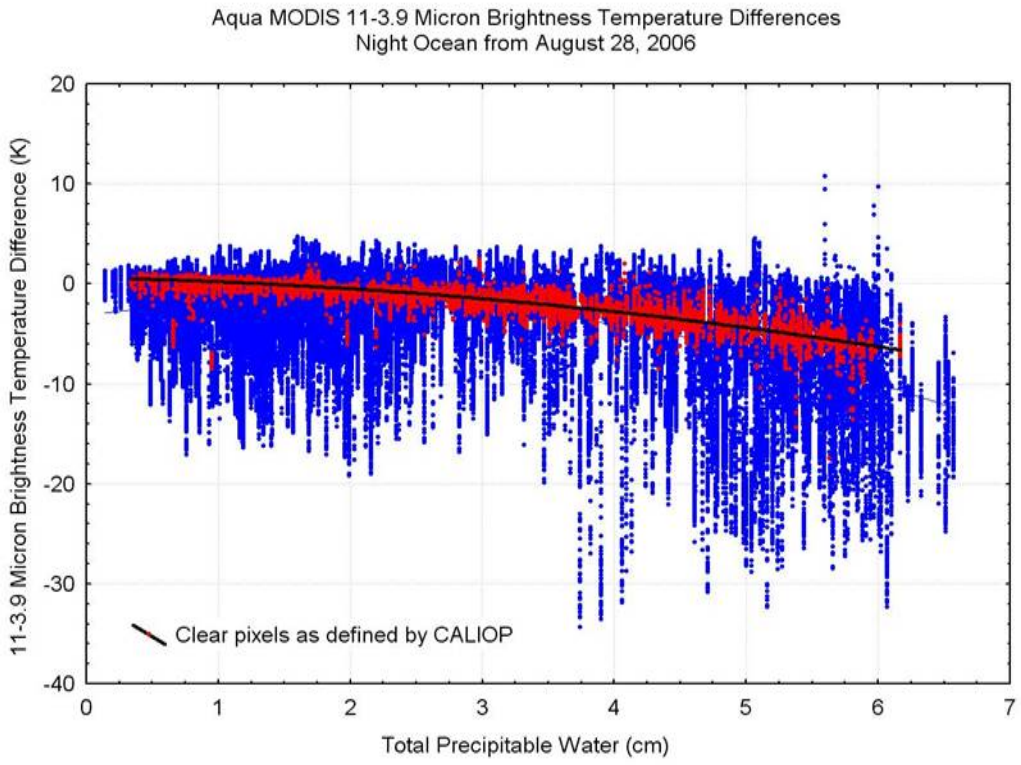

Figure 4. Aqua MODIS BT_{11}-$BT_{3.9}$ night ocean observations on August 28, 2006. Blue is cloudy, red is clear.

Table 6. Some simple thresholds used in the BT11-BT3.9 cloud tests.

Scene Type	Threshold	High confidence clear	Low confidence clear
Day ocean	-8.0 K	-6.0 K	-10.0 K
Night ocean (stratus)	1.0 K	-1.0 K	1.25 K
Day land	-13.0 K	-11.0 K	-15. 0 K
Day non-polar snow/ice	-7.0 K	-4.0 K	-10.0 K
Night non-polar snow/ice	0.60 K	0.50 K	0.70 K
Day desert	-18.0, 0 K	>-16, <-2 K	<-20, >2 K

$BT_{3.9}$ - BT_{12} TEST (BIT 17)

This window brightness temperature difference test is applied during the nighttime over land and polar snow/ice surfaces. This difference is useful for separating thin cirrus and cloud free conditions and is relatively insensitive to the amount of water vapor in the atmosphere (Hutchison and Hardy 1995). The non-polar land thresholds are 15, 10, and 5 K, for low confidence, mid-point, and high confidence of clear sky, respectively. Over non-polar snow-covered surfaces, the thresholds are 4.5, 4.0, and 3.5K.

The 3.9-12 μm BTD high cloud test has different thresholds in polar night conditions. For reasons not well understood, the thresholds for this test need to be increased with decreasing temperatures below 265K. This is counter-intuitive from arguments based on atmospheric water vapor loading and absorption at these two wavelengths. Perhaps the calibration of one or both bands is of reduced accuracy at cold temperatures. In addition, the test cannot be used on the very coldest and driest scenes such as are found in Antarctica and Greenland during the winter season. Therefore, the test is not performed in polar night conditions when the elevation exceeds 2000 m. Test thresholds vary linearly from +4.5K to +2.5K as the observed 11 μm *BT* varies between 235K and 265K. The threshold is constant below 235K and above 265K.

$BT_{7.3}$ - BT_{11} TEST (BIT 23)

A test for identifying high and mid-level clouds over land at night uses the brightness temperature difference between 7.3 and 11 μm. Under clear-sky conditions, $BT_{7.3}$ is sensitive to temperature and moisture in middle levels of the atmosphere while BT_{11} measures radiation mainly from the warmer surface. Clouds reduce the absolute value of this difference. The thresholds used are -8K, -10K, and -11K for low, mid-point, and high confidences, respectively.

The polar night algorithm also utilizes a 7.3-11μm BTD cloud test with different thresholds that are functions of the observed 11 μm *BT*. Since the weighting function of the 7.3 μm band peaks at about 800 hPa, the BTD is related to the temperature difference between the 800 hPa layer and the surface, to which the 11 μm band is most sensitive. In the presence of low clouds under polar night conditions with a temperature inversion, radiation from the 11 μm band comes primarily from the relatively warm cloud top, decreasing the 7.3-11 μm BTD compared to the clear-sky value. For a complete discussion of the theory, see Liu et al. (2004). In conditions of deep polar night, even high clouds may be warmer than the surface and will often be detected with this test. The test as configured in MOD35 is applicable only over nighttime snow and ice surfaces. Because the 7.3 μm band is sensitive to atmospheric water vapor and also because inversion strength tends to increase with decreasing surface temperatures (Liu et al., 2004), thresholds for this test are a function of the observed 11 μm *BT*. The thresholds vary linearly in three ranges: BTD +2K to –4.5K for 11 μm *BT* between 220K and 245K, BTD –4.5K to –11.5K for 11 μm *BT* between 245 and 255K, and BTD –11.5 to –21K for 11 μm *BT* between 255K and 265K. Thresholds are constant for 11 μm *BT* below 220K or above 265K. The thresholds are slightly different over ice (frozen water surfaces): BTD +2K to –4.5K for 11 μm *BT* between 220K and 245K, BTD –4.5K to –17.5K for 11 μm *BT* between 245 and 255K, and BTD –17.5 to –21K for 11 μm *BT* between 255K and 265K. These somewhat larger BTDs presumably reflect a lesser tendency for strong inversions and higher water vapor loading over frozen water surfaces as opposed to snow-covered land areas. These thresholds also differ slightly from those reported

in Liu et al. (2004), a result of extensive testing over many scenes and the necessity of meshing this test with other cloud mask tests and algorithms. Note that this test was also implemented for non-polar (latitude < 60º), nighttime, snow-covered land. Figure 5 (left) shows imagery from the 7.3 μm band for a scene from Canada and the results of the test (right). Note the difference in texture between cloudy and clear on the right in the 7.3 μm *BT* imagery, even though the gray scale indicates similar temperatures for much of the scene.

A 7.3-11 μm BTD test is utilized to find clear sky because of the prevalence of polar night temperature inversions. This test works in the same way as the 6.7-11 μm BTD clear-sky restoral test (see below), where 11 μm BTs are sometimes significantly lower than those measured in the 6.7 μm band because the 6.7 μm weighting function peaks near the top of a warmer inversion layer in some cases. However, since the 7.3 μm band peaks lower in the atmosphere, a 7.3-11 μm BTD test can detect lower and weaker inversions. Pixels are restored to clear if the 7.3-11 μm BTD > 5K.

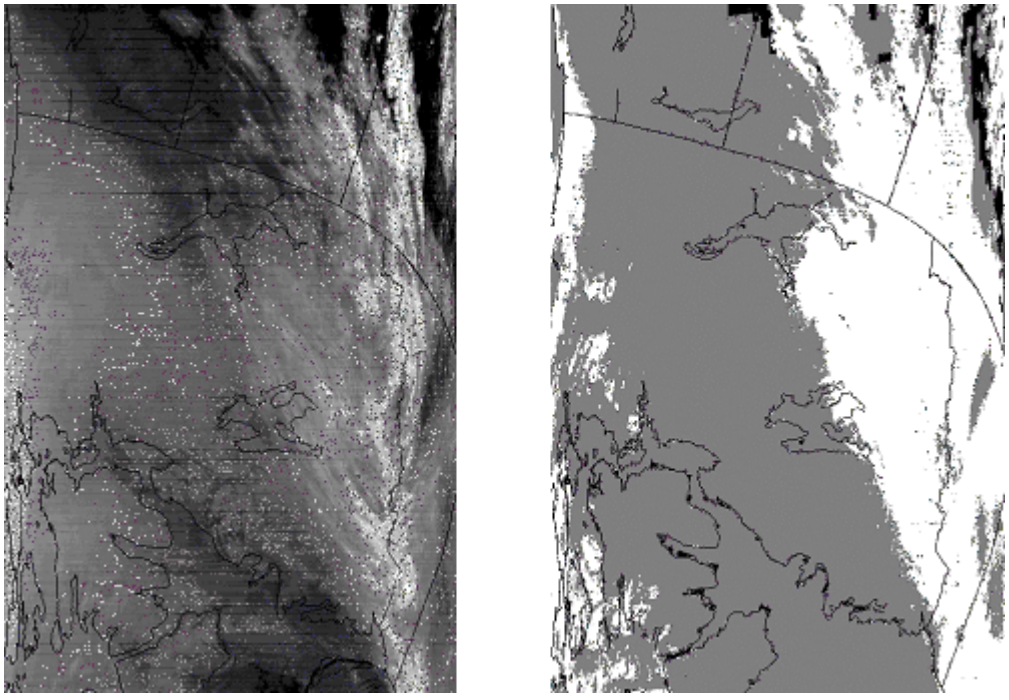

Figure 5. Canadian scene from Aqua MODIS on April 1, 2003 at 05:05UTC. $BT_{7.3}$ on left, 7.3-11 μm BTD test result on right.

$BT_{8.6}$ - $BT_{7.3}$ TEST (BIT 29)

The 8.6-7.3 μm BTD test is designed primarily to detect thick mid-level clouds over night ocean surfaces but can also detect lower clouds in regions where middle atmosphere relative humidity is low. It is sometimes more effective than the SST test for finding stratocumulus clouds of small horizontal extent. It can also detect high, thick clouds. Both this and the surface temperature (SST) test are needed in order to find those clouds that are thick but that also show very small thermal spatial variability. The test thresholds are 16.0K, 17.0K, and 18.0K for 0.0, 0.5, and 1.0 confidence of clear sky, respectively.

BT_{11} VARIABILITY CLOUD TEST (BIT 30)

The 11 μm variability test is utilized to detect clouds of small spatial extent (a pixel or two) and cloud edges over nighttime oceans. Most thick clouds are detected by other spectral measures but a spatial variability test is very effective at night for detecting the thinner, warmer cloud edges (including clouds extending only over a few pixels) over the uniform ocean surface. Beginning with Collection 5, this test counts the number of surrounding pixels where differences in 11 μm BT are ≤ 0.5K. The higher the number (8 possible), the more likely the center pixel is clear. The confident cloud, mid-point, and confident clear thresholds are 3, 6, and 7, respectively.

$BT_{6.7}$ HIGH CLOUD TEST (BIT 15)

In clear-sky situations, the 6.7 μm radiation measured by satellite instruments is emitted by water vapor in the atmospheric layer between approximately 200 and 500 hPa (Soden and Bretherton 1993; Wu et al. 1993) and has a brightness temperature ($BT_{6.7}$) related to the temperature and moisture in that layer. The 6.7 μm radiation emitted by the surface or low clouds is absorbed in the atmosphere above and is generally not sensed by satellite instruments. Therefore, thick clouds found above or near the top of this layer have colder brightness temperatures than surrounding pixels containing clear skies or lower clouds. The 6.7 μm thresholds for this test are

215K, 220K, and 225K for low confidence, mid-point, and high confidence, respectively. This test is performed on all scenes except Antarctica during polar night.

Detection of clouds over polar regions during winter is difficult. Under clear-sky conditions, strong surface radiative temperature inversions often exist. Thus, IR channels whose weighting function peaks low in the atmosphere will often have a larger *BT* than a window channel. For example, $BT_{8.6} > BT_{11}$ in the presence of a surface inversion. A surface inversion can also be confused with thick cirrus cloud; this can be mitigated by other tests (e.g., the magnitude of BT_{11} or the $BT_{11} - BT_{12}$). Analysis of $BT_{11} - BT_{6.7}$ has shown large negative differences during winter over the Antarctic Plateau and Greenland, which may be indicative of a strong surface inversion and thus clear skies (Ackerman 1996). Under clear-sky conditions, the measured 11 μm radiation originates primarily at the surface, with a small contribution by the near-surface atmosphere. Because the surface is normally warmer than the upper troposphere, BT_{11} is normally warmer than the 6.7 μm brightness temperature; thus the difference, $BT_{11} - BT_{6.7}$, is normally greater than zero.

In polar regions, strong surface radiation inversions can develop as a result of long wave energy loss at the surface due to clear-skies and a dry atmosphere. Figure 6 is a temperature (solid-line) and dew point temperature (dashed-line) profile measured over the South Pole at 0000 UTC on 13 September 1995 and illustrates this surface inversion. On this day the temperature inversion was approximately 20 K over the lowest 100 m of the atmosphere. The surface temperature was more than 25 K colder than the temperature at 600 hPa. Temperatures over Antarctica near the surface can reach 200 K (Stearns et al. 1993), while the middle troposphere is ~235 K. Under such conditions, satellite channels located in strong water vapor absorption bands, such as the 6.7 μm channel, have a warmer equivalent brightness temperature than the 11 μm window channel. A simulation of the HIRS/2 BT_{11} - $BT_{6.7}$ difference using Figure 6 temperature and moisture profile was -14 K. This brightness temperature difference between 11 and 6.7 μm is an asset for detecting cloud-free conditions over elevated surfaces in the polar night (Ackerman

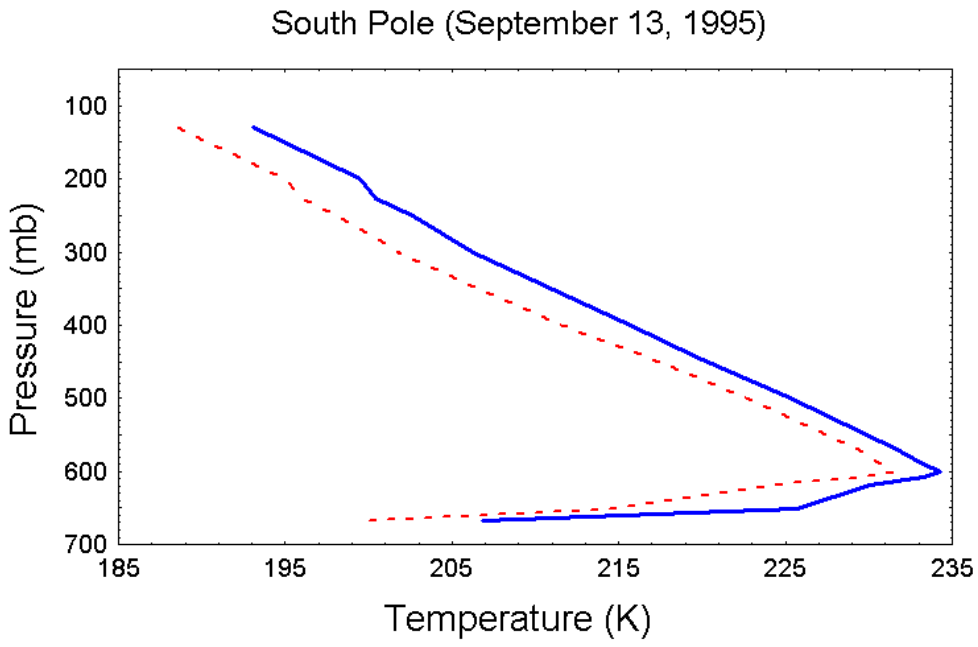

Figure 6. Vertical profile of atmospheric temperature and dew point temperature over the South Pole on 13 September 1995. The deep surface radiation inversion is useful for clear-sky detection.

1996). Clouds inhibit the formation of the inversion and obscure the inversion from satellite detection if the IWP is greater than approximately 20 g m^{-2}. In the cloud mask, under polar night conditions, pixels with differences $< -10°C$ are labeled clear and reported in bit 26.

$BT_{13.9}$ HIGH CLOUD TEST (BIT 14)

CO_2 slicing (Smith and Platt, 1978; Wylie et al., 1994, Menzel et al., 2008) is a useful method for determining heights and effective cloud amounts of ice clouds in the middle and upper troposphere. CO_2 slicing is not wholly incorporated into the cloud mask. A separate product, MOD06, includes results from CO_2 slicing. However, simple threshold tests using CO_2 absorption channels are useful for high cloud detection. Whether or not a particular cloud is observed at these wavelengths (MODIS bands 33-36) depends on the weighting function of the particular channel and the altitude of the cloud.

MODIS band 35 (13.9 μm) provides good sensitivity to the relatively cold regions of the upper troposphere. Only clouds above 500 hPa have strong contributions to the radiance to space observed at 13.9 μm; negligible contributions come from the earth's surface. Thus, a threshold test for cloud versus ambient atmosphere can reveal clouds above 500 hPa.

Figure 7 depicts a histogram of brightness temperature at 14.0 and 13.6 μm derived from the HIRS/2 instrument (channels 5 and 6 respectively) using the CHAPS (Frey, et al., 1996) data set. The narrow peaks at the warm end are associated with clear-sky conditions, or with clouds that reside low in the atmosphere. Based on these observations, clear-sky threshold would be about 240 K. The thresholds for MODIS are somewhat different due to the variation of spectral characteristics between the two instruments. The low confidence, mid-point, and high confidence of clear sky thresholds are independent of scene type and are 222, 224 and 226 K, respectively. This test is not performed poleward of 60 degrees latitude.

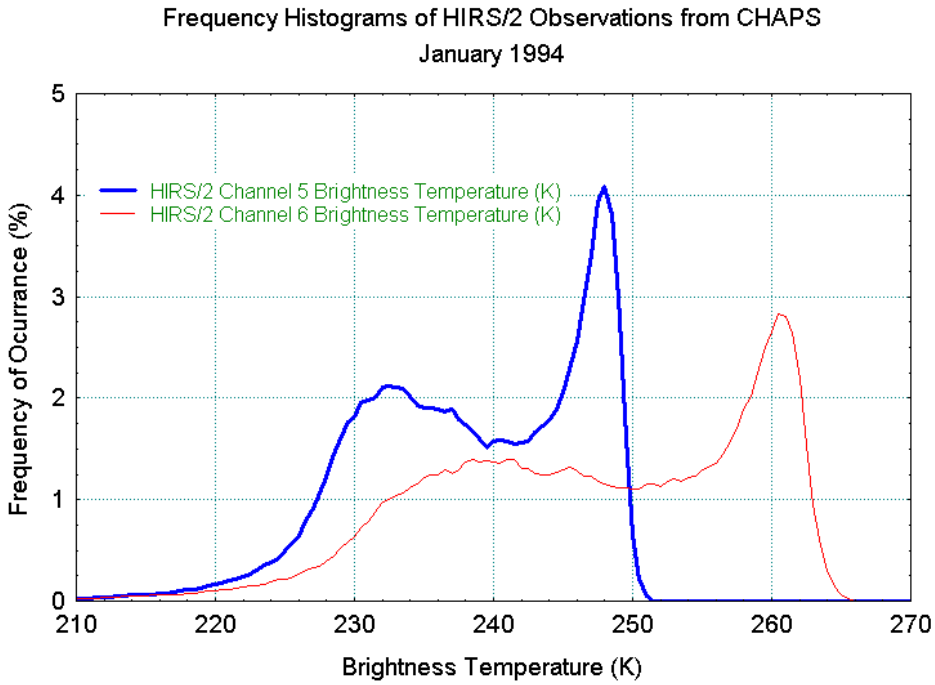

Figure 7. Histogram of BT_{14} and $BT_{13.6}$ HIRS/2 global observations for January 1994, where channel 5 (6) is centered at 14.0 (13.6) µm.

A BTD test similar to BT_{11} - $BT_{6.7}$ is used for detecting polar inversions at night. $BT_{13.3}$ - BT_{11} (MODIS bands 33, 31) is used to identify deep polar inversions likely characterized by clear skies. A pixel is labeled clear if this difference is > 3.0K.

INFRARED THIN CIRRUS TEST (BIT 11)

This bit indicates that IR tests detected a thin cirrus cloud. This test is independent of the 1.38 µm thin cirrus test described below and applies the split window technique (11-12 µm BTD) to detect the presence of thin cirrus. It is the same as the cirrus cloud test described above except that the thresholds are set to detect only thinner cirrus clouds. Thin cirrus is indicated when the observed 11-12 µm BTD is greater than the mid-point threshold but less than the confident cloud threshold (0.5 confidence of clear sky threshold < 11-12 µm BTD < 0.0 confidence

of clear sky threshold).

BT_{11} SPATIAL UNIFORMITY (BIT 25)

The infrared window spatial uniformity test (applied on 3 by 3 pixel segments) is performed for water scenes. Most ocean regions are well suited for spatial uniformity tests; such tests may be applied with less confidence in coastal regions or regions with large temperature gradients (e.g., the Gulf Stream). In addition to the cloud test mentioned above (reported in bit 30), the MODIS cloud mask uses spatial variability as a clear-sky restoral test over oceans and lakes. The tests are used to modify the confidence of a pixel being clear. If the confidence flag of a pixel is ≤ 0.95 but > 0.05, the variability test is implemented. If the difference between the pixel of interest and any of the surrounding pixel brightness temperatures is $\leq 0.5°C$, the scene is considered uniform and the confidence is increased by one output confidence level (e.g., from uncertain to probably clear).

3.1.2 VISIBLE AND NEAR-INFRARED THRESHOLD TESTS

VISIBLE/NIR REFLECTANCE TEST (BIT 20)

This is a single-channel threshold test where discriminating bright clouds from dark surfaces (e.g., stratus over ocean) is its strength. Three different bands are used depending on ecosystem type. Reflectances from 0.65 μm (band 1) are used for vegetated land (background NDVI $\geq$ 0.25) and coastal regions, from 0.413 μm (band 8) for arid regions (background NDVI < 0.25) as discussed in Hutchison and Jackson (2003), while 0.86 μm reflectances are used over water scenes. The thresholds for water surfaces (band 2) are given in Table 7. For land scenes (bands 1 or 8), the thresholds are functions of background NDVI and scattering angle (Hutchison et al., 2005). Default land thresholds are also listed in Table 7, used when no background NDVI is available. Note that these were also the thresholds used for Collection 5 and earlier versions of the cloud mask and were not view-angle dependent. Band 8 is used for the first time in Collection 6. The background NDVIs are taken from Moody et al., 2005, where snow-free NDVIs are

Table 7. Water and default land thresholds used for the VIS/NIR test in the MODIS cloud mask algorithm.

Scene Type	Threshold	High confidence clear	Low confidence clear
$R_{0.65}$			
Land	0.18	0.14	0.22
$R_{0.86}$			
Terra day water	0.030	0.040	0.055
Aqua day water	0.030	0.045	0.065
Desert	0.30	0.26	0.34

calculated at one-minute spatial resolution. We use five-year means (2000-2004) of NDVI calculated for constant 16-day intervals throughout the calendar year.

Band 1 and 8 land thresholds were constructed by sorting clear and cloudy sky reflectances into cumulative histograms, one clear-sky and one cloudy-sky histogram for each 10 degrees of scattering angle and 0.1 interval of background NDVI. The reflectances were from Aqua Collection 5 Level 1b data and clear and cloudy designations were taken from Collection 5 cloud mask (MOD35) output. Collocated CALIOP clear vs. cloudy data could not be used in this case because a wide range of viewing zenith angles are required to fill out the scattering angle classes. Individual pixel observations were used from the months of August 2006 and February 2007. Figure 8 shows example histograms for background NDVI from 0.7-0.8 and scattering angles from 110-120º. The cumulative histograms for clear (blue) and cloudy (red) observations are oriented in opposite directions, with the numbers of cloudy pixels per band 1 reflectance class

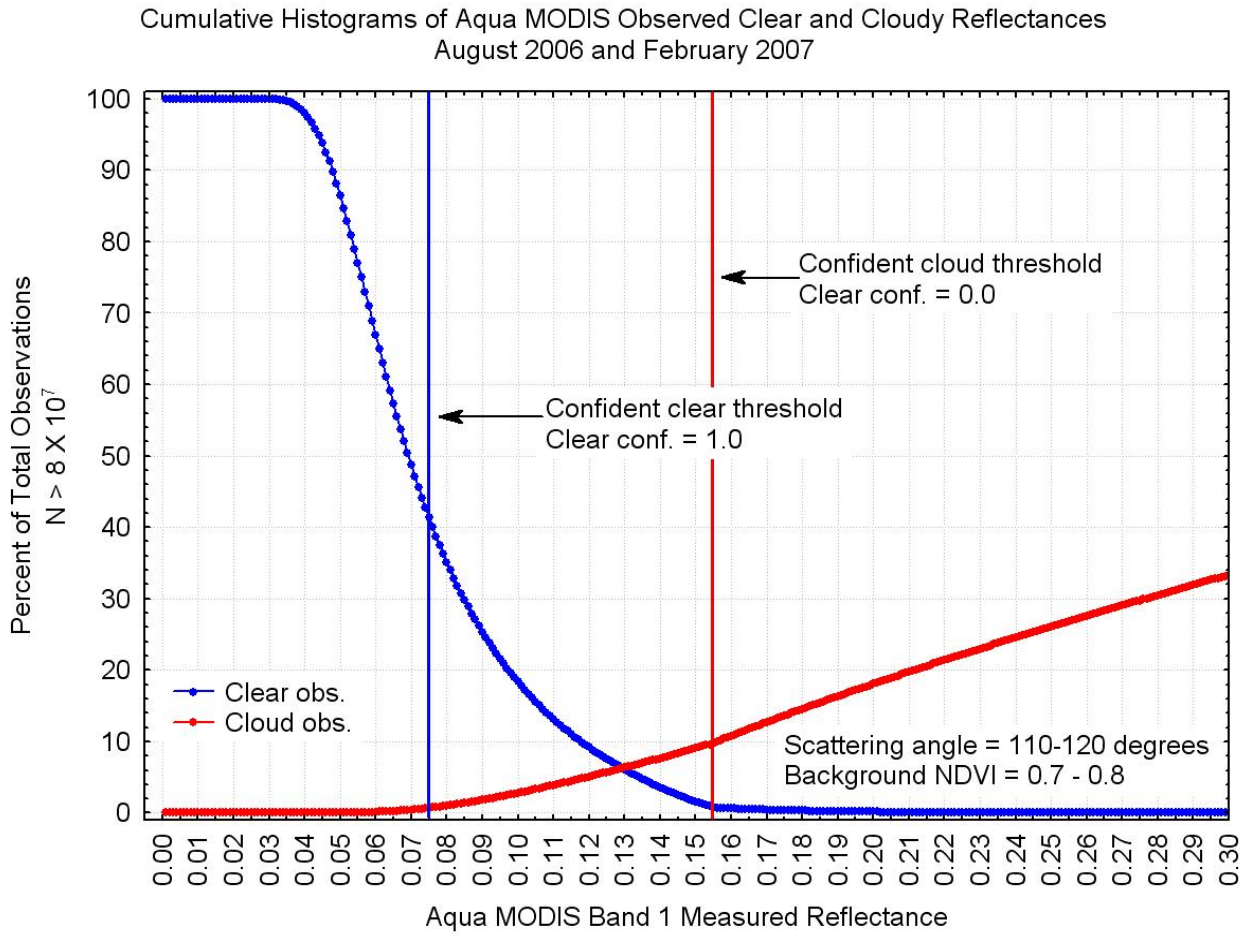

Figure 8. Clear (blue) and cloudy (red) cumulative histograms of 0.65 µm Aqua MODIS reflectances from which a confident clear threshold (vertical blue line) and a confident cloudy threshold (vertical red line) may be defined.

increasing towards higher reflectances and the number of clear observations increasing towards lower reflectances. For each scattering angle and NDVI class, confident clear thresholds were defined as reflectances where the "darkest" one percent of cloudy pixels were found, as shown in the figure. Likewise, confident cloud thresholds were defined where the "brightest" one percent of clear-sky pixels were found. Middle confidences (0.5 confidence of clear sky) were calculated as a simple average between the confident clear and confident cloudy thresholds.

Then, for each background NDVI class (0.1 interval), fourth-order polynomial fits were generated to the three sets of reflectance thresholds (confident clear, mid-point, confident cloud) as a function of scattering angle. With the knowledge of background NDVI and scattering angle for a given pixel, dynamic visible cloud test thresholds are calculated within the MOD35 algorithm from the polynomial fit coefficients.

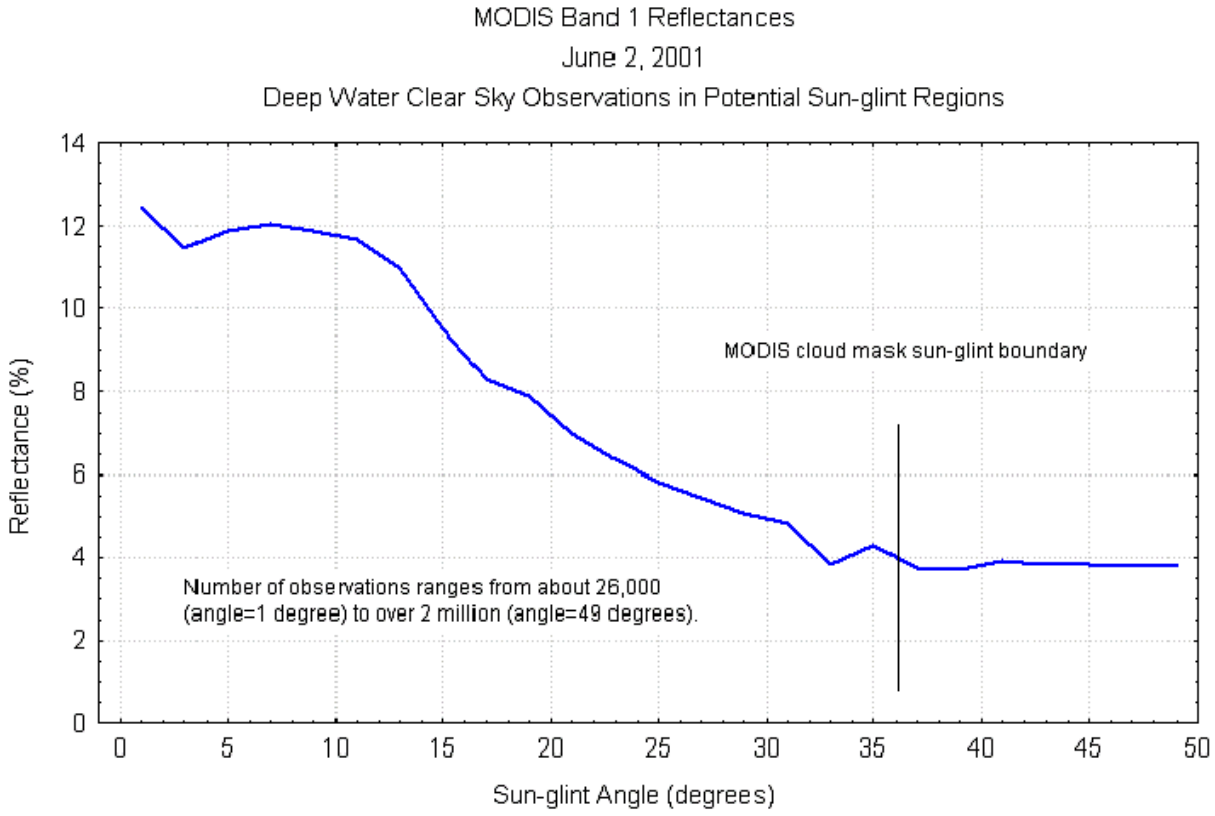

Figure 9. MODIS channel 2 reflectance as a function of reflectance angle, on June 2, 2001 over ocean regions.

The reflectance test is view-angle dependent when applied in sun-glint regions as identified by sun-Earth geometry (see Bit 4 above). Figure 9 demonstrates this angular dependence of the 0.86 μm reflectance test using MODIS observations. The reflectance thresholds in sun-glint regions are therefore a function of θ_r (sun-glint angle on the x-axis) and are divided into three parts. For θ_r from 0-10 degrees, the mid-point threshold is constant at .105, for θ_r from 10 to 20 degrees the threshold varies linearly from .105 to .075, and for θ_r from 20 to 36 degrees it varies linearly from .075 to .055. The low and high confidence limits are set to ± .01 of the mid-point values.

REFLECTANCE RATIO TEST (BIT 21)

The reflectance ratio test uses channel 2 divided by channel 1 ($R_{0.86}/R_{0.65}$). This test makes use of the fact that the spectral reflectance at these two wavelengths is similar over clouds (ratio

is near 1) and different over water and vegetation. Using AVHRR data this ratio has been found to be between 0.9 and 1.1 in cloudy regions. If the ratio falls within this range, cloud is indicated. McClain (1993) suggests that the minimum value may need to be lowered to about 0.8, at least for some cases. For cloud-free ocean the ratio is expected to be less than 0.75 (Saunders and Kriebel 1988). This ratio is generally observed to be greater than 1.0 over vegetation. The MODIS cloud mask thresholds for oceans are 0.85, 0.90, and 0.95 for confident clear, mid-point and confident cloudy, respectively. In sun-glint regions and for glint angles < 10º, the middle confidence value is 0.105. For glint angles between 10º and 20º, the threshold varies linearly from 0.105 to 0.075, for glint angles between 20º and 36º, from 0.075 and 0.045 (0.040 for Terra).

Figure 10 illustrates some of the complexities of arid and semi-arid ecosystems as demonstrated by the reflectance ratio. The observations were taken from AVHRR on NOAA-9 and are over the Arabian Sea, the Arabian Peninsula, and surrounding regions. The figure shows histograms of reflectance ratio values for coastal/water scenes, as well as desert and more densely vegetated areas in the Persian Gulf region from approximately 15-25° N latitude and 50-70° E longitude. Almost all of the observations recorded in the histograms were from clear-sky conditions, as determined by inspection of visible and IR imagery. As suggested by the histograms of $R_{0.86}/R_{0.65}$, clear-sky ocean scenes have a ratio of less than 0.75. One can immediately see that clear-sky desert values of the ratio cover a large range of values, including values one might normally associate with cloudy skies over vegetated surfaces.

Beginning with Collection 6 and the improved visible reflectance test (see above), the reflectance ratio test becomes somewhat redundant over vegetated surfaces. However, additional information is always helpful in the more difficult arid and semi-arid ecosystems. A modified form of the reflectance ratio test (Global Environment Monitoring Index or GEMI) was developed by Pinty et al., 1992 for use in such ecosystems. The test is very effective if thresholds are chosen carefully. The MOD35 GEMI thresholds are functions of background NDVI as listed in Table 8.

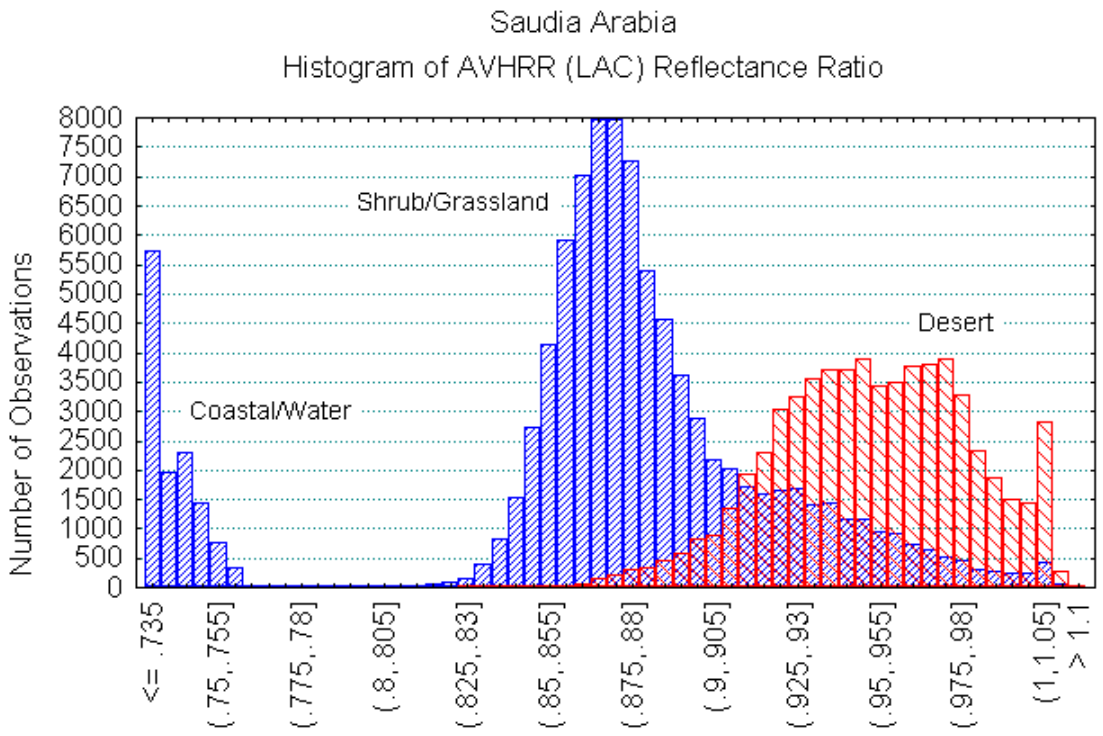

Figure 10. Histogram of the frequency of occurrence of the AVHRR reflectance ratio $R_{0.86}/R_{0.63}$ for a scene over the Arabian peninsula and Arabian Sea.

Table 8. GEMI cloud test thresholds for arid and semi-arid regions.

NDVI	Confident Clear GEMI Threshold	Mid-point GEMI Threshold	Confident Cloud GEMI Threshold
0.0-0.1	0.050	0.0250	0.000
0.1-0.2	0.200	0.150	0.100
0.2-0.3	0.350	0.325	0.300

The test is not performed when background NDVI is > 0.3.

NEAR INFRARED 1.38 μM CIRRUS TEST (BITS 9 AND 16)

The cloud mask uses MODIS band 26 (1.38 μm) reflectance thresholds to detect the presence of transmissive cirrus clouds in the upper troposphere under daytime viewing conditions. The strength of this cloud detection channel lies in the strong water vapor absorption in the 1.38

μm region (Gao et al., 1993). With sufficient atmospheric water vapor present (estimated to be about 1 cm precipitable water) in the beam path, no upwelling reflected radiance from the earth's surface reaches the satellite. This means that much, but not all, of the earth's surface will be obscured in this channel; precipitable water is often less than 1 cm over polar regions, in midlatitude winter, and at high elevations. With relatively little of the atmosphere's moisture located high in the troposphere, high clouds appear bright; reflectance from low and mid level clouds is partially attenuated by water vapor absorption.

Simple thresholds are used to separate thin cirrus (subjectively defined as a cloud that has a small impact on the visible reflectance, enabling atmospheric correction to be applied to retrieve land surface properties such as NDVI) from clear and thicker cirrus (near infrared cloud optical depth $> \sim 0.5$) cloud scenes. These thresholds were set initially using a multiple-scattering model with the assumption of no surface reflectance contribution to the satellite observed radiance, i.e., a dark background. Ben-Dor (1994) analyzed a scene from the AVIRIS to demonstrate that thin cirrus detection using 1.38 μm observations may be more difficult for elevated surfaces, dry atmospheric conditions, and high albedo surfaces. For these reasons, cloud tests using 1.38 μm reflectances are not performed in Antarctica or Greenland, anywhere the surface elevation is above 2000 meters, or when the total precipitable water over land surfaces falls below 0.75 cm.

There are two cloud tests performed in the MOD35 algorithm that use 1.38 μm reflectances: 1) a general cloud test with confident clear, middle, and confident cloud thresholds and 2) a test that uses the confident clear and middle thresholds (see Table 9) to define the range of expected reflectances from thin cirrus. The result of the first is included along with other cloud tests in calculating the final confidence of clear sky for a given pixel and is reported in Bit 16. The second indicates that a thin cirrus cloud is likely to be present and is reported in Bit 9. The various 1.38 μm reflectance thresholds are listed in Table 9.

Table 9. Various 1.38 μm reflectance cloud test thresholds.

Scene Type	Confident Clear	Mid-point	Confident Cloud
Land	0.0300	0.0350	0.0400
Snow/Ice	0.0450	0.0525	0.0600
Ocean	0.0050	0.0125	0.0350

250-METER VISIBLE TESTS (BITS 32-47)

The visible/NIR reflectance test and the reflectance ratio test (see above) are used for clear-sky determination in the 250 m resolution data. The results are a simple yes/no decision and incorporate the results from the 1 km resolution tests to maintain consistency with the 1-km mask.

3.1.3 ADDITIONAL CLEAR SKY RESTORAL TESTS (BITS 22 AND 26)

There are additional clear-sky restoral tests not mentioned elsewhere in the test descriptions. A simple NDVI (Normalized Difference Vegetation Index) test is invoked during daylight hours in areas characterized by a land/water mix and also in regions identified as shallow water. Spectral signatures of clear vs. cloudy skies are often convoluted and difficult to separate when land and water surfaces coexist in the same small region. Also, sediments at the bottom of shallow water bodies or suspended in water near river discharges can lead to ambiguous spectral signatures. The NDVI is calculated from ratios of 0.86 and 0.65 μm reflectances (band 2 - band 1 / band 2 + band 1). If no spectral tests found evidence of high cloud and if this value is < -0.18 or > 0.40, then the pixel in question is labeled clear. Low values imply clear water while high values indicate clear land. When the values are between the two thresholds, the initial cloud mask

result is not changed. The result is reported in bit 22.

Another test that may "restore" the cloud mask value to clear is performed in sun-glint regions. If the initial result for a given pixel is uncertain or cloudy and if no tests found evidence of high cloud, the following conditions are checked. If the following are met the pixel is labeled as probably clear.

1. $BT_{3.75} - BT_{11} > 15\text{K}$ (band 20 – band 31)
2. $R_{0.895} / R_{0.935} > 3.0$ (band 17 / band 18)

   AND

$R_{0.443}$ not saturated (band 9)

   OR

standard deviation of $R_{0.86}$ * mean $R_{0.86} < 0.001$ (band 2)

These tests are an attempt to discriminate bright, low clouds from almost equally bright sun-glint off cloud-free water surfaces. The thresholds are based largely on experience with the MODIS data. Thick water clouds often drive the band 17/18 ratio to low values due to lessened differential water vapor absorption and band 9 is often saturated over bright clouds. The standard deviation multiplied by the mean of band 2 reflectances over the pixel of interest and surrounding eight pixels is a textural measure aimed at detection of very smooth scenes. As pixels brighten and the possibility of clouds increases, variability must decrease in order to meet the clear-sky test criterion. The brightness temperature difference threshold is set to indicate reflective surfaces so that initial cloud mask results are not modified in an area that is fairly dark and already handled well by other cloud tests. The result is reported in bit 26.

The $R_{1.2} / R_{0.55}$ ratio test is used to minimize false cloud and uncertain determinations in daytime land situations. If the confidence flag is less than 0.95 and $R_{1.2} / R_{0.55} > 3.0$ (2.0 for desert scenes), and if $BT_{3.7} - BT_{3.9} < 11.0$ and $BT_{3.7} - BT_{11} < 15$, the scene is considered probably clear and reported in bit 26.

3.1.4 NON-CLOUD OBSTRUCTION FLAG (BIT 8) AND SUSPENDED DUST FLAG (BIT 28)

An atmosphere laden with heavy aerosol may result in a lowered confidence of clear sky or even a confident cloudy determination. Tests may be constructed that indicate an aerosol contaminated FOV and not a cloudy one (Hutchison et al., 2008); however, it must be noted that simple threshold tests are usually not completely adequate for this task except in cases of very thick aerosol. Also, many times aerosols and clouds are present in close proximity and it is more difficult to separate the two (Hutchison, et al., 2010). The MOD35 algorithm employs several series of threshold tests to detect smoke and/or fires, heavily polluted atmospheres (bit 8), and airborne dust (bit 28). Note that these tests are not performed when a strong spectral cloud signal is reported by high cloud tests. Other cloud test results may preclude performance of aerosol tests in specific situations, e.g., no smoke test over water surfaces when a strong thermal signal (observed BT_{11} << SST) is found. No non-cloud obstruction tests are attempted over snow or ice surfaces.

A fire test finds hot spots using a 3.75 μm threshold of 350K and a brightness temperature difference between 3.75 and 11 μm which must be > 10K. Over solar illuminated land surfaces, smoke is indicated when the reflectance in band 7 (2.1 μm) is < .20 and the band 1 (0.65 μm) reflectance is greater than the value of a function based on the 2.1 μm reflectance. Thick smoke is dark at 2.1 μm relative to 0.65 μm. However, this test will give false indications of smoke over some brighter land surfaces and should be used with caution.

Smoke and pollution tests are performed over solar illuminated water surfaces. Smoke is indicated when the standard deviation of $R_{0.86}$ over the pixel of interest and the surrounding eight pixels is < 0.003, $R_{1.24}$ is between 0.022 and 0.050, $R_{0.47} \geq 0.12$, $R_{0.47} / R_{1.24} \geq 5.0$, and $R_{2.1} / R_{1.24} <$ 0.5. In addition, smoke is indicated when the standard deviation of $R_{0.86} < 0.003$, the simple $R_{0.86}$ water threshold test indicated cloud, and $R_{0.47} / R_{1.24} \geq 2.5$. In cases where the above standard deviation criterion is not met, smoke may still be indicated if $R_{0.47} / R_{1.24} \geq 2.5$ and $R_{2.1} / R_{1.24} <$ 0.3.

Several tests are performed to detect the presence of suspended dust in the atmosphere. The general procedure is to first perform spectral checks to screen out potential clouds, then compute other spectral measures to indicate dust. For daytime land surfaces, the following criteria must be met:

1. BT_{11}-$BT_{12} \leq$ -0.5, $BT_{3.7}$-$BT_{11} \geq$20.0, and $R_{1.38} < 0.035$
2. $\{(R_{0.65}-R_{0.47}) / (R_{0.65}+R_{0.47})\}^2 / R_{0.65}^2 > 0.005$ and $(\text{NDVI}^2 / R_{0.65}^2) < 0.08$

   OR

   $BT_{3.7}$-$BT_{11} \geq 25.0$

Independent of 1 and 2 above is a test for very thick dust:

BT_{11}-$BT_{12} <$ -0.5, $BT_{3.7}$-$BT_{11} \geq 25.0$, $R_{1.38} < 0.055$, and $(\text{NDVI}^2 / R_{0.65}^2) < 0.20$

For nighttime land regions, the following criteria must be met to indicate dust:

1. $BT_{11} > 273.0$, standard deviation $BT_{11} < 2.0$, BT_{11}-$BT_{12} <$ -0.5, and $BT_{8.6}$-$BT_{11} >$ -7.0
2. $BT_{3.7}$-$BT_{11} \leq$ -2.5

   OR

   $BT_{3.7}$-$BT_{11} > 6.0$

For water surfaces, a surface temperature (SST) test and a variability test are first performed to screen out potential low-level clouds. The SST test thresholds are a function of water vapor loading in the atmosphere as indicated by the value of BT_{11}-BT_{12}. During the day, the standard deviation of $R_{0.86}$ must be < 0.005, at night the standard deviation of BT_{11} must be < 0.25. The remaining criteria must be met for daytime cases:

1. $R_{0.47} \leq 0.30$, $R_{0.47} / R_{0.65} < 2.0$, $BT_{3.7}$-$BT_{11} > 4.0$, and $BT_{3.7}$-$BT_{11} \leq 20.0$
2. BT_{11}-$BT_{12} <$ 0.10, NDVI $\leq$ 0.0, and NDVI $\geq$ -0.3

   OR

   $R_{0.47} / R_{0.65} < 1.2$

   OR

   $BT_{3.7}$-$BT_{11} >$ 10.0 and BT_{11}-$BT_{12} <$ -0.1

   OR

$BT_{3.7}$-BT_{11} > 20.0, BT_{11}-BT_{12} < 0.0, NDVI ≥ -0.3, and NDVI ≤ 0.05

In addition, even if the above standard deviation criterion is not met, the following indicates dust:

$R_{0.65}$ / $R_{0.55}$ ≥ 1.15 and $R_{0.55}$ / $R_{0.47}$ ≥ 1.15

In the case of nighttime water, the following is necessary to indicate dust:

1. BT_{11}-BT_{12} < -1.0 and $BT_{3.7}$-BT_{11} < 0.0

   OR

   BT_{11}-BT_{12} < 0.0, $BT_{3.7}$-BT_{11} < 5.0, and $BT_{3.7}$-BT_{11} > 1.0

3.2 Confidence Flags

The spectral tests employed to discriminate between clear and cloudy pixels that are discussed in Section 3.1 rely on thresholds. Thresholds are never global, there are always exceptions. For example, the ratio of reflectances at 0.86 to 0.65 μm identifies oceanic cloud for values > 0.95. It seems unrealistic to label a pixel with $R_{0.86}/R_{0.656}$ = 0.96 as cloudy, and a neighboring pixel with the ratio of 0.95 as non-cloudy. Rather, as one approaches threshold limits, the certainty or confidence in the labeling becomes more and more uncertain. The uncertainty is a function of instrument noise in that channel and the magnitude of the correction that was necessary due to surface spectral radiative properties, as well as atmospheric moisture and/or aerosol reflection contributions. An individual confidence value is assigned to each single pixel test and is a function of how close the observation is to the threshold. After all tests are performed, individual confidences are combined to produce the final cloud mask confidence of clear sky, recorded in bits 1 and 2 as one of four categories: *clear*, *probably clear*, *probably cloudy* and *cloudy*. These categories correspond to confidences of clear sky > 0.99, > 0.95, > 0.66, and ≤ 0.66, respectively.

Many cloud detection schemes have a single threshold for a given test. For example, one might determine that if the visible reflectance for an ocean pixel is greater than 6%, then it would be labeled cloudy. The MODIS cloud masking algorithm is designed to provide information on

how much confidence a user can place on the result. Each test is assigned a value between 0 and 1 representing increasing confidence in clear-sky conditions. Figure 11 is a graphical representation of how confidence levels are assigned when performing clear vs. cloudy threshold tests. The abscissa represents the observation and the ordinate the clear-sky confidence level. In this test, an observation greater than a value of γ is determined to be a high confidence clear scene and assigned a value of 1. An observation with a value less than α is cloudy and assigned a confidence level of 0. These high confidence clear and cloud thresholds, γ and α respectively, are

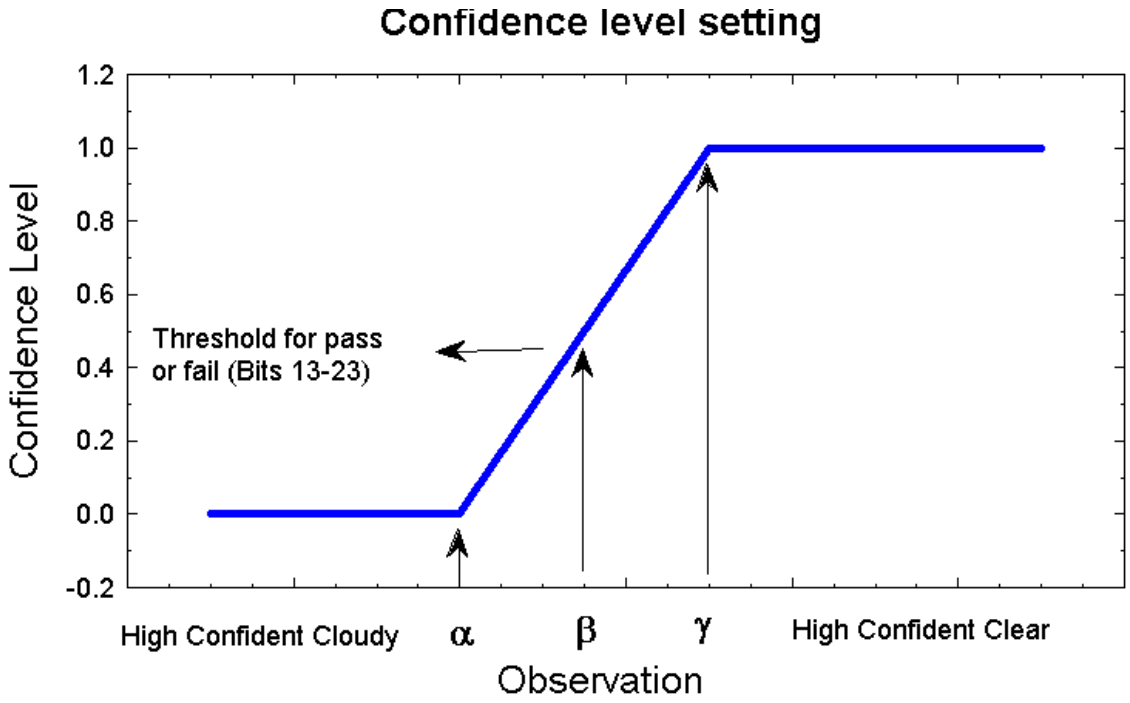

Figure 11. A graphical depiction of three thresholds used in cloud screening.

determined from observations and/or theoretical simulations. Values between α and γ are assigned a value between 0 and 1 (or 1 and 0). In the figure, assignment is based on a linear function though other types may be used (e.g., Sigmoid curves).

Bits 13-21, 23, 24, 27, and 29-31 represent results from individual cloud tests. The β value

in Figure 11 represents the "pass/fail" threshold used when reporting test results in those bits. Thus, each test has three thresholds: pass/fail (also called middle or mid-point), high confidence pass and high confidence fail. Some tests, such as the $BT_{3.9}$-BT_{11} BTD, identify cloud if the observations fall within a given range. For these tests, there are six thresholds, three for each end of the range.

Each of the tests performed returns a confidence value ranging from 1 (high confidence that the pixel is clear) to 0 (high confidence that the pixel is cloudy). These must be combined to determine a final decision on the state of cloudiness. We denote the confidence level of an individual test as F_i and the final result as Q. We have experimented with a variety of methods for combining the confidences of individual tests. The differences due to the various methods are seen mostly on the boundaries of cloud systems.

The final cloud mask confidence could be derived as a product of all the individual tests:

$$Q = \prod_{i=1}^{N} F_i \tag{22}$$

Using this product assures that any test with a high confident cloudy result (confidence of 0) will set the final cloud mask as cloudy. This is the proper formulation if all the tests are conditionally independent; however, this is not the case. Different spectral tests are sensitive to the same type of cloud conditions as discussed below. A disadvantage of this product approach is that one cannot improve on the confidence level by increasing the number of tests (N) since $F_i \leq 1$. Thus, if 5 tests have a confidence of 0.95, the final result is $0.95^5 \approx 0.63$.

The final result could also be set to the minimum confidence level of all applied tests:

$$Q = \min[F_i]. \tag{23}$$

This approach would be a clear-sky conservative approach. It makes it insensitive to any test other than the test that produces the minimum. That is, no matter what the other tests are indicating, a single low confidence test will set the output flag to obstructed or cloudy. On the other hand, a cloud conservative approach would be to select the maximum confidence level.

$$Q = \max[F_i]. \tag{24}$$

This can be improved upon by

$$Q = 1 - \prod_{i=1}^{N}\left[1 - F_i\right], \tag{25}$$

another cloud conservative case. A test with a high confident clear result sets the bit to clear.

In most cloud masking schemes, not all tests are independent of one another. For example, consider daytime over oceans in regions without sun glint. If stratocumulus clouds are present, the visible reflectance test, the reflectance ratio test and the $BT_{11} - BT_{3.7}$ will likely detect them. These same tests will likely miss the presence of thin uniform cirrus clouds, which would probably be detected by the BT_{11}-BT_{12} test. Very thin cirrus clouds would best be detected by the 1.38 and 13.9 μm tests, two tests that have difficulty detecting low-level clouds.

Because of this overlap in the types of clouds different tests detect, each test is considered in one of four groups. The five groups are:

Group I (Simple IR threshold test)

BT_{11}

$BT_{13.9}$

$BT_{6.7}$

Surface Temperature

Group II (Brightness temperature difference)

$BT_{8.6}$ - BT_{11}

BT_{11} - BT_{12}

$BT_{7.3}$ - BT_{11}

BT_{11} - $BT_{3.9}$

$BT_{8.6} - BT_{7.3}$

Group III (Solar reflectance tests)

$R_{0.65}$ or $R_{0.86}$

$R_{0.86}/R_{0.65}$

Group IV (NIR thin cirrus)

$R_{1.38}$

Group V (IR thin cirrus)

$BT_{3.9}$ - BT_{12}

A minimum confidence is determined for each group,

$$G_{i=1,5} = \min[F_i]. \tag{26}$$

The final cloud mask is then determined from the product of the results from each group;

$$Q = \sqrt[N]{\prod_{i=1}^{N} G_i} \ . \tag{27}$$

This approach is still clear-sky conservative. If any test is highly confident that the scene is cloudy ($F_i = 0$), the final cloud mask is $Q = 00$.

4.0 Practical Application of Cloud Detection Algorithms

4.1 MODIS cloud mask examples

This section shows three examples of cloud mask results that illustrate some of the challenges of global cloud vs. clear-sky discrimination and some insights into the algorithm methodology. Final results of MOD35 are shown in the color panels. Green represents high confidence clear, blue is probably clear, red is probably cloudy, and white is confident cloudy. In the black and white pictures, white is cloud, gray is clear, and black means test not performed. MODIS radiance data is shown in gray shades where white is cold and dark is warm in the 11 μm images.

Figure 12 shows an example of Collection 6 cloud mask output for a scene near Lake Chad recorded by Aqua on March 6, 2006 at 12:45 UTC. Lake Chad may be seen in the visible image (band 1) in Panel A as the dark region at middle right. The 11 μm (band 31) image is shown in Panel B. Panel C shows the results of the visible/NIR test where white indicates a confidence of clear sky < 0.5 (β or mid-point in Figure 11). This data is from the Sahel region of Africa where surface reflectances increase rapidly from south to north. Note that the test performs well except

for the region at upper right. Without clear-sky restoral tests, this region would be labeled cloudy in the final mask result, shown in Panel D. The non-binary nature of the cloud mask is seen near the edges of cirrus clouds where the output category changes from confident cloud to probably cloudy (white to red). Panel F shows the result of the 1.38 μm test that is sensitive to thin cirrus. At the top of Panel B, one may see several regions of lowered BT_{11} that are areas of airborne dust. Panel E shows the output of the MOD35 dust test where white denotes a positive indication. As noted in Section 3.1.4, it is difficult to discriminate between aerosols, clouds, and surface with simple thresholding algorithms. However, the cloud mask shows many probably clear pixels in the dusty areas (as opposed to probably or confident cloudy) and the dust detection algorithm finds most of the thicker dust, indicated by the cooler BT_{11} values. Note the higher cirrus cloud overlaying the dust in the top left of the scene. It is labeled as either confident cloudy or probably cloudy (white or red, respectively). This cloud is invisible in the band 1 image.

MODIS band 26 (1.38 μm channel) and the thermal bands (bands 20-36) are subject to varying amounts of cross-detector striping and cross-talk. A correction algorithm has been developed at the University of Wisconsin (after Weinreb et al., 1989) and is implemented at the beginning of cloud mask processing. A dramatic example of band 26 correction is shown in Figure 13 (different scene than in Figure 12). Even with the destriping correction applied, one notices some minor striping in the cloud mask result in Panel D of Figure 12, seen as alternating regions of confident clear and probably clear. This demonstrates the sensitivity of the algorithm to small fluctuations in radiometric quality from detector to detector.

Figure 14 is a complicated scene from 18:10 UTC December 10, 2000, recorded by Terra MODIS. Surface skin temperatures are very cold, about –28C in North Dakota and southern Manitoba and Saskatchewan. Panels A and B are visible and NIR images of MODIS bands 1 (0.65 μm) and 6 (1.64 μm). Note the feature extending southeastward from the top left of the image in Panel C (1.38 μm) toward the center and terminating in southern North Dakota. This feature is not obvious in bands 1 and 6 (see Panels A, and B), appearing to be a very thin ice

cloud although further analysis confirmed it to be a tropospheric water vapor feature. Such features prohibit the use of the 1.38 μm test in very dry regions where total precipitable water is < 0.75 cm (see Near Infrared 1.38 μm Cirrus Test in Section 3.1.2). In Panel E, gray indicates snow or ice cover was determined to be on the surface. The effects on the final cloud mask may be seen in Panel D. Areas not determined to be snow-covered are sometimes incorrectly labeled as cloudy. Variations in vegetation, topography, and the age, depth, and microphysical properties of snow lead to complex spatial fluctuations in 1.6 μm reflectances that cannot be captured in a simple thresholding algorithm (see Snow/Ice Processing Flag in Section 2.3.1). This is not a solved problem for cloud detection methods and will be a matter for continuing research.

In North Dakota, a long, narrow region near the center of this scene is labeled probably cloudy (red color in Panel D) but the MODIS imagery (Panels A-C) indicates clear skies. The BT_{11}-BT_{12} high cloud test is finding somewhat lowered clear sky confidences in this case though confidences are rarely below 0.5 (white color in Panel F). This illustrates the clear-sky conservative nature of the cloud mask, where one test may change the category of the final result but also shows how other tests that did not indicate cloud keep the output in one of the "uncertain" categories (i.e., not confident clear or confident cloudy). This test does identify the cirrus clouds found just north of the U.S.-Canada border in Saskatchewan.

By definition, a clear-sky conservative cloud detection method (as in MOD35) allows more false clouds than false clear; however, the following case shows that some clouds identified by the human eye still cannot be successfully labeled as such by MOD35. Figure 15 shows a scene from eastern North America and adjacent ocean. Indeed, by looking only at Panel A (MODIS band 1, 0.65 μm) and C (MOD35 final result), one would logically conclude that clouds were over-determined. But note the large area of very thin cirrus clouds near the center of Panel D, a heavily contrasted image of MODIS band 26 (1.38 μm) reflectance. Very little of this cloud has computed clear sky confidences < 0.5 by the 1.38 μm reflectance test (reported in bit 16 and colored white in Panel D), but some lowered final confidences are seen in the final product. Panel F shows the result of the 1.38 μm thin cirrus test, reported in bit 9 (see Near Infrared 1.38 μm Cir-

rus Test of Section 3.1.2). This test finds many of the clouds in question, but still not all. This example illustrates the challenges of "balancing" a cloud detection algorithm in order to find as many of the obvious and most radiatively important clouds while minimizing the numbers of false clear determinations. If thresholds were set to detect this optically thin cloud, many more clear pixels would be labeled cloudy. The thin cirrus test result does not contribute to the final output clear-sky confidence (bits 1 and 2).

Panel E shows the result of the visible/NIR cloud test. Comparing this to Panel A, one can see that the NDVI-dependent test thresholds are appropriate for the land areas in this scene. This scene also encompasses some sun-glint, seen at the very bottom of Panel A and manifested as a region of "probably clear" results (colored blue in Panel C). Many pixels in the sun-glint area were initially determined to be cloudy by the visible/NIR reflectance test but were "restored" by a combination of the BT_{11} ocean variability and sun-glint clear-sky restoral tests (see BT_{11} Spatial Uniformity of Section 3.1.1 and Section 3.1.3, respectively). The use of cloud tests (exploiting cloud vs. clear-sky spectral signatures for the most common Earth scenes) and clear-sky tests (ability to override cloud tests in less common and/or difficult scenes) is another attempt to realistically balance cloud mask results between clear and cloudy.

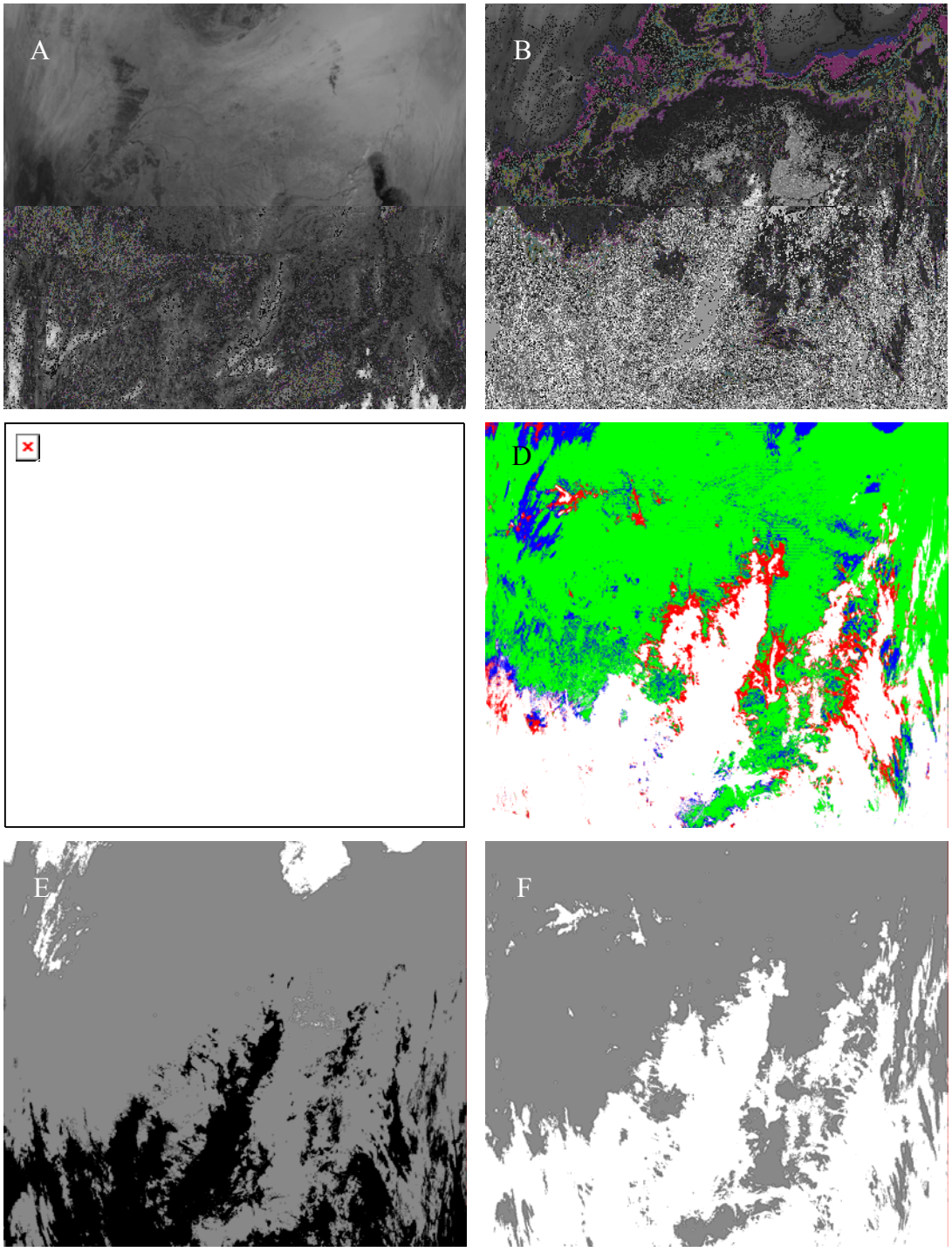

Figure 12. A scene from the Sahel region taken from Aqua on March 6, 2006 at 12:45 UTC. Panels A-E show MODIS band 1, MODIS band 31, visible/NIR cloud test, cloud mask final result, dust test, and 1.38 μm cirrus test, respectively. Cloud mask output is from Collection 6. See text for color definitions.

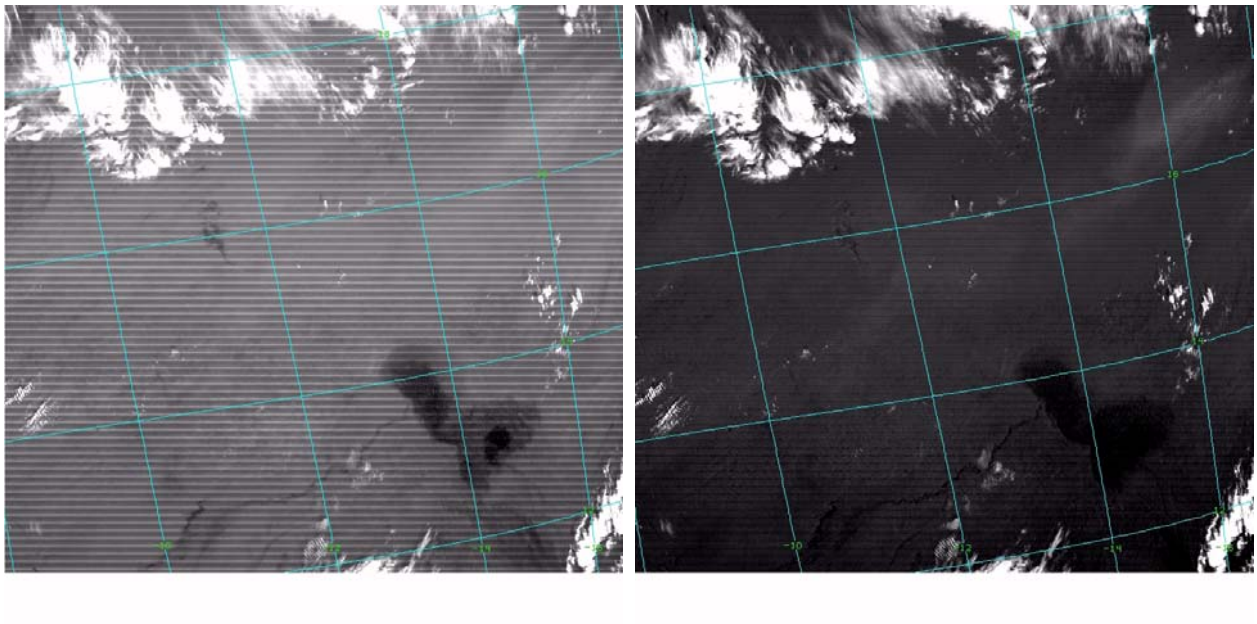

Figure 13. Improvement when Band 26 is corrected for destriping and cross-talk influences. This is a scene located in north central Africa from 10:05 UTC December 10, 2000. Lake Chad is seen in the uncorrected image (left) but surface features are almost invisible after the correction (right).

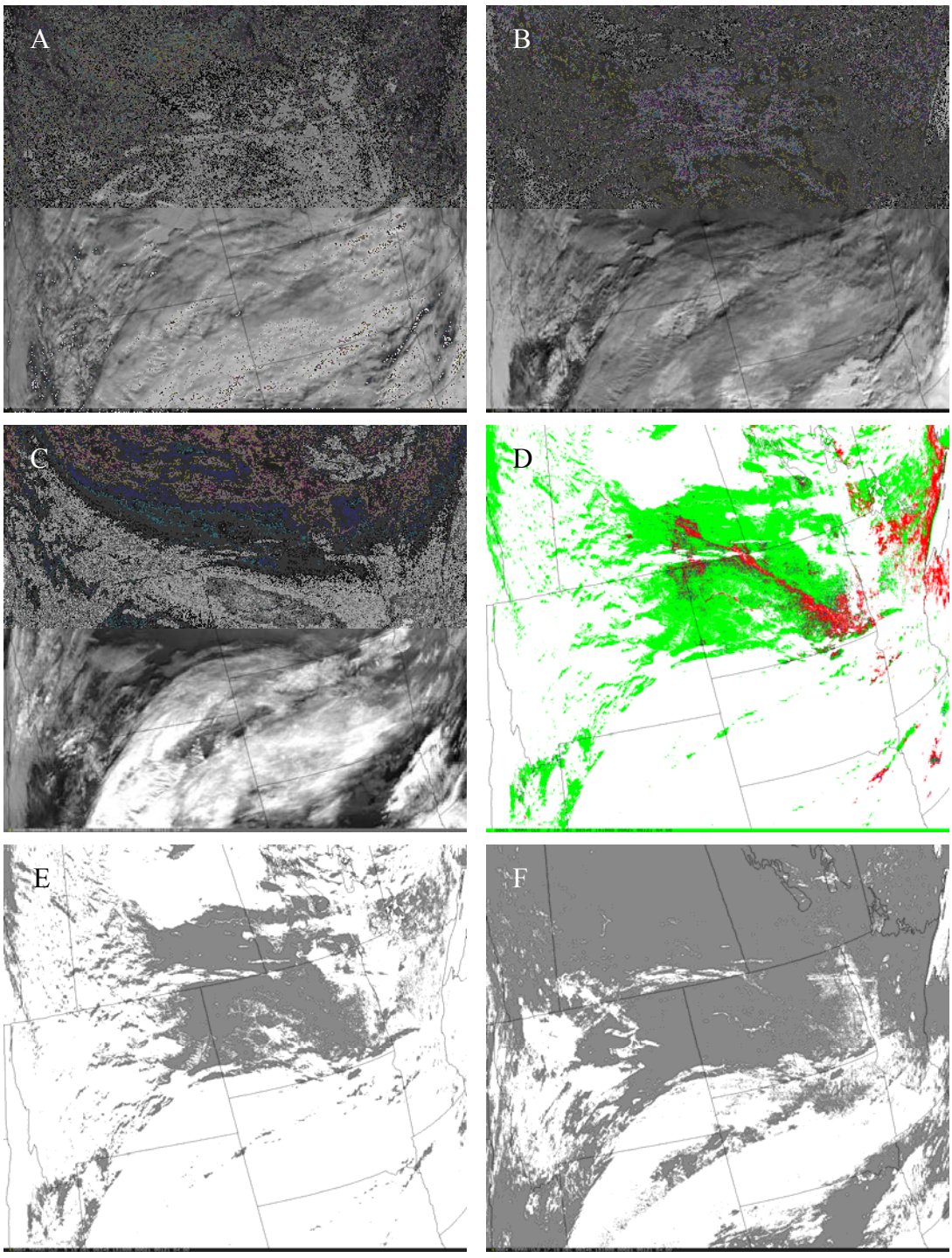

Figure 14. A scene from North Ameria taken from Terra on Dec. 10, 2000 at 18:10 UTC. Panels A-E show MODIS band 1, MODIS band 6, MODIS band 26, cloud mask final result, surface snow/ice test, and BT_{11}-BT_{12} µm high cloud test, respectively. Cloud mask output is from Collection 6. See text for color definitions.

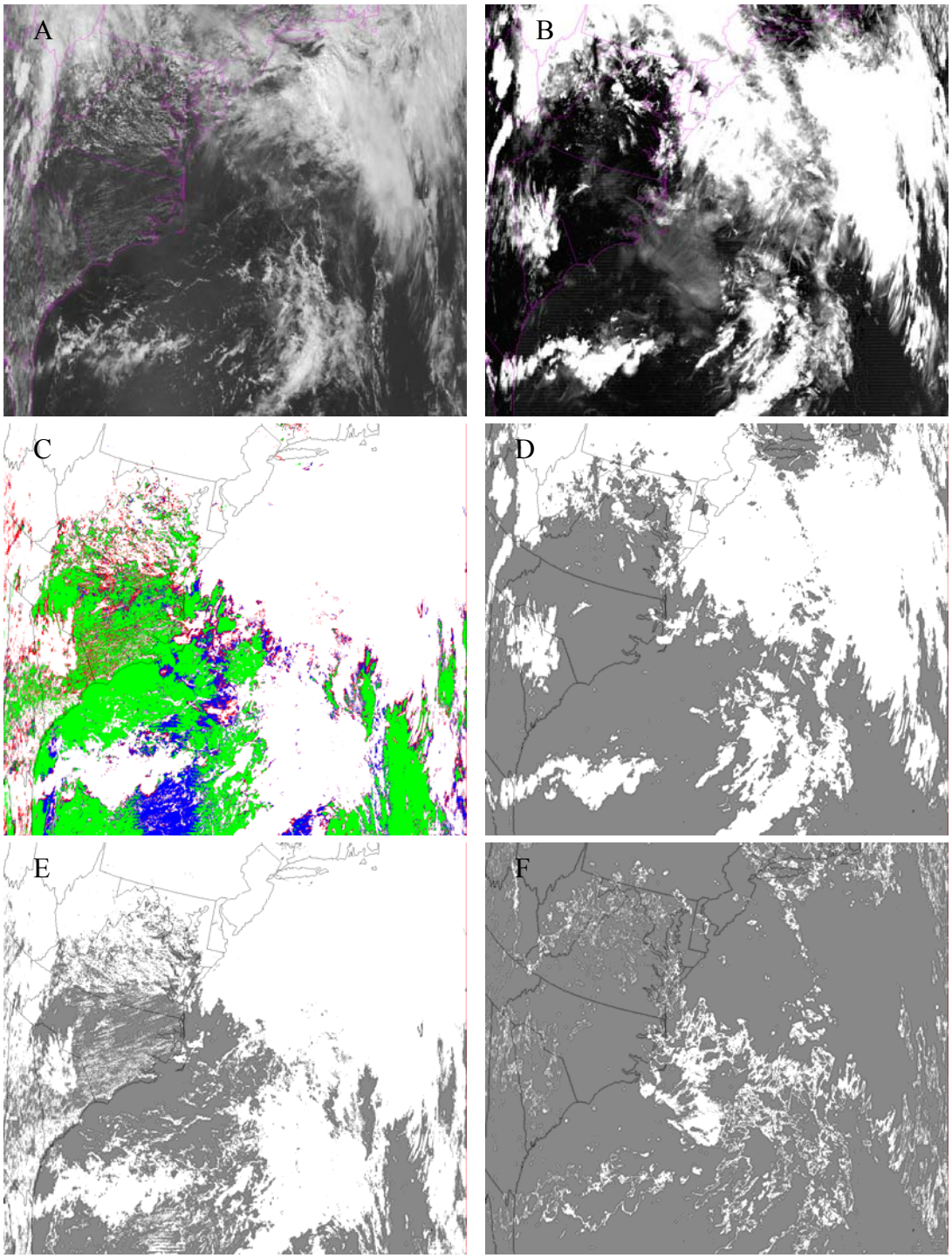

Figure 15. A scene from eastern North Ameria and adjacent ocean taken from Aqua on Aug. 28, 2006 at 18:05 UTC. Panels A-E show MODIS band 1, MODIS band 26, cloud mask final result, 1.38 µm high cloud test, vis/NIR reflectance test, and the 1.38 µm thin cirrus test, respectively. Cloud mask output is from Collection 6. See text for color definitions.

4.2 Interpreting the cloud mask

This section provides examples of how to interpret output from the cloud mask algorithm. They are suggested approaches and not strict rules, and recognize that each MODIS science team member will know how to best use the cloud mask for their applications.

4.2.1 CLEAR SCENES ONLY

Certain applications have little tolerance for cloud contamination. This is an example of how these applications (e.g., bi-directional reflectance models) might interpret the cloud mask output.

1. Read bit 0 to determine if a cloud mask was determined; if this bit is 0 no further processing of the pixel is required.
2. If necessary, read bits 3 through 7 to determine scene domain.
3. Read bits 1 and 2; if both bits are *not* equal to 1, then some tests suggest the presence of cloud, and the pixel is skipped.
4. Read bit 9 to determine if a thin cirrus cloud is present (bit value of 0). An optically thin cirrus cloud may be flagged but not be classified as a cloudy pixel.
5. Daytime algorithms may (depending on application) read bits 32 through 47 to assess potential subpixel contamination or scene variability.

4.2.2 CLEAR SCENES WITH THIN CLOUD CORRECTION ALGORITHMS

Some algorithms may be insensitive to the presence of thin cloud or may apply appropriate correction algorithms. Two examples are given, one that might be appropriate for Normalized Difference Vegetation Index (NDVI) and the second for sea surface temperature (SST) retrievals.

Interpretation procedure that might be useful for NDVI retrievals:

1. Read bit 0 to determine if a cloud mask was determined; if this bit is 0, no further processing of the pixel is required.

2. Read bits 3 through 7 to determine if scene domain is appropriate (e.g., land and day-time)
3. Read the confidence flag—bits 1 and 2. If high confident cloudy (value of 00), do not process pixel. A value of 01 for bits 1 and 2 (probably cloudy) often occurs around cloud edges and retrieving NDVI may not be appropriate with this confidence level. If both bits are equal to 1, then most tests are suggesting clear scenes; proceed with steps 4-7. If confidence bits are 10 (probably clear), then detailed checking of bits 13 through 31 (1-km flags) and bits 32-47 (250-m cloud flags) may be required to determine if NDVI algorithm processing should continue.
4. Read bit 9 to determine if a thin cirrus cloud is present (bit value of 0). An optically thin cirrus cloud may be flagged but not be classified as a cloudy scene. Some of the MODIS solar channels are not as sensitive to thin cirrus as the 1.38 μm band (see Figure 1 for an example). If thin cirrus is detected, apply appropriate correction algorithms.
5. Check that reflectance tests (bits 20 and 21) did not detect cloud. Note that a value of 0 indicates that either a cloud is present or the test was not run. This test is not run if over snow or solar zenith angles greater than 85°.
6. Read bits 32 through 47 to assess cloud contamination. This would not be recommended if snow were indicated.

Interpretation procedure that might be useful for SST retrievals.

1. Read bit 0 to determine if a cloud mask was determined; if this bit is 0, no further processing of the pixel is required.
2. Read bits 3 through 7 to determine if the scene is water or if sun glint is present.
3. Read the clear confidence flag—bits 1 and 2. If high confident cloudy (value of 00), do not process pixel. A value of 01 for bits 1 and 2 (possibly cloudy) often occurs around cloud edges and retrieving SST may not be appropriate with this confidence level. If both bits are equal to 1, then most tests are suggesting clear scenes; proceed

with steps 4-9. If the confidence is 10 (probably clear), then detailed checking of bits 13 through 31 (1-km flags) may be required to determine if the SST algorithm should continue. For example, if confidence bits are 10 and pixel is in a sun glint region, determine how many IR tests are detecting cloud. If all IR tests are passing (indicate clear), then continue with steps 4-8. If the IR tests are indicating cloud, then pixel contamination is likely. In this case the SST should either be retrieved with caution, or appropriate corrections to the IR channels should be made.

4. Read bit 9 to determine if a thin cirrus cloud is present (bit value of 0). An optically thin cirrus cloud may be flagged but not be classified as a cloudy scene. If thin cirrus is detected, apply appropriate IR correction algorithms. Corrections require other cloud products, such as cloud emissivity and cloud effective temperature (MOD06).
5. Check that IR tests did not detect cloud. The greater the number of IR tests that did not detect cloud, the more confidence one has in the SST product. Note that a value of 0 indicates that either a cloud is present or the test was not run.
6. Read bits 32 through 47 to assess subpixel cloud contamination. This would not be recommended in sun glint regions.

4.2.3 CLOUDY SCENES

Use of the cloud mask for cloud scene processing may require a more in-depth analysis than clear-sky applications, as the mask is clear-sky conservative and minimizes false clear determinations. Here we consider a few approaches to interpret the cloud mask for cloud property retrievals during the day, which are a function of processing path.

Daytime ocean scene, no sun glint:

1. Read bit 0 to determine if a cloud mask was determined; if this bit is 0, no further processing of the pixel is required.
2. Read bit 3, if this bit is 0 no further processing of the pixel is required (night).
3. Read bits 6 and 7, if 00 then water scene so proceed.

4. Read bit 4, if 0 then sun-glint region, may want to place less confidence on product retrieval.
5. Read the confidence flag—bits 1 and 2.
    - If high confident clear (value of 11), Read bit 9 to determine if a thin cirrus cloud is present (bit value of 0). An optically thin cirrus cloud may be flagged but not be classified as a cloudy scene. If thin cirrus is detected, apply appropriate algorithms or place less confidence on product retrieval. If bit 9 is 1, it is clear sky and no further processing is required.
    - If both bits are equal to 00, then the scene is cloudy. Check bit 8 and 28 for possible heavy aerosol loading. If either is 0 then pixel may be aerosol-contaminated; no further processing or place less confidence on product retrieval. Check individual test to determine ice or water phase. For example, if bit 21 is 0 and bit 13 is 1, probably water cloud scene. If bits 16 and 18 are 0, probably an ice cloud.
    - If confidence is 10 (probably clear) or 01 (probably cloudy), then detailed checking of bits 13 through 31 may be required to determine if algorithm should be executed. For example, if confidence bits are 01 and pixel is in a sun glint region, additional testing is advised.
6. Check how many tests detected cloud. The greater the number of tests that detected cloud, the more confidence one has in the cloud property product. Note that a value of 0 indicates that either a cloud is present or the test was not run.
7. Read bits 32 through 47 to assess subpixel cloud contamination. This would not be recommended for region with sun glint.

Daytime dark vegetated land regions (for example, forests):

1. Read bit 0 to determine if a cloud mask was determined; if this bit is 0, no further processing of the pixel is required.
2. Read bit 3, if this bit is 0 no further processing of the pixel is required (night).

3. Read bits 6 and 7, if 11 then land scene so check ecosystem for correct type.
4. Read the confidence flag—bits 1 and 2.
    - If high confident clear (value of 11), Read bit 9 to determine if a thin cirrus cloud is present (bit value of 0). An optically thin cirrus cloud may be flagged but not be classified as a cloudy scene. If thin cirrus is detected, apply appropriate algorithms or place less confidence on product retrieval. If bit 9 is 1, it is clear sky, no further processing is required.
    - If both bits are equal to 00, then the scene is cloudy. Check bit 8 and 28 for possible heavy aerosol loading. If either bit is 0 then pixel may be aerosol-contaminated, no further processing or place less confidence on product retrieval. Check individual test to determine ice or water phase. For example, if bit 21 is 0 and bits 14, 15, 16, and 18 are 1, probably water cloud scene. If bits 16 and 18 are 0, probably an ice cloud.
    - If confidence is 10 (probably clear) or 01 (probably cloudy), then detailed checking of bits 13 through 31 may be required to determine if algorithm should be executed. For example, check the number of solar tests passed, if bits 16, 20, and 21 are 1 then IR and not solar tests are indicating cloud, probably do not want to process retrieval that depends on solar techniques or place less confidence on product retrieval.
5. Check how many tests detected cloud. The greater the number of tests that detected cloud, the more confidence one has in the cloud property product.

Detection of clouds over snow and ice is a difficult problem. One procedure for interpreting the cloud mask output for daytime snow/ice retrieval algorithms follows.

1. Read bit 0 to determine if a cloud mask was determined; if this bit is 0, no further processing of the pixel is required.
2. Read bits 3 through 7 to determine if scene domain is appropriate (e.g., daytime and non-desert).

3. Read bits 5 and/or 10 to determine if snow processing path (bit 5) or ancillary data indicates snow (bit10).
4. Read bits 1 and 2 - the final confidence flag.
    - If not confident clear (value of 11), do additional testing. Check bit 19, if 0 (cloud indicated) probably low level water cloud. Check bits 16 and 18, if either is 0, probably ice cloud.
    - If high confidant clear (value of 11), check for the possible presence of thin cirrus (bit 9 and bit 11).

4.2.4 SCENES WITH AEROSOLS

An interpretation procedure for application with aerosol retrieval algorithms is:

1. Read bit 0 to determine if a cloud mask was determined; if this bit is 0, no further processing of the pixel is required.
2. Read bits 3 through 7 to determine scene domain is appropriate for aerosol retrieval (e.g., daytime land, daytime water)
3. Read bit 4 for sun glint contamination, proceed as appropriate.
4. Read bit 5 for snow/ice indication.
5. Read bits 1 and 2 - the final confidence flag.
    - If high confident clear (value of 11), search for aerosol. If bit 9 is 0, possible contamination by thin cirrus or high aerosol.
    - If bits 1 and 2 are 00, 01, or 10, check bits 8 and 28 for heavy aerosol condition. If either are 0, run aerosol retrieval algorithm.
    - If bits 1 and 2 are 00, check all high cloud flags. If any of bits 14, 15, 16, or 18 are 0, cloudy and not aerosol.

4.3 Quality Control

An entire document has been written by the atmosphere group relating to Quality Assessment and Quality Control. Please refer to the MODIS Atmosphere Group QA Plan at

http://modis-atmos.gsfc.nasa.gov/_docs/QA_Plan_2000_07.pdf.

4.4 Validation

Validating cloud detection is difficult (Ackerman and Cox 1981; Rossow et al., 1993; Baum et al., 1995, Ackerman et al, 1998). The performance of the MODIS cloud mask has been addressed in several papers (King et al. 2003; Platnick et al. 2003; Lee et al. 2004; Li et al. 2007). Two important steps in validation are image interpretation and quantitative analysis. In image interpretation, an analyst conducts a validation through visual inspection of the spectral, spatial, and temporal features in a set of composite images. Visual inspection is an important first step in validating any cloud mask algorithm. The analyst uses knowledge of and experience with cloud and surface spectral properties to identify obvious problems. However, visual inspection provides poor quantitative evaluation. More quantitative validation can be attained through direct pixel by pixel comparison with collocated surface, aircraft, or space-born observations. While this approach provides quantitative accuracy, it possesses the problem that the two measurement systems often observe different cloud properties (Baum et al., 1995).

4.4.1 IMAGE ANALYSIS

Figure 16 is a visual analysis of the MODIS cloud mask performance over the DOE Southern Great Plains ARM site. Validation of this scene consists of visual inspection of the imagery. For example, an analysis of multi-spectral MODIS imagery reveals that the cloud mask in the above case properly discriminates cloud from both snow and non-snow covered surfaces. The image on the right shows the cloud mask result. A great many scenes have been evaluated from all regions, surface types, and seasons.

4.4.2 COMPARISON WITH SURFACE REMOTE SENSING SITES

We have compared cloud mask results with ground-based lidar and radar data from the SGP CART Site in Lamont, Oklahoma (Stokes and Schwartz 1994), located at the red dot on the left-hand image of Figure 16. Data used for validation in this case includes cloud top height derived from

a Department of Energy (DOE) Atmospheric Radiation Measurement (ARM) Program Active Remotely Sensed Cloud (ARSCL) product that combines ground-based observations from a micropulse lidar (MPL) and a millimeter-wavelength cloud radar (MMCR) to determine cloud presence and cloud-top heights (Clothiaux et al. 2000). The ARSCL algorithm processes and combines data from the MPL and MMCR to determine cloud-base and cloud-top altitude at a vertical spatial resolution of 45 m and a temporal resolution of 10 s. The present comparison focuses on the cloud detection of the algorithm, using ARSCL cloud-top height retrieval only as an analysis tool.

There are inherent difficulties in comparing data with vastly different spatial and temporal resolutions and sensitivities. MPL/MMCR output is every ten seconds and is subject to attenuation effects and local cloud top height deviations at the single observation point over the CART site, therefore the data need to be adjusted to better match the MODIS observations. This was achieved by using a range binning process which entailed placing every MPL/MMCR observation surrounding the MODIS sounder observation time (five minutes before and after the MODIS observation time was used) into range bins of 250m. Each range bin must have a given number of observations in it to be considered valid, in this case 16% of the observations. A direct comparison was made between the MODIS and MPL/MMCR cloud detection. This is a yes/no comparison; either the instrument is reporting a cloud top height or it is not. The MODIS cloud detection algorithm and MPL/MMCR agree on the existence of clear or probably clear 86% of the time (85+65/175), and 92% of the time that a cloud was present (Table 10).

Table 10. Agreement between MOD35 and MPL/MMCR cloud vs. clear-sky discrimination.

Radar/lidar	MODIS Cloud	MODIS Uncertain	MODIS probably clear	MODIS Clear	
Clear	19	6	85	65	175
Low Cloud	82	0	4	3	89
Middle Cloud	44	3	13	0	60
High Cloud	14	1	6	3	24
	159	10	108	71	

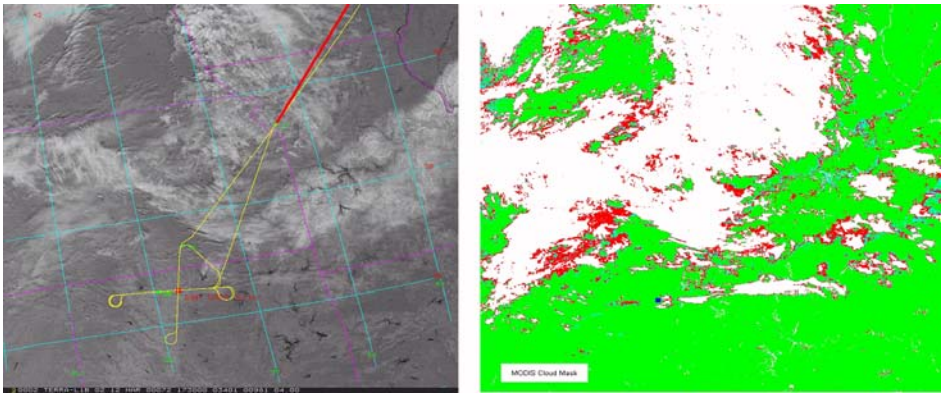

Figure 16. An example cloud mask result over the DOE ARM Southern Great Plains Site. The left image shows the ER-2 flight track (yellow line) superimposed on the MODIS 0.86 μm image from 17:10 UTC March 12, 2000 during WISC-T2000. The cloud mask result is shown at right.

In a longer-term comparison, three years (2003–05) of Collection 5 cloud mask algorithm results were compared with those from the MPL/MMCR. A group of 5 × 5 MODIS observations centered on the ARM site was used in the comparison, averaging the final cloud mask confidences and assuming that a value of greater than 0.95 represents a clear scene. The radiances were collected from the MODIS direct broadcast system at the University of Wisconsin—Madison and used as input to the Collection 5 MODIS cloud mask. The ARSCL cloud fraction is defined as the fraction of samples determined cloudy over a 30-min time period, with a cloud fraction of less than 5% considered to be clear.

Table 11 lists the comparison between the MODIS cloud mask and the ARCL data set for both the Terra and Aqua data set. There is agreement for more than 80% of the observations. There is little difference in the skill score with season. Those observations that are determined by MODIS as cloudy while ARCL is indicating clear are mostly associated with the average MODIS confidence flag of 0.90 (Figure 17), where we have defined a value of greater than 0.95 as clear. Those cases in which MODIS defines clear and ARCL cloudy occur primarily for cloud top altitudes greater than 8 km.

Table 11. Comparison of MODIS cloud detection with the ARCL over the ARM site of the Southern Great Plains.

	ARCL clear	ARCL cloudy
MODIS clear	Terra: 146 Aqua: 117	Terra: 45 Aqua:58
MODIS cloudy	Terra: 38 Aqua: 12	Terra: 298 Aqua:185

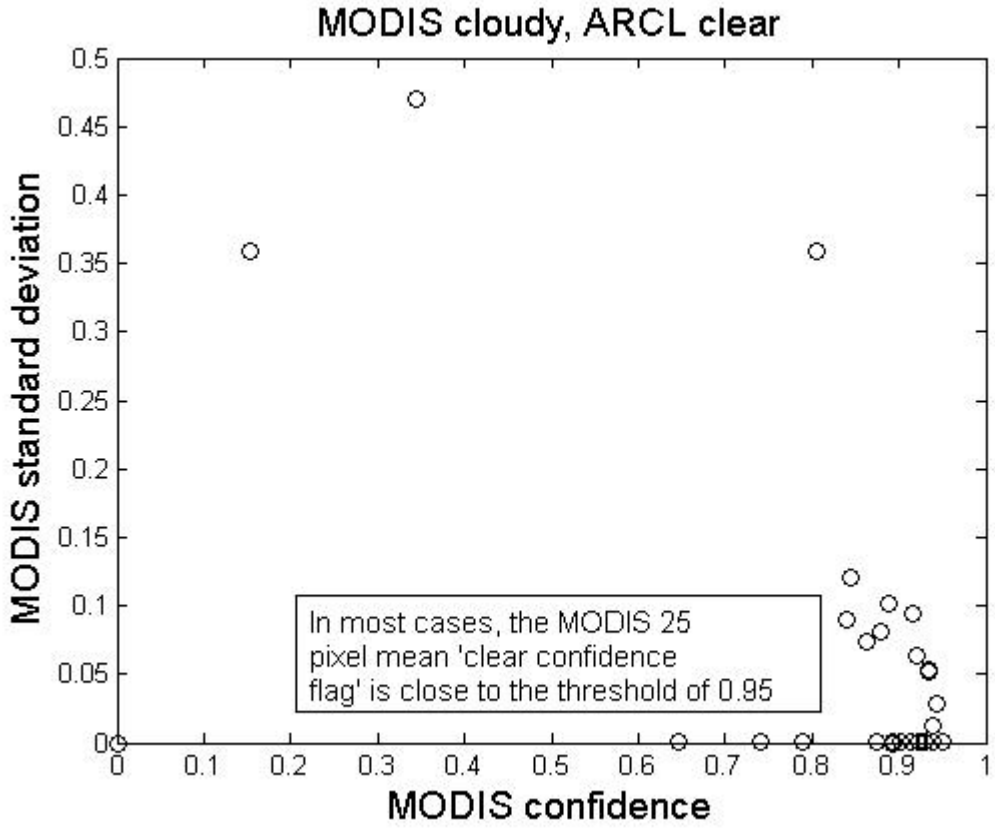

Figure 17. MODIS average confidence versus standard deviation for cases labeled by MODIS as cloudy and by the ARCL algorithm as clear. The clear-sky threshold is 0.95.

4.4.3 INTERNAL CONSISTENCY TESTS

Figure 18 shows histograms of visible ratios as a function of final clear sky confidences according to the MODIS cloud mask. The vertical lines near the center define the threshold interval for this cloud test (confidence of 1.0 at left to 0.0 at the right). One may conclude that the thresholds have been chosen properly as very few, if any, clear sky confidences > 0.95 fall

within the interval.

In addition, we can compare results from the MODIS instruments on the Aqua and Terra platforms. Figure 19 shows a comparison of the cloud mask from the two instruments over East Africa on July 11, 2002 Terra at 08:05 UTC, Aqua at 11:00 UTC. Results of the cloud detection appear consistent, given the time difference between the two overpasses.

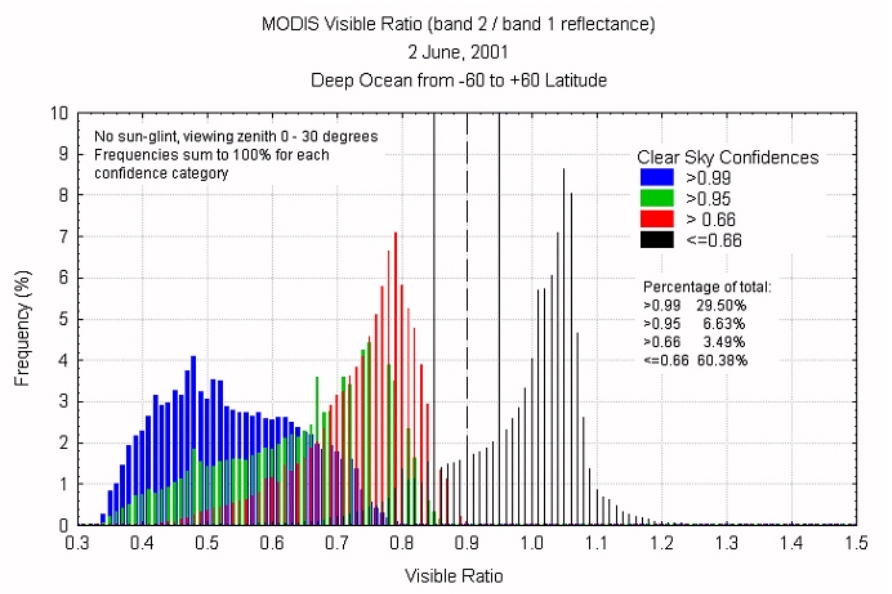

Figure 18. Histograms of Terra MODIS observations on June 2, 2001 over deep ocean regions between 60 degrees north and south latitude as a function of the final cloud mask result. See text for details.

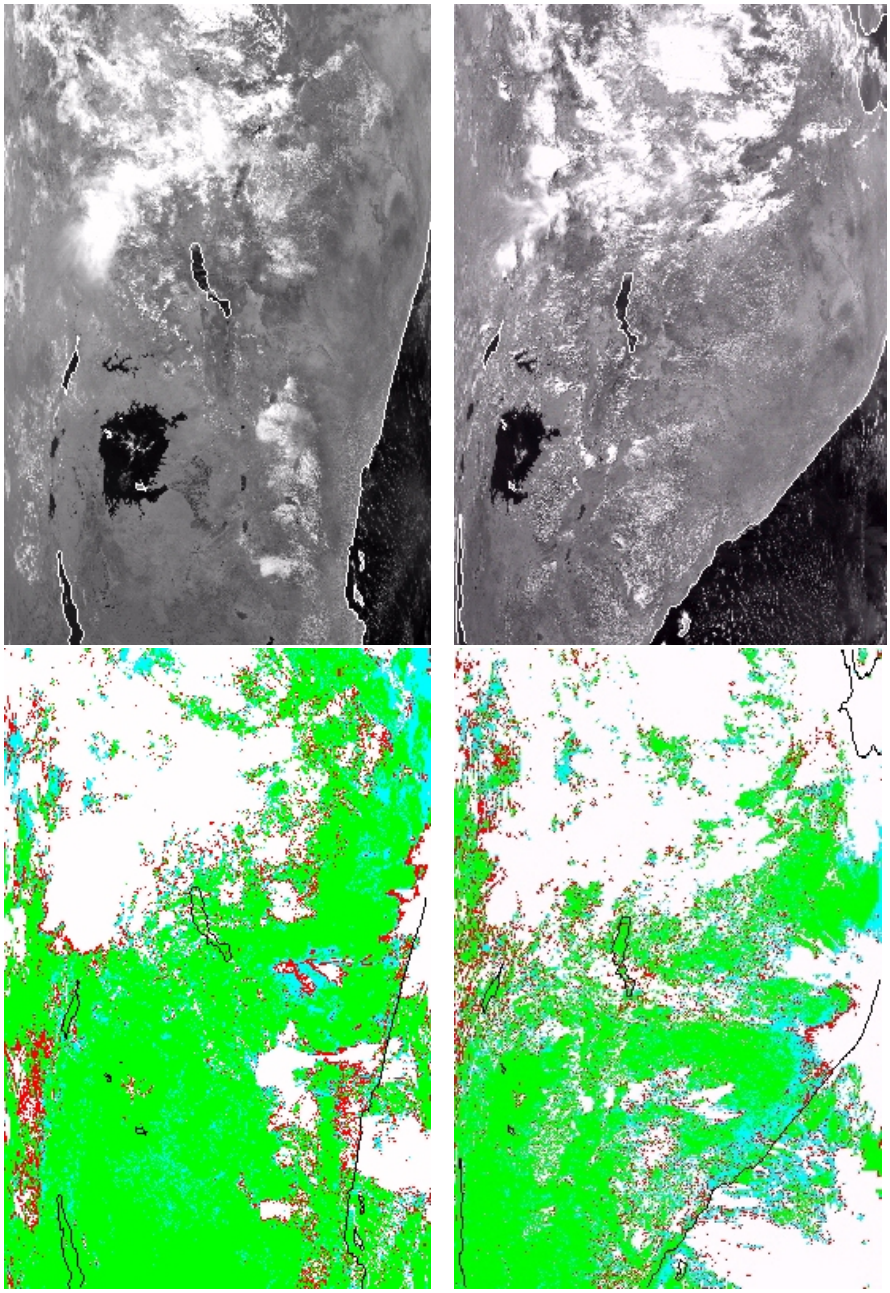

Figure 19. East African Scene from July 11, 2002 Terra at 08:05 UTC, Aqua from 11:00 UTC. MODIS Terra (left) and Aqua (right), Band 2 (top) and cloud mask (bottom). Colors: green is confident clear; cyan is probably clear; red is uncertain; white is cloudy.

Sun-glint and Daytime Ocean

Ocean areas characterized by sun-glint are some of the most difficult scenes in which to perform cloud vs. clear-sky discrimination. These areas are mostly very remote as well, where validation data for comparison is scarce or non-existent. A region of the Pacific Ocean between –30 and +45 latitude was chosen for a detailed study of the effectiveness of the MOD35 algorithm in sun-glint areas. The longitudinal domain was –180 to –130 and the temporal range was Apri1 1-8, 2003. Figure 20a shows total cloud amount as a function of glint angle binned in 6-degree increments. Sun-glint is defined in the cloud mask algorithm as glint angles from 0 to 36 degrees, where 0 defines the specular point. Because increasing sun-glint angles on the Earth's surface are characterized by a series of concentric circles, larger glint angles also imply a wider range of latitudes, as well as increasing surface area and viewing zenith angles. At first glance, the total cloud amount from the combined confident cloudy and uncertain decisions from MOD35 (top curve) would appear to be seriously biased in the sun-glint regions, but other indications of cloud (bottom curves) show the same pattern. Sub-freezing observations in the 11 μm band are independent of sun-glint, and thin and thick cirrus as determined by 1.38 μm reflectances, are generally very insensitive to glint especially in moist, tropical regions. The numbers in brackets along the top curve indicate the minimum and maximum latitudes from which the corresponding values originated. Figure 20b shows total cloud frequency from the same region but from non-glint pixels and as a function of latitude. It can be seen from comparing the latitude ranges from the first plot to the cloud frequencies of those latitudes on the second, that the trend toward lower cloud amounts in the latitudes most affected by glint is reasonable. Using the total number of observations from each glint angle bin as a surrogate for areal coverage (not exact), a reasonably accurate weighted average may be obtained over the entire region. The non-glint cloud amount was 70.8% while the cloud percentage from the glint region was 64.5%, a difference of 6.3%. Although not proven by this analysis, we suspect that the majority of missed cloudy pixels in glint areas are those warm clouds of small extent that are detected only by visi-

ble and NIR cloud tests. In areas affected by glint, the background ocean reflectance is often about the same or greater than that from these clouds, rendering them invisible. The bottom curve on Figure 26b shows zonal means of the frequencies of these clouds as defined by the cloud mask from non-glint regions.

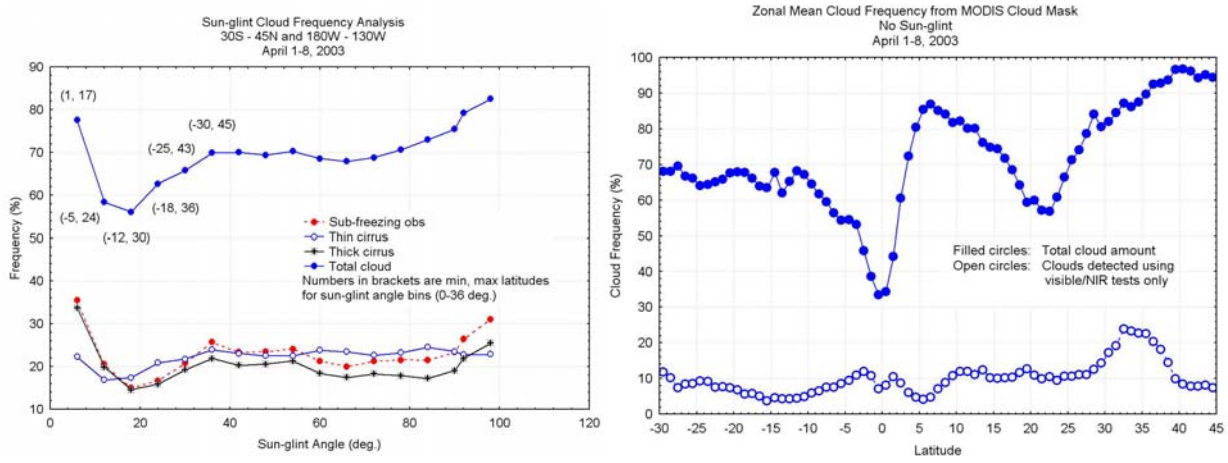

Figure 20 a and b: Cloud frequencies as a function of sun-glint angle (a) and as a function of latitude (b). The cloud frequencies in (b) do not contain any observations from sun-glint conditions. Data is from April 1-8, 2003.

4.4.4 COMPARISONS WITH COLLOCATED SATELLITE DATA

Since 2006, a very effective validation tool has been available for use with Aqua MODIS cloud algorithms. The Cloud-Aerosol Lidar with Orthogonal Polarization (CALIOP) (Winker, et al., 2007) on board the Cloud-Aerosol Lidar and Infrared Pathfinder Satellite Observations (CALIPSO) platform detects clouds and measures cloud altitudes with high accuracy (Vaughn, et al., 2009). The CALIPSO platform flies in formation as part of the "A-Train" constellation of satellites, lagging Aqua by about 95 seconds. This results in both MODIS and CALIOP observing the same clouds and/or Earth surface nearly simultaneously.

We use the 1-km Layer Product from CALIOP that includes cloud detection and cloud altitude collocated with 1-km MODIS cloud mask results (Ackerman et al., 2008). CALIOP observations are from nadir only with locations that precess across collocated MODIS scans but do not include sun-glint regions or MODIS pixels from far-limb areas.

Figure 21 shows global overall agreement (hit rate) between CALIOP and MODIS cloud detection algorithms for the period July 2007 through June 2008 where only those CALIOP 1-km footprints that are completely cloudy or completely clear are considered. As expected, day-time results are better than night, as more information is available to distinguish clear skies from cloudy. Note that this comparison is a rather harsh one for an algorithm based on a passive sensor (MODIS). Figures 22-24 show the same comparisons for global land and water, polar, and 60S-60N land and water.

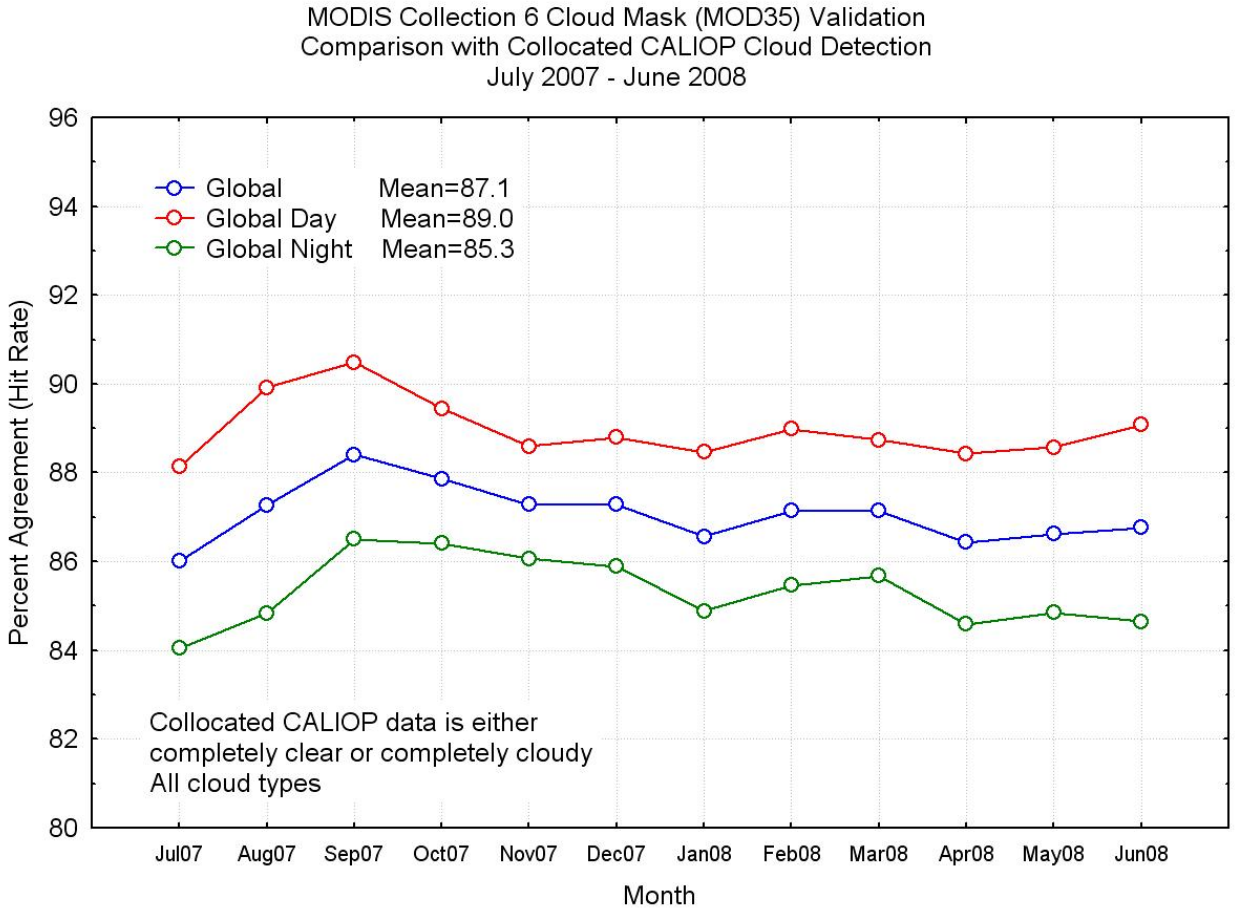

Figure 21. Global day and night percent agreement (hit rate) between CALIOP and MOD35 cloud detection.

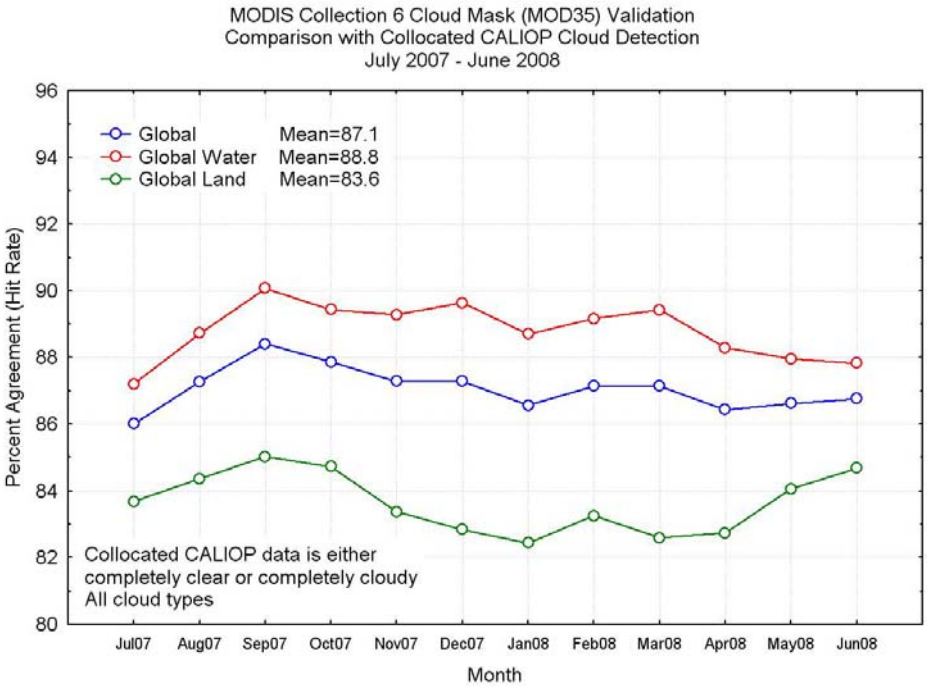

Figure 22. Global land and water percent agreement (hit rate) between CALIOP and MOD35 cloud detection.

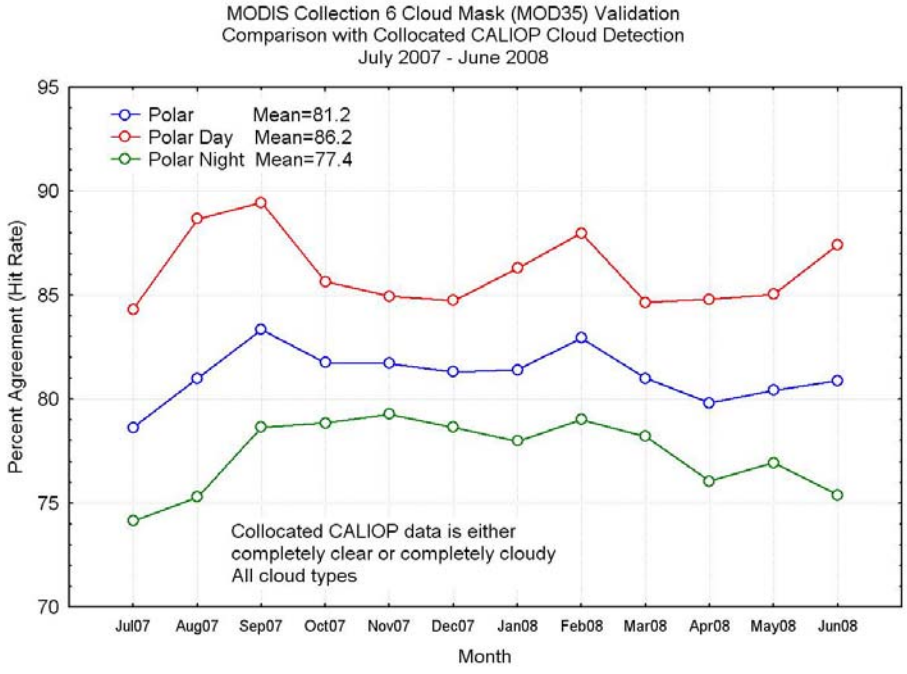

Figure 23. Polar day and night percent agreement (hit rate) between CALIOP and MOD35 cloud detection.

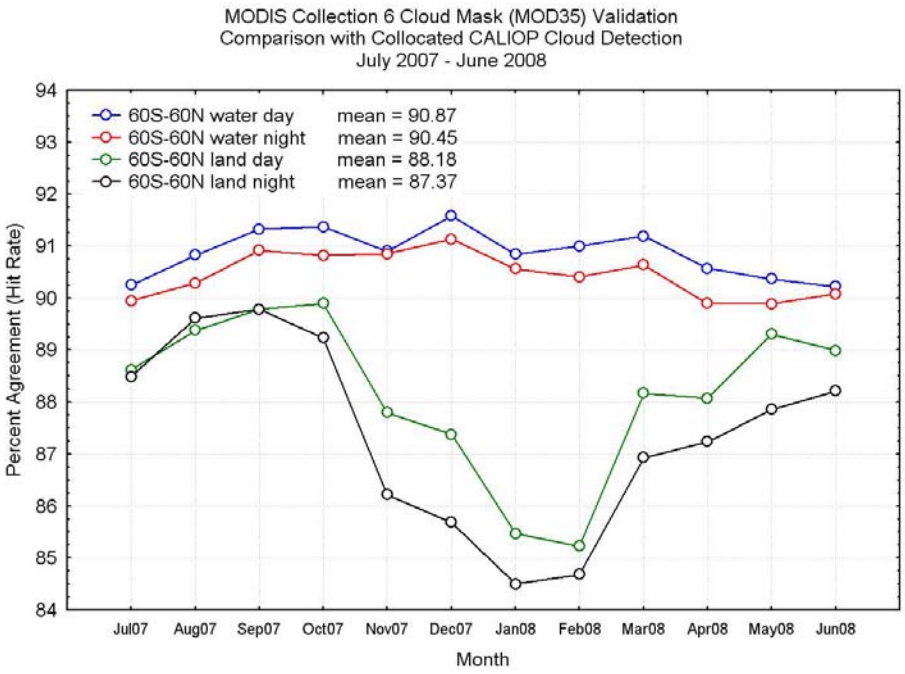

Figure 24. 60S-60N water and land, day and night percent agreement (hit rate) between CALIOP and MOD35 cloud detection.

The global agreements shown above are very consistent from month to month; however, for land surfaces from 60S-60N latitudes there is a dip during the northern hemisphere winter months. This is due to the difficulty of detecting snow cover (especially partial snow cover) over vegetated surfaces. Even when the detection of snow is correct, the lowered contrast in both visible and infrared measurements between surface and clouds greatly hinders cloud detection efficiency.

5.0 References

Ackerman, S. A., and S. K. Cox, 1981: Comparison of satellite and all-sky camera estimates of cloud cover during GATE. Journal of Applied Meteorology, Volume 20, 581-587.

Ackerman, Steven A., Smith, W. L., Spinhirne, J. D. and Revercomb, H. E.. The 27-28 October 1986 FIRE IFO cirrus case study: Spectral properties of cirrus clouds in the 8-12 micron window. Monthly Weather Review, Volume 118, Issue 11, 1990, 2377-2388. Call Number: Reprint # 1040

Ackerman, S. A.; Smith, W. L.; Collard, A. D.; Ma, H. E.; Revercomb, H. E. and Knuteson, R. O.. Cirrus cloud properties derived from High Spectral Resolution Infrared Spectrometry during FIRE II. Part II: Aircraft HIS results. Journal of the Atmospheric Sciences, Volume 52, Issue 23, 1995, 4246-4263. Call Number: Reprint # 2222

Ackerman, Steven A.. Global satellite observations of negative brightness temperature differences between 11 and 6.7 microns. Journal of the Atmospheric Sciences, Volume 53, Issue 19, 1996, 2803-2812. Call Number: Reprint # 2299

Ackerman, Steven A.. Remote sensing aerosols using satellite infrared observations. Journal of Geophysical Research, Volume 102, 1997, 17,069-17,079. Call Number: Reprint # 2413

Ackerman, Steven A.; Strabala, Kathleen I.; Menzel, W. Paul; Frey, Richard A.; Moeller, Christopher C. and Gumley, Liam E.. Discriminating clear sky from clouds with MODIS. Journal of Geophysical Research, Volume 103, 1998, 32,141-32,157. Call Number: Reprint # 2513

Ackerman, S. A., R. E. Holz, R. A. Frey, E. W. Eloranta, B. C. Maddux, and M. McGill, 2008: Cloud detection with MODIS. Part II: validation. Journal of Atmospheric and Oceanic Technology, Volume 25, 1073-1086.

Baum, B. A., T. Uttal, M. Poellot, T. P. Ackerman, J. M. Alvarez, J. Intrieri, D. O'C. Starr, J.Titlow, V. Tovinkere, and E. Clothiaux, 1995: Satellite remote sensing of multiple cloud layers. Journal of the Atmospheric Sciences, Volume 52, 4210-4230.

Baum, Bryan A.; Soulen, Peter F.; Strabala, Kathleen I.; King, Michael D.; Ackerman, Steven A.; Menzel, W. Paul and Yang, Ping. Remote sensing of cloud properties using MODIS airborne simulator imagery during SUCCESS. 2. Cloud thermodynamic phase. Journal of Geophysical Research, Volume 105, 2000, 11,781-11,792. Call Number: Reprint # 2787

Ben-Dor, 1994: A precaution regarding cirrus cloud detection from airborne imaging spectrometer data using the 1.38 um water vapor band. Journal of Remote Sensing, Volume 50, 346-350.

Brown, O. B., P. J. Minnett, R. Evans, E. Kearns, K. Kilpatrick, A. Kumar, R. Sikorski, and A. Zavody, 1999: MODIS infrared sea surface temperature algorithm. Algorithm Theoretical Basis Document. NASA Contract. Number NAS5-31361, 10 November 1994.

Otis B. Brown and Peter J. Minnett, 1999: MODIS Infrared Sea Surface Temperature Algorithm, Tech. Report ATBD25, University of Miami, Miami, FL 33149-1098.

Chung, Sunggi; Ackerman, Steven; van Delst, Paul F. and Menzel, W. Paul, 2000: **Model calculations and interferometer measurements of ice-cloud characteristics**. Journal of Applied Meteorology, Volume 39, Issue 5, 634-644. Call Number: Reprint # 2792

Clothiaux, E. E., T. P. Ackerman, G. G. Mace, K. P. Moran, R. T. Marchand, M. A. Miller and B. E. Martner, 2000: Objective Determination of Cloud Heights and Radar Reflectivities Us-

ing a Combination of Active Remote Sensors at the ARM CART Sites. Journal of Applied Meterology, Volume 39, Issue 5, 645-665.

Coakley, J. A. and F. P. Bretherton, 1982: Cloud cover from high-resolution scanner data: Detecting and allowing for partially filled fields of view. Journal of Geophysical Research Oceans, Volume 87, No. C7, 4917-4932.

Collard, A. D.; Ackerman, S. A.; Smith, W. L.; Ma, H. E.; Revercomb, H. E.; Knuteson, R. O. and Lee, S. -C., 1995: **Cirrus cloud properties derived from High Spectral Resolution Infrared Spectrometry during FIRE II. Part III: Ground-based HIS results**. Journal of the Atmospheric Sciences, Volume 52, Issue 23, 4264-4275. Call Number: Reprint # 2223

DeSlover, Daniel H.; Smith, William L.; Piironen, Paivi, K. and Eloranta, Edwin W., 1999: **A methodology for measuring cirrus cloud visible-to-infrared spectral optical depth ratios**. Journal of Atmospheric and Oceanic Technology, Volume 16, Issue 2, 251-262. Call Number: Reprint # 2576

Duda, D. P. and J. D. Spinhirne, 1996: Split-window retrieval of particle size and optical depth in contrails located above horizontally inhomogeneous ice clouds. Geophysical Research Letters, Volume 23, No. 25, 3711-3714.

Frey, Richard A.; Ackerman, S. A. and Soden, Brian J., 1996: **Climate parameters from satellite spectral measurements. Part I: Collocated AVHRR and HIRS/2 observations of spectral greenhouse parameter**. Journal of Climate, Volume 9, Issue 2, 1996, 327-344. Call Number: Reprint # 2260

Frey, Richard A.; Baum, Bryan A.; Menzel, W. Paul; Ackerman, Steven A.; Moeller, Christopher C. and Spinhirne, James D., 1999: **A comparison of cloud top heights computed from airborne lidar and MAS radiance data using CO2 slicing**. Journal of Geophysical Research, Volume 104, 24547-24555. Call Number: Reprint # 2644

Gao, B. C. and A. F. H. Goetz, 1991: Cloud area determination from AVIRIS data using water vapor channels near 1 um. Journal of Geophysical Research Atmospheres, Volume 96, No. D2, 2857-2864

Gao, B.-C., Goetz, A. F. H., & Wiscombe, W. J., 1993: Cirrus cloud detection from airborne imaging spectrometer data using the 1.38 micron water vapor band. Geophysical Research Letters, 20(4), 301-304.

Gesell, G., 1989: An algorithm for snow and ice detection using AVHRR data: An extension to the APOLLO software package. International Journal of Remote Sensing, Volume 10, Issue 4, 897-905

Gustafson, G. B., R. G. Isaacs, R. P. d'Entremont, J. M. Sparrow, T. M. Hamill, C. Grassotti, D. W. Johnson, C. P. Sarkisian, D. C. Peduzzi, B. T. Pearson, V. D. Jakabhazy, J. S. Belfiore,

and A.S. Lisa, 1994: Support of environmental requirements for cloud analysis and archive (SERCAA): algorithm descriptions. PL-TR-94-2114, Phillips Laboratory, Hanscom AFB, MA. ADA-PL-283240, 100 pp.

Hall, D. K., G. A. Riggs and V. V. Salomonson, 1995: Development of methods for mapping global snow cover using Moderate Resolution Imaging Spectroradiometer data. Remote Sensing of Environment, Volume 54, No. 2, 127-140

Hawkinson, James A.; Feltz, W.; Schreiner, A. J. and Schmit, T. J., 2003: Validation of the GOES sounder cloud top pressure product. Conference on Satellite Meteorology and Oceanography, 12th, Long Beach, CA, 9-13 February 2003 (preprints). American Meteorological Society, Boston, MA, 2003.

Hutchison, K. D. and K. R. Hardy, 1995: Threshold functions for automated cloud analyses of global meteorological satellite imagery. International Journal of Remote Sensing, Volume 16, Issue 18, 3665-3680.

Hutchison, K.D., Hauss, B. I., Iisager, B. D., Agravante, H., Mahoney, R. L., Sei, A., and J. M. Jackson, 2010: Differentiating between Clouds and Heavy Aerosols in Sunglint Regions, J. Atmospheric & Oceanic Technology, **27**, 1085-1094.

Hutchison, K.D., Iisager, B., Kopp, T., and J. M. Jackson, 2008: Discriminating between Clouds and Aerosols in the VIIRS Cloud Mask Algorithms, J. Atmospheric & Oceanic Technology, **25,** 501–518.

Hutchison, K.D., Roskovensky, J.K., Jackson, J.M., Heidinger, A.K., Kopp, T. J., Pavolonis, M.J, and R. Frey, 2005: Automated Cloud Detection and Typing of Data Collected by the Visible Infrared Imager Radiometer Suite (VIIRS), International Journal of Remote Sensing, **20**, 4681 - 4706.

Hutchison, K. D. and J. M. Jackson, 2003: Cloud detection over desert regions using the 412 nanometer MODIS channel, Geophysical Research Letters, **30**, 2187-2191.

Inoue, T., 1987: A cloud type classification with NOAA 7 split window measuremenets. Journal of Geophysical Research, Volume 92, No. D4, 3991-4000.

Key, J. and R. G. Barry, 1989: Cloud cover analysis with Arctic AVHRR, part 1: cloud detection. Journal of Geophysical Research, Volume 94, No. D15, 18521-18535.

Key, J., 2002, The cloud and surface parameter retrieval (CASPR) system for polar AVHRR, User's Guide. Cooperative Institute for Meteorological Satellite Studies, University of Wisconsin, Madison, 59 pp.

Kim, D. and S. G. Benjamin, 2000: Assimilation of cloud-top pressure derived from GOES sounder data into MAPS/RUC. Preprints, *10th Conf. on Satellite Meteorology and Oceanography,* Long Beach, CA, Amer. Meteor. Soc., 110–113.

King, M. D., M. G. Strange, P. Leone and L. R. Blaine, 1986: Multiwavelength scanning radiometer for airborne measurements of scattered radiation within clouds. Journal of Atmospheric and Oceanic Technology, Volume 3, Issue 3, 513-522.

King, M. D., W. P. Menzel, P. S. Grant, J. S. Myers, G. T. Arnold, S. E. Platnick, L. E. Gumley, S. C. Tsay, C. C. Moeller, M. Fitzgerald, K. S. Brown and F. G. Osterwisch, 1996: Airborne scanning spectrometer for remote sensing of cloud, aerosol, water vapor and surface properties. Journal of Atmospheric and Oceanic Technology, Volume 13, issue 4, 777-794.

King, M. D., W. P. Menzel, Y. J. Kaufman, D. Tanré, B. C. Gao, S. Platnick, S. A. Ackerman, L. A. Remer, R. Pincus, and P. A. Hubanks, 2003: Cloud and aerosol properties, precipitable water, and profiles of temperature and humidity from MODIS. *IEEE Trans. Geosci. Remote Sens.*, **41**, 442-458.

King, M. D., S. Platnick, P. Yang, G. T. Arnold, M. A. Gray, J. C. Riedl, S. A. Ackerman and K.-N Liou, 2004: Remote Sensing of Liquid Water and Ice Cloud Optical Thickness and Effective Radius in the Arctic: Application of Airborne Multispectral MAS Data. *J. Atmos. Oceanic Tech.* **21**, 857-875.

Kriebel, K. T., 1978: Measured spectral bidirectional reflection properties of four vegetated surfaces. Applied Optics, Volume 17(2), 253-259.

Kriebel, K. T. and R. W. Saunders, 1988: An improved method for detecting clear sky and cloudy radiances from AVHRR data. International Journal of Remote Sensing, Volume 9(1) 123-150.

Kriebel, K.T., R.W. Saunders and G. Gesell 1989: Optical properties of clouds derived from fully cloudy AVHRR pixels. *Beitr. Phys. Atmosph* **62** (1989), pp. 165–171.

Lee, Y., G. Wahba, and S. A. Ackerman, 2004: Cloud Classification of Satellite Radiance Data by Multicategory Support Vector Machines. *J. Atmos. Oceanic Tech.* **21**, 159-169.

Liu, Y. H., J. R. Key, R. A. Frey, S. A. Ackerman, and W. P. Menzel, 2004: Nighttime polar cloud detection with MODIS. *Remote Sens. Environ*., **92**, 181-194.

Leprieur, C., Y. H. Kerr and J. M. Pichon, 1996: Critical assessment of vegetation indices from AVHRR in a semi-arid environment. International Journal of Remote Sensing, Volume 17 (13), 2549-2563.

McMillin, L. M., and C. Dean, 1982: Evaluation of a new operational technique for producing clear radiances. Journal of Applied Meteorology, Volume 21, 1005–1014.

Menzel, W. P., R. A. Frey, H. Zhang, D. P. Wylie., C. C. Moeller, R. A. Holz, B. Maddux, B. A. Baum, K. I. Strabala, and L. E. Gumley, 2008: MODIS global cloud-top pressure and amount estimation: algorithm description and results. Journal of Applied Meteorology and Climatol-

ogy, 47, 1175-1198.

Li, J., W. P. Menzel and A. J. Schriener, 2001: Variational retrieval of cloud parameters from GOES sounder longwave cloudy radiance measurements. Journal of Applied meteorology, Volume 40(3), 312-330.

Li, J., W. P. Menzel, Z. Yang, R. A. Frey and S. A. Ackerman, 2002: High spacial resolution surface and cloud type classification from MODIS multi-spectral band measurements. Journal of Applied Meteorology and Climatology, Volume 42(2), 204-226.

Li, Zhenglong; Li, Jun; Menzel, W. Paul; Schmit, Timothy J. and Ackerman, Steven A. Comparison between current and future environmental satellite imagers on cloud classification using MODIS. Remote Sensing of Environment, Volume 108, 2007, pp.311-326.

Liu, Y., J. Key, R. Frey, S. Ackerman, and W. Menzel, 2004: Nighttime polar cloud detection with MODIS, Remote Sensing of Environment, **92**, 181-194, 2004.

Liou, K. N., 1973: A numerical experiment on Chandrasekhar's discrete-ordinate method for radiative transfer: Applications to cloudy and hazy atmospheres. Journal of Atmospheric Sciences, Volume 30(7), 1303-1326.

Mace, G. G., T. P. Ackerman, P. Minnis and D. F. Young, 1998: Cirrus layer microphysical properties derived from surface-based millimeter radar and infrared interferometer data. Journal of Geophysical Research, Volume 103, No. D18, 23207-23216.

Matthews, E. and W. B. Rossow, 1987: Regional and seasonal variations of surface reflectance from satellite observations at 0.6 um. Journal of Applied Meteorology, Volume 26 (1), 170-203.

McClain, E. P., 1993: Evaluation of CLAVR Phase-I algorithm performance. Final Report, U. S. Department of Commerce/NOAA/NESDIS, Report 40-AANE-201-424.

Menzel, W. P., D. P. Wylie and K. I. Strabala, 1992: Seasonal and diurnal changes in cirrus clouds as seen in four years of observations with the VAS. Journal of Applied Meteorology, Volume 31, 370-385.

Menzel, W. Paul; R. A. Frey, H. Zhang, D. P. Wylie, C. C. Moeller, R. E. Holz, B. Maddux, B. A. Baum, K. I. Strabala, and L. E. Gumley, 2008. MODIS global cloud-top pressure and amount estimation: Algorithm description and results**.** Journal of Applied Meteorology and Climatology, Volume 47, Issue 4, 2008, 1175-1198.

Minnis, P. and E. F. Harrison, 1984a: Diurnal variability of regional cloud and clear sky radiative parameters derived from GOES data: Part I: Analysis method. Journal of Climate and Applied Meteorology, Volume 23 (7), 993-1011.

Minnis, P. and E. F. Harrison, 1984b: Diurnal variability of regional cloud and clear sky radia-

tive parameters derived from GOES data: Part III: November 1978 radiative parameters. Journal of Climate and Applied Meteorology, Volume 23 (7), 1032-1051.

Minnis, P., J. W. L. Smith, D. P. Garber, J. K. Ayers and D. R. Doelling, 1995: Cloud properties derived from GOES-7 for the Spring 1994 ARM Intensive Observing Period using version 1.0.0 of the ARM satellite data analysis program. NASA Reference Publication 1366, Hampton, VA.

Minnis, P., D. P. Garber, D. F. Young, R. F. Arduini and Y. Takano, 1998: Parameterization of reflectance and effective emittance for satellite remote sensing of cloud preperties. Journal of the Atmospheric Sciences, Volume 55, 3313-3339.

Moeller, C. C., S. A. Ackerman, K. I. Strabala, W. P. Menzel, W. L. Smith, 1994: Negative 11 micron minus 12 micron brightness temperature differences: A second look. Poster presented at *8th Conference on Satellite Meteorology and Oceanography*, Feb 1996 Amer. Meteor. Soc.

Moody, E. G., M. D. King and S. Platnick, 2005: Spatially complete global spectral surface albedos: value-added datasets derived from Terra MODIS land products, IEEE Trans. Geosci. Rem. Sci. 43, pp. 144–158.

Penaloza, M. A. and R. M. Welch, 1996: Feature selection for classification of polar regions using a fuzzy expert system. Remote Sensing of Environment, Volume 58 (1), 81-100.

Pinty, B. and M. M. Verstraete, 1992: GEMI: A non-linear index to monitor global vegetation from satellites. Vegetatio, Volume 101, 15-20.

Platnick, S., M. D. King, S. A. Ackerman, W. P. Menzel, B. A. Baum, J. C. Riédi, and R. A. Frey, 2003: The MODIS cloud products: Algorithms and examples from Terra. *IEEE Trans. Geosci. Remote Sens.*, **41**, 459-473.

Prabhakara, C., J.-M. Yoo, D. P. Kratz and G. Dalu, 1993: Boundary layer stratus clouds: Inferred from satellite infrared spectral measurements over oceans. Journal of Quantitative Spectroscopy and Radiative Transfer, Volume 49 (6), 559-607.

Prata, A. J., 1989: Infrared radiative transfer calculations for volcanic ash clouds. Geophysical Research Letters, Volume 16 No. 11, 1293-1296.

Rizzi, R., C. Serio, G. Kelly, V. Tramutoli, A. McNally and V. Cuomo, 1994: Cloud clearing of infrared sounder radiances. Journal of Applied Meteorology, Volume 33, 179-194.

Rossow, W. B., 1989: Measuring cloud properties from space: A review. Journal of Climate, Volume 2, (3) 201-213.

Rossow, W. B., L. C. Garder and A. A. Lacis, 1989: Global, seasonal cloud variations from sat-

ellite radiance measurements. Part I: Sensitivity of analysis. Journal of Climate, Volume 2 (5), 419-458.

Rossow, W. B. and L. C. Garder, 1993: Cloud detection using satellite measurements of infrared and visible radiances for ISCCP. Journal of Climate, Volume 6 (12), 2341-2369.

Rossow, W. B., A. W. Walker and L. C. Garder, 1993: Comparison of ISCCP and other cloud amounts. Journal of Climate, Volume 6 (12), 2394-2418.

Saunders, R. W. and K. T. Kriebel, 1988: An improved method for detecting clear sky and cloudy radiances from AVHRR data. International Journal of Remote Sensing, Volume 9 (1), 123-150.

Schreiner, A. J., T. J. Schmit and W. P. Menzel, 2001: Observations and trends of clouds based on GOES Sounder data. Journal of Geophysical Research, Volume 106 No. D17, 20349-20363.

Seze, G. and W. B. Rossow, 1991a: Time-cumulated visible and infrared radiance histograms used as descriptors of surface and cloud variations. International Journal of Remote Sensing, Volume 12 (5), 877-920.

Seze, G. and W. B. Rossow, 1991b: Effects of satellite data resolution on measuring the space-time variations of surfaces and clouds. International Journal of Remote Sensing, Volume 12 (5), 921-952.

Simpson, J. J., 1992: Image masking using polygon fills and morphological transformations. Remote Sensing of Environment, Volume 40 (3), 161-183.

Simpson, J. J. and R. H. Keller, 1996: An improved fuzzy logic segmentation of sea ice, clouds, and ocean in remotely sensed artic imagery. Remote Sensing of Environment, Volume 54 No. 3, 290-312.

Smith, W. L., 1968: An improved method for calculating tropospheric temperature and moisture profiles from satellite radiometer measurements. Monthly Weather Review, Volume 96 (6), 387-396.

Smith, W. L. and C. M. R. Platt, 1978: Comparison of satellite-deduced cloud heights with indications from radiosonde and ground-based laser measurements. Journal of Applied Meteorology, Volume 17 (12), 1796-1802.

Smith, W. L. and R. A. Frey, 1990: On cloud altitude determinations from High Resolution Interferometer Sounder (HIS) observations. Journal of Applied Meteorology, Volume 29, 658-662.

Smith, W. L., X. L. Ma, S. A. Ackerman, H. E. Revercomb and R. O. Knuteson, 1992: Remote

Sensing Cloud Properties from High Spectral Resolution Infrared Observations. Journal of the Atmospheric Sciences, Volume 50, 1708-1720.

Smith, W. L., H. E. Revercomb, R. O. Knuteson, F. A. Best, R. Dedecker, H. B. Howell and H. M. Woolf, 1995: Cirrus cloud properties derived from high spectral resolution infrared spectrometry during FIRE II. Part I: The high resolution interferometer sounder (HIS) systems. Journal of Atmospheric Sciences, Volume 52, 4238-4245.

Smith, W. L., S. Ackerman, H. Revercomb, H. Huang, D. H. DeSlover, W. Fletz, L. Gumley and A. Collard, 1998: Infrared spectral absorption of nearly invisible cirrus clouds. Geophysical Research Letters, Volume 25 (8), 1137-1140.

Soden, B. and F. P. Bretherton, 1993. Upper tropospheric relative humidity from GOES 6.7 μ*m* channel: Method and climatology for July 1987. *J. Geophys. Res.* **98,** 16669–16688.

Spinhirne, J. D., R. Boers and W. D. Hart, 1989: Cloud top liquid water from lidar observations of marine stratocumulus. Journal of Applied Meteorology, Volume 28 (2), 81-90.

Spinhirne, J. D. and W. D. Hart, 1990: Cirrus structure and radiative parameters from airborne lidar and spectral radiometer observations. Monthly Weather Review, Volume 118, 2329-2343.

Spinhirne, J. D. and T. Nakajima, 1994: Glory of clouds in the near infrared. Applied Optics, Volume 33 (21), 4652-4662.

Spinhirne, J. D., W. D. Hart and D. L. Hlavka, 1996: Cirrus infrared parameters and shortwave reflectance relations from observations. Journal of the Atmospheric Sciences, Volume 53 (10), 1438-1458.

Stackhouse, P. W. and G. L. Stephens, 1991: A theoretical and observational study of the radiative properties of cirrus: Results from FIRE 1986. Journal of the Atmospheric Sciences, Volume 48 (18), 2044-2059.

Stamnes, K. and R. A. Swanson, 1981: A new look at the discrete ordinate method for radiative transfer calculations in the anisotropically scattering atmospheres. Journal of the Atmospheric Sciences, Volume 38, 387-399.

Stearns, C. R., R. H. Keller, G. A. Weidner and M. Sievers, 1993: Monthly mean climatic data for Antarctic automatic weather stations. *Antarctic Meteorology and Climatology: Studies Based on Automatic Weather Stations*, D. H. Bromwich and C. R. Stearns, Eds., Antarctic Research Series, Volume 61, American Geophysical Union, 1-21.

Stokes, G. M., and S. E. Schwartz, 1994: The atmospheric radiation measurement (ARM) program: Programmatic background and design of the cloud and radiation test bed. Bulletin of the American Meteorological Society, Volume 75, 1201–1221.

Stowe, L. L., E. P. McClain, R. Carey, P. Pellegrino, G. Gutman, P. Davis, C. Long and S. Hart, 1991: Global distribution of cloud cover derived from NOAA/AVHRR operational satellite data. Advances in Space Research, Volume 11 (3), 51-54.

Stowe, L. L., S. K. Vemury and A. V. Rao, 1994: AVHRR clear sky radiation data sets at NOAA/NESDIS. Advances in Space Research, Volume 14 (1), 113-116.

Stowe, L. L., P. A. Davis, and E. P. McClain, 1998: Scientific basis and initial evaluation of the CLAVR-1 global clear/cloud classification algorithm for the Advanced Very High Resolution Radiometer. Journal of Atmospheric and Oceanic Technology, Volume 16, 656-681.

Strabala, K. I., S. A. Ackerman and W. P. Menzel, 1994: Cloud properties inferred from 8-12 um data. Journal of Applied Meteorology, Volume 33, 212-229.

Suttles, J. T., R. N. Green, P. Minnis, G. L. Smith, W. F. Staylor, B. A. Wielicki, I. J. Walker, D. F. Young, V. R. Taylor and L. L. Stowe, 1988: Angular radiation models for Earth-atmosphere system: Volume I - Shortwave radiation. NASA Reference Publication (1988), p. 1184.

Tarpley, J. D., 1979: Estimating incident solar radiation at the surface from geostationary satellite data. Journal of Applied Meteorology, Volume 18, 1172-1181.

Tsonis, A. A., 1984: On the separability of various classes from GOES visible and infrared data. Journal of Climate and Applied Meteorology, Volume 23, 1393-1410.

Vane, G., R. O. Green, T. G. Chrien, H. T. Enmark, E. G. Hansen and W. M. Porter, 1993: The Airborne Visible/Infrared Imaging Spectrometer (AVIRIS). Remote Sensing of Environment, Volume 44, 127-143.

Vaughan, M., K. A. Powell, D. M. Winker, C. A. Hostetler, R. E. Kuehn, W. H. Hunt, B. J. Gezewich, S. A. Young, Z. Liu, and M. J. McGill, 2009: Fully automated detection of cloud and aerosol layers in the CALIPSO lidar measurements. Journal of Atmospheric and Oceanic Technology, Volume 26, 2034–2050.

Wang, J. R., P. Racette, J. D. Spinhirne, K. F. Evans and W. D. Hart, 1998: Observations of cirrus clouds with airborne MIR, CLS, and MAS during SUCCESS. Geophysical Research Letters, Volume 25, No. 8, 1145-1148.

Weinreb, M. P., R. Xie, J. H. Lienesch, and D. S. Crosby, 1989: Destriping GOES images by matching empirical distribution functions. Remote Sensing of Environment, Volume 29, 185-195.

Wielicki, B. A., J. T. Suttles, A. J. Heymsfield, R. W. Welch, J. D. Spinhirne, M. L. Wu, D. O. C. Starr, L. Parker and R. F. Arduini, 1990: The 27-28 October 1986 FIRE IFO cirrus case study: Comparison of radiative transfer theory with observations by satellite and aircraft. Monthly Weather Review, Volume 118, 2356-2376.

Winker, D. M., W. H. Hunt, and M. J. McGill, 2007: Initial performance assessment of CALIOP, Geophysical Research Letters, Volume 34, L19803, doi:10.1029/2007GL030135.

Wu, X., J. J. Bates and S. Singhkhalsa, 1993: A climatology of the water vapor band brightness temperatures for NOAA operational satellites. Journal of Climate, Volume 6, 1282-1300.

Wylie, D. P. and W. P. Menzel, 1989: Two years of cloud cover statistics using VAS. Journal of Climate, Volume 2 (4), 380-392.

Wylie, D. P., W. P. Menzel, H. M. Woolf and K. I. Strabala, 1994: Four years of global cirrus cloud statistics using HIRS. Journal of Climate, Volume 7 (12), 1972-1986.

Yamanouchi, T., K. Suzuki and S. Kawaguci, 1987: Detection of clouds in Antarctica from infrared multispectral data of AVHRR. Journal of the Meteorological Society of Japan, Volume 65, 949-962.

Yang, P., B.-C. Gao, B. A. Baum, Y. X. Hu, W. Wiscombe, M. I. Mischenko, D. M. Winker and S. L. Nasiri, 2000: Asymptotic solutions of optical properties of large particles with strong absorption. Applied Optics, Volume 40 (9), 1532-1547.

Yang, P., B.-C. Gao, B. A. Baum, Y. X. Hu, W. J. Wiscombe, S.-C. Tsay and D. M. Winker, 2000: Radiative properties of cirrus clouds in the infrared (8-13 um) spectral region. Journal of Quantitative Spectroscopy and Radiative Transfer, Volume 70 (4), 473-504.

Appendix A. Example Code for reading Cloud Mask Output

This is an example FORTRAN program to read the MODIS cloud mask. The code picks out the first byte of data from the six byte product, and returns -1 in the CldMsk data array (one scan cube) if the product is not defined at a certain pixel, a 1 if it is clear and a 0 if cloudy. This particular version just passes a binary (0 or 1) value for cloud or clear, where clear is defined by this user to be anything greater than 66% probability of clear. It also returns the value of the land sea flag from the 2 bit product in the cloud mask product (0-3) to the LandSea_Flag variable. This is a good example of how a user can design what they extract out of the cloud mask file based upon their needs. It also includes the appropriate MAPI and SDP toolkit calls used in Version 1.

========== Begin Example Cloud Mask Reader ==========

```
      INTEGER FUNCTION ReadCldMsk_MOD05(Modfil,Scan_No,Buf_Size1,
           &                 Buf_Size2,Data_Size,CldMsk,LandSea_Flag)
      IMPLICIT NONE
            INCLUDE 'mapi.inc'
            INCLUDE 'hdf.inc'
            INCLUDE 'PGS_SMF.f'
            INCLUDE 'PGS_MODIS_39500.f'
      C-------------------------------------------------------------------------
      C !F77
      C
      C !DESCRIPTION: Retrieves one scan cube of MODIS Cloud Mask data from
      C               an HDF target array of 100 scan cubes (a granule).
      C
      C !INPUT PARAMETERS:
      C    INTEGER  Modfil(3)    File handle structure for HDF files
      C    INTEGER  Scan_No      Scan Number
      C    INTEGER  Buf_Size1/2  Size of dimension 1/2 of 'Cloud Mask' output
      C                          buffer as dimensioned in calling program
      C
      C !OUTPUT PARAMETERS:
      C    INTEGER  Data_Size(2) Array specifying the size of 'Cloud Mask'
      C                          data block within output buffer.
      C             In definitions below, x = Buf_Size1
```

```
C                                  y = Buf_Size2
C    INTEGER  CldMsk(x,y)  Buffer storing Cloud Mask.
C    INTEGER  LandSea_Flag(x,y)  Buffer storing LandSea_Flag.
C
C !TEAM-UNIQUE HEADER:
C
C    This software is developed by the MODIS Science Data Support
C    Team for the National Aeronautics and Space Administration,
C    Goddard Space Flight Center, under contract NAS5-32373.
C
C !REFERENCES AND CREDITS
C
C    WRITTEN BY:
C    Xiao-Yang Ding                09/12/95
C    Research and Data systems Corporation
C    SAIC/GSC MODIS Science Data Support Office
C    7501 Forbes Blvd, Seabrook MD 20706
C
C !DESIGN NOTES:
C
C    ReadCldMsk_MOD05 checks the return status of all MODIS Application
C    Program Interface (M-API) function calls.  A successful M-API
C    call is indicated by a return value of MAPIOK (0).  If unsuccessful,
C    a warning error message (i.e., type .._W_..) is written to the
C    LogStatus file, and control reverts back to the calling routine.
C    Subroutine MODIS_SMF_SETDYNAMICMSG is used for message passing to
C    the LogStatus file.
C
C   Externals:
C
C      Function:
C        GMAR                       (libmapi.a)
C        GMARDM                     (libmapi.a)
C
C      Subroutines:
C        MODIS_SMF_SETDYNAMICMSG
C        CONCATENATE
C
C      Named Constant:
C        DFACC_READ                 (hdf.inc)
```

```
C        MAPIOK                     (mapi.inc)
C        MODIS_W_GENERIC            (MODIS_39500.f)
C
C   Internals Variables:
C        arrnam      Name of the SDS array.
C        grpnm       Name of the data group containing the target
C        data_type   String describing the data type of the array.
C        Edge(3)     Array specifying the number of data value to read.
C        Start(3)    Array specifying the starting location of data.
C        Fmax        Maximum frame number per scan line.
C        Lmax        Maximum line number per scan cube.
C        Rank        The number of dimensions in an array
C        ReadCldMsk_MOD05 The function return value
C        MaxScan_No  Total Swath Number.
C        count(15000) A temporary buffer for data of the target array
C        LinesPerScan The number of lines per scan cube
C
C !END
C--------------------------------------------------------------------------

C Declarations
      CHARACTER*80 arrnm,grpnm,data_type,msgbuf,msgbuf1
      INTEGER      Scan_No,LinesPerScan,Rank,I,j,k,L,Fmax,
     2             Lmax,MaxScan_No,No_Bytes
      LOGICAL      error_flag
      PARAMETER    (No_Bytes=6,Fmax=1500,Lmax=10)
      BYTE         count(No_Bytes*Fmax*Lmax)
      INTEGER      Temp1,Temp2,Start(3),Edge(3),Data_Size(2),
     2             Dim_Size(3),Buf_Size1,Buf_Size2,Modfil(3),
     3             CldMsk(Buf_Size1,Buf_Size2),
     4             LandSea_Flag(Buf_Size1,Buf_Size2)

C Initialization
      grpnm = ' '
      arrnm = 'Cloud_Mask'
      error_flag = .false.
      ReadCldMsk_MOD05 = -1
      LinesPerScan = 10
      Rank  =  3
      Start(1) = 0
```

```
      Start(2) = 0
      Start(3) = (Scan_No-1)*LinesPerScan

C Check for valid file and band numbers
      IF (Modfil(1).le.0 .or. Modfil(3).ne.DFACC_READ) THEN
          CALL MODIS_SMF_SETDYNAMICMSG(MODIS_W_GENERIC,
     &    'Invalid SD_ID or invalid file access type','ReadCldMsk_MOD05')
          error_flag = .true.
      End If

C Retrieve the rank, dimensions and data type of SDS data.
      IF (GMARDM(Modfil, arrnm, grpnm, data_type, Rank, Dim_Size)
     &  .ne.MAPIOK) THEN
          CALL MODIS_SMF_SETDYNAMICMSG(MODIS_W_GENERIC,
     &  'GMARDM failed','ReadCldMsk_MOD05')
          error_flag = .true.
      End If

C  Additional input check of Scan_No and buffer size
      MaxScan_No=Dim_Size(3)/LinesPerScan

      IF (Scan_No.lt.1 .or. Scan_No.gt.MaxScan_No) THEN
         write(msgbuf,'(i4)') MaxScan_No
         call Concatenate('Scan_No out of bounds; range 1 -',
     &   msgbuf, msgbuf1)
         CALL MODIS_SMF_SETDYNAMICMSG(MODIS_W_GENERIC,
     &   msgbuf1,'ReadCldMsk_MOD05')
         error_flag = .true.
      End If

      IF (Buf_Size1 .lt. Dim_Size(2)) THEN
         CALL MODIS_SMF_SETDYNAMICMSG
     2   (MODIS_W_GENERIC,'Buffer size too small','ReadCldMsk_MOD05')
         error_flag = .true.
      END IF

C Get Cloud MASK data
       Edge(1) = Dim_Size(1)
       Edge(2) = Dim_Size(2)
       Edge(3) = LinesPerScan
```

```
C Read HDF target array into 'count' buffer
      IF (GMAR(Modfil,arrnm,grpnm,Start,Edge,count).ne.MAPIOK) THEN
         CALL MODIS_SMF_SETDYNAMICMSG(MODIS_W_GENERIC,'GMAR failed',
     &   'ReadCldMsk_MOD05')
         error_flag = .true.
      END IF

      IF (.not.error_flag) THEN

C Set size of output data.  Note Data_Size(1) set in previous call
C to GMARDM.
         Data_Size(1) = Dim_Size(2)
         Data_Size(2) = LinesPerScan
         L = -5

         Do 30 k=1,Edge(3)
         Do 40 j=1,Edge(2)

C The Cloud mask consists of 6 separate 1-byte words.
C Increment memory buffer index by 6 for each successive pixel.
            L = L + 6

C Examine first byte of cloud mask at each pixel.
C First, find out whether cloud mask for pixel was determined.
C Zero-based bit 0 is 1 for determined, 0 for not determined.
C If cloud mask not determined, set CldMsk(j,k) to -1.
C In Version 1, LandSea_Flag takes 5 values:  0 (water), 1 coastal,
C 2 (wetland), 3 (land), and -1(invalid data marker).

           Temp1 = ibits(count(L),0,1)

           if (Temp1 .EQ. 0) then
              CldMsk(j,k) = -1
              LandSea_Flag(j,k) = -1
           else

C Go to clear/cloud confidence level bits (zero-based bits 1 and 2)
C Note: We treat the clear confidence levels of 66%, 95%, and 99% as
C all clear.  Modifications are expected if the Cloud MASK data are
```

```
C used as more than a simple switch.  Set default Cloud value to
C clear (1).  If cloud is found, re-assign Cloud value to 0.

              CldMsk(j,k) = 1
              Temp2 = ibits(count(L),1,2)
              if (Temp2 .EQ. 0) CldMsk(j,k) = 0

C Go to bits 6 and 7 to set Version 1 land/sea flag, 0 for water;
C 1 coastal, 2 wetland, 3 land.
              Temp2 = ibits(count(L),6,2)
              LandSea_Flag(j,k) = Temp2
           end if

   40    continue
   30    continue
         ReadCldMsk_MOD05 = 0
      END IF

      RETURN
      END
```

========== End Example Cloud Mask Reader ==========

This is an example MATLAB program to read the MODIS cloud mask.

```
function cloudmask = readModisCloudMask(maskFilename, byteList, area)

% function cloudmask = readModisCloudMask(maskFilename, byteList)
%
% DESCRIPTION:
% Reads the mask product information from a MODIS MOD35 HDF file
%
% REQUIRED INPUT:
%   maskFilename (string)        Name of MODIS MOD35 HDF file
%
% ---------------------------------------------------------------------
%
% OPTIONAL INPUT:
%   byteList       Byte numbers of data to return.  If this argument is
%            specified, all bits of the selected byte are
%            returned.  If this argument is not specified, ONLY
%            bits 1 & 2 of byte 1 (cloud mask probability of clear,
%            with QA) is returned.
%
%            byteList can be either an array of byte #s
%            (1 through 6) or the string 'all' to return all
%            bytes.  Note that to get the 250m cloud mask, only
%            byte 5 or 6 (not both) needs to be requested.
%
%            See list below (under "Output") for a description of the
%            bits in each byte.
%
%            For each byte requested, QA information is also read in
%            A separate QA array is not returned, instead this information
%            is incorporated into the cloud mask fields that are returned.
%            The cloud mask values corresponding to QA "not useful" or
%            "not applied" are set to -1.
%
% ---------------------------------------------------------------------
%
% OUTPUT:
%   cloudmask (struct) with contents determined by the byte
%   numbers selected in byteList:
%
%   BYTE 1
%    cloudmask.flag (bit 0)
%                  0 = Not determined
%                  1 = Determined
```

```
%          .mask (bits 1 & 2)
%                -1 = Not Useful (from QA)
%                  0 = Cloud
%                  1 = 66% Probability of clear
%                  2 = 95% Probability of clear
%                  3 = 99% Probability of clear
%           .confidenceQA (QA byte 1, bits 1,2,3)
%                 0 - 7 confidence level for cloudmask.mask
%          .dayOrNight (bit 3)
%                  0 = Night   1 = Day  -1 = Not Useful (from QA)
%          .sunglint (bit 4)
%                  0 = Yes     1 = No   -1 = Not Useful (from QA)
%          .snowIce (bit 5)
%                  0 = Yes     1 = No   -1 = Not Useful (from QA)
%          .landWater (bits 6 & 7)
%                -1 = Not Useful (from QA)
%                  0 = Water
%                  1 = Coastal
%                  2 = Desert
%                  3 = Land
%
%    BYTE 2 (0 = Yes;  1 = No; -1 = Not Applied, from QA)
%     cloudmask.bit0 (Non-cloud obstruction flag)
%          .bit1 (Thin cirrus detected, solar)
%          .bit2 (Shadow found)
%          .bit3 (Thin cirrus detected, IR)
%          .bit4 (Adjacent cloud detected -- implemented
%               post-launch to indicate cloud found within
%               surrounding 1km pixels)
%          .bit5 (Cloud Flag, IR threshold)
%          .bit6 (High cloud flag, CO2 test)
%          .bit7 (High cloud flag, 6.7 micron test)
%
%    BYTE 3 (0 = Yes;  1 = No; -1 = Not Applied, from QA)
%     cloudmask.bit0 (High cloud flag, 1.38 micron test)
%          .bit1 (High cloud flag, 3.7-12 micron test)
%          .bit2 (Cloud flag, IR temperature difference)
%          .bit3 (Cloud flag, 3.7-11 micron test)
%          .bit4 (Cloud flag, visible reflectance test)
%          .bit5 (Cloud flag, visible reflectance ratio test)
%          .bit6 (0.935/0.87 reflectance test)
%          .bit7 (3.7-3.9 micron test)
%
%    BYTE 4 (0 = Yes;  1 = No; -1 = Not Applied, from QA)
%     cloudmask.bit0 (Cloud flag, temporal consistency)
%          .bit1 (Cloud flag, spatial variability)
```

```
%            .bit2 (Final confidence confirmation test)
%            .bit3 (Cloud flag, night water spatial variability)
%            .bit4 (Suspended dust flag)
%
%    BYTES 5 & 6 250m Cloud Flag Visible Tests
%              (0 = Yes;  1 = No; -1 = Not Applied, from QA)
%      cloudmask.visibleTest250m          250m resolution array
%
%
%  24 April: removed this field, it is memory intensive and not
%           too useful so far.
%                       .sumVisibleTest250m            1km resolution, sum of all
%                                  16 elements in each 1km grid
%
% ------------------------------------------------------------------------
%
% Time to run this code for:   Byte 1        1 minute
%                              Bytes 1-4     1.5 minutes
%                              Bytes 5 & 6   3.3 minutes
%
% Note: With 1G of RAM, I run out of memory if I try to read all bytes at
%       once.  Instead, I read bytes 1-4, then 5-6 separately.
%
% ------------------------------------------------------------------------
%
% Written By:
%    Suzanne Wetzel Seemann
%    swetzel@ssec.wisc.edu
%    April 2001
%
% update 23 April 2001 -- added QA for bytes 5 & 6
% update 24 April 2001 -- removed .sumVisibleTest250m field because it
%                         is memory intensive and not very useful so far
%
% Code History: Based on a code by Shaima Nasiri (modis_mask_read.m) that
%               reads Byte 1 of the cloud mask.
%
% RESTRICTIONS:
%    Only tested on Matlab version 5.3.1 (R11.1) - performance under
%    other versions of Matlab is unknown
%
% ------------------------------------------------------------------------
%
% SAMPLE RUN STATEMENTS:
%  dataPath = '/home/swetzel/data/gomo310/';
%
```

```
    %  readModisCloudMask([dataPath
'MOD35_L2.A2000310.1750.002.2000332030507.hdf'], ...
    %                  [1 4]);
    %  readModisCloudMask([dataPath
'MOD35_L2.A2000310.1750.002.2000332030507.hdf'], ...
    %                  5);
    %  readModisCloudMask([dataPath
'MOD35_L2.A2000310.1750.002.2000332030507.hdf'], ...
    %                  1,'all');

    %%%%%%%%%%%%%%%%%%%%%%%%%%%%%%%%%%%%%%%%%%%%%%%%%%%%%%%%%%%%%%%%%%%%%%%%%%%%
    % Error check inputs
    %%%%%%%%%%%%%%%%%%%%%%%%%%%%%%%%%%%%%%%%%%%%%%%%%%%%%%%%%%%%%%%%%%%%%%%%%%%%
    onlyBits1and2 = 0;

     if nargin < 1
       error(['readModisCloudMask requires at least one input: maskFilename']);
     elseif nargin == 1
       byteList = 1;
       onlyBits1and2 = 1;
     elseif nargin > 1
       if ischar(byteList)
         if strcmp(byteList,'all')
             byteList = [1:6];
         else
             error(['Second input argument, byteList must either ' ...
                'be an array of integers 1-6 or the string "all"']);
         end
       else
         if any(byteList > 6) | any(byteList < 1)
             error(['Second input argument, byteList must either ' ...
                'be an array of integers 1-6 or the string "all"']);
         end
       end
     end

    % Check for valid MOD35 HDF file
     if (~exist(maskFilename,'file'))
       error(['Filename : ' maskFilename ' was not found']);
     end

     len_filename = length(maskFilename);
     if (~strcmp( maskFilename(len_filename-3:len_filename), '.hdf'))
       error(['Filename: ' maskFilename ' is not an HDF file']);
```

```
    end

   %% Add byte 5 to byteList if byte 6 was given or add
   %% byte 6 to byteList if byte 5 was given

     if ismember(5,byteList) & ~ismember(6,byteList)
         byteList = [byteList 6];
     elseif ~ismember(5,byteList) & ismember(6,byteList)
         byteList = [byteList 5];
     end

   %% Find the largest cloud mask and QA byte number, to minimize
   %% the amount of data we need to read in.

     minBytes = min(byteList);
     maxBytes = max(byteList);
     cloudMaskDataByteList = [minBytes:1:maxBytes];

   %%%%%%%%%%%%%%%%%%%%%%%%%%%%%%%%%%%%%%%%%%%%%%%%%%%%
%%%%%%%%%%%%%%%%%%%%%%%%%%%%%%%%%%
   % Open cloud mask file and read data, dimensions, and attributes
   %%%%%%%%%%%%%%%%%%%%%%%%%%%%%%%%%%%%%%%%%%%%%%%%%%%%
%%%%%%%%%%%%%%%%%%%%%%%%%%%%%%%%%%
    SD_id = hdfsd( 'start', maskFilename, 'read' );
    if (SD_id < 0)
       error(['HDF file' maskFilename ' was not opened.']);
    end

   % data we want is 'Cloud_Mask'
    mask_ex = hdfsd('nametoindex', SD_id, 'Cloud_Mask');
    mask_id = hdfsd('select',SD_id, mask_ex);
    [name,rank,dimsizes,data_type,nattrs,status(1)] = hdfsd('getinfo',mask_id );

   nbytes = dimsizes(1);
   npixels_across =  dimsizes(2);
   npixels_along = dimsizes(3);

   start = [minBytes-1; 0 ; 0];
   count = [1 ; 1 ; 1];
   edge = [1 ; npixels_across ;  npixels_along];


    if (nargin == 3)
       start(2) = min( [max([area(1) 0]) (npixels_across - 1)] );
       start(3) = min( [max([area(2) 0]) (npixels_along - 1)] );
       edge(2) = min( [max([area(3) 0]) (npixels_across - start(2))] );
```

```
    edge(3) = min( [max([area(4) 0]) (npixels_along - start(3))] );
  end

 %  if maxBytes <= nbytes
 %    edge = [maxBytes-minBytes+1; npixels_along; npixels_across];
 %  else
 %    error(['maxBytes cannot be greater than the number of bytes in the file']);
 %  end

  [cloudMaskData,status(2)] = hdfsd('readdata',mask_id,start,count,edge);
  cloudMaskData  = double(cloudMaskData);
  attr_ex = hdfsd('findattr', mask_id, 'scale_factor');
  [scale, status(3)] = hdfsd('readattr', mask_id,attr_ex) ;

  attr_ex = hdfsd('findattr', mask_id, 'long_name');
  [longname, status(4)] = hdfsd('readattr', mask_id,attr_ex) ;

  attr_ex = hdfsd('findattr', mask_id, 'Cell_Along_Swath_Sampling');
  [sampling, status(5)] = hdfsd('readattr', mask_id,attr_ex) ;

  attr_ex = hdfsd('findattr', mask_id, 'add_offset');
  [offset, status(6)] = hdfsd('readattr', mask_id,attr_ex) ;
  if offset ~= 0 | scale ~= 1
    error(['Cloud_Mask offset ~= 0 or slope ~= 1']);
  end

 % stop accessing data
  status(7) = hdfsd('endaccess',mask_id);

  if any(status == -1)
    error('Trouble reading Cloud_Mask data, dimensions, or attributes');
  end

  clear status

 % close HDF file
  status = hdfsd('end', SD_id);
  if (status < 0)
    warning(['HDF file' maskFilename ' was not closed.']);
  end

 %%%%%%%%%%%%%%%%%%%%%%%%%%%%%%%%%%%%%%%%%%%%%%%%%%%%%%%%%%%%%%%%%%%%%%%%%
%%%%%%%%%%%%%%%%%%%%%%%%%%%
 %% Read all bits from the selected bytes
 %%%%%%%%%%%%%%%%%%%%%%%%%%%%%%%%%%%%%%%%%%%%%%%%%%%%%%%%%%%%%%%%%%%%%%%%%
%%%%%%%%%%%%%%%%%%%%%%%%%%%
```

```
%% For each byte, before reading the bits, we must separate
%% the bytes and adjust image array for use in Matlab :
%%        convert values to double precision
%%        rotate and flip the image
%%        convert from MOD35's signed integers to Matlab's unsigned
%%       integers where [0:127 -128:-1] is mapped to [0:1:255]

  clear cloudmask
  cloudmask.filename = maskFilename;


%%%%%%%%%%%%%%%%%%%%%%%%%%%%%%%%%%%%%%%%%%%%%%%%%%%%%%%%%%%
%%%%%%%%%%%%%%%
  %% Cloud_Mask: BYTE 1

%%%%%%%%%%%%%%%%%%%%%%%%%%%%%%%%%%%%%%%%%%%%%%%%%%%%%%%%%%%
%%%%%%%%%%%%%%%
  if any(byteList == 1)

    byteInd = find(1 == cloudMaskDataByteList);
    byte1 = flipud(rot90(squeeze(cloudMaskData(:,:,byteInd)) ));
    % find negative integers and remap them
    ind = find(byte1 < 0);
    byte1(ind) = 256 + byte1(ind);
    clear ind

    %% BITS 1,2 - Unobstructed FOV Quality Flag
    %%   0 = Cloud
    %%   1 = 66% Probability of clear
    %%   2 = 95% Probability of clear
    %%   3 = 99% Probability of clear

    bit3 = bitget(byte1,3);
    bit2 = bitget(byte1, 2);
    clear99prob_ind = find(bit3 & bit2);
    clear95prob_ind = find(bit3 & ~bit2);
    clear66prob_ind = find(~bit3 & bit2);
    cloud_ind = find(~bit3 & ~bit2);

    cloudmask.byte1.mask = NaN * ones(size(byte1));
    cloudmask.byte1.mask(clear99prob_ind) = 3;
    cloudmask.byte1.mask(clear95prob_ind) = 2;
    cloudmask.byte1.mask(clear66prob_ind) = 1;
    cloudmask.byte1.mask(cloud_ind) = 0;
```

```
    clear bit3 bit2 clear99prob_ind clear95prob_ind clear66prob_ind cloud_ind

    if onlyBits1and2 == 0
      %% BIT 0 - CloudMask Flag
      %%   0 = Not determined
      %%   1 = Determined
      cloudmask.byte1.flag = bitget(byte1, 1);

      %% BIT 3 - Day or Night Path
      %%   0 = Night   1 = Day
      cloudmask.byte1.dayOrNight = bitget(byte1,4);

      %% BIT 4 - Sunglint Path
      %%   0 = Yes     1 = No
      cloudmask.byte1.sunglint = bitget(byte1,5);

      %% BIT 5 - Snow/Ice Background Path
      %%   0 = Yes     1 = No
      cloudmask.byte1.snowIce = bitget(byte1,6);

      %% BITS 6,7 - Land or Water Path
      %%   0 = Water
      %%   1 = Coastal
      %%   2 = Desert
      %%   3 = Land
      cloudmask.byte1.landWater = NaN * ones(size(byte1));

      bit7 = bitget(byte1,7); bit8 = bitget(byte1,8);
      land_ind  = find(bit8 & bit7);
      desert_ind = find(bit8 & ~bit7);
      coastal_ind = find(~bit8 & bit7);
      water_ind = find(~bit8 & ~bit7);

      cloudmask.byte1.landWater(land_ind) = 3;
      cloudmask.byte1.landWater(desert_ind) = 2;
      cloudmask.byte1.landWater(coastal_ind) = 1;
      cloudmask.byte1.landWater(water_ind) = 0;

      clear bit7 bit8 land_ind desert_ind coastal_ind water_ind
    end
    clear byte1
  end % byte 1


%%%%%%%%%%%%%%%%%%%%%%%%%%%%%%%%%%%%%%%%%%%%%%%%%%%%%%
%%%%%%%%%%%%%%%
```

```
%% Cloud_Mask: BYTES 2-4
%%   0 = Yes     1 = No

%%%%%%%%%%%%%%%%%%%%%%%%%%%%%%%%%%%%%%%%%%%%%%%%%%%%%%%%%%%%%%%%%%%%%%%%%%%%%%%%%%%%%%%%%%%%%%%%%%%%%%%%%%%%%%%%%%%%%%%%%%%%%%%%%%%%%%%%%%

    if any(byteList == 2 | byteList == 3 | byteList == 4)
      indBytes234 = find(byteList == 2 | byteList == 3 | byteList == 4);
      for j = 1:length(indBytes234)

        byteInd = find(byteList(indBytes234(j)) == cloudMaskDataByteList);
        byteData = flipud(rot90(squeeze(cloudMaskData(:,:,byteInd)) ));
      clear byteInd

        % find negative integers and remap them
        ind = find(byteData < 0);
        byteData(ind) = 256 + byteData(ind);
        clear ind

        if byteList(indBytes234(j)) < 4
          %% 8 bits (0-7) in bytes 2 and 3
          numBits = 8;
        else
          %% 5 bits (0-4) in byte 4
          numBits = 5;
        end

        % assign data to cloudmask structure: cloudmask.byte#.bit#
        for k = 1:numBits
          eval(['cloudmask.byte' num2str(byteList(indBytes234(j))) ...
            '.bit' num2str(k-1) ' = bitget(byteData,k);']);
        end
        clear byteData

      end %% for
    end  %% bytes 2, 3, 4


%%%%%%%%%%%%%%%%%%%%%%%%%%%%%%%%%%%%%%%%%%%%%%%%%%%%%%%%%%%%%%%%%%%%%%%%%%%%%%%%%%%%%%%%%%%%%%%%%%%%%%%%%%%%%%%%%%%%%%%%%%%%%%%%%%%%%%%%%%
    %% Cloud_Mask: BYTES 5 & 6: 250-m Cloud Flag, Visible Tests
    %%   0 = Yes     1 = No

%%%%%%%%%%%%%%%%%%%%%%%%%%%%%%%%%%%%%%%%%%%%%%%%%%%%%%%%%%%%%%%%%%%%%%%%%%%%%%%%%%%%%%%%%%%%%%%%%%%%%%%%%%%%%%%%%%%%%%%%%%%%%%%%%%%%%%%%%%
    if any(byteList == 5) | any(byteList == 6)
```

```
%% BYTE 5

  byteInd = find(5 == cloudMaskDataByteList);
  byte5 = flipud(rot90(squeeze(cloudMaskData(:,:,byteInd)) ));
  clear byteInd

  % find negative integers and remap them
  ind = find(byte5 < 0);
  byte5(ind) = 256 + byte5(ind);
  clear ind

  %% create an array of all NaNs 4x the size of one element
  %% repmat is faster than ones*NaN
  elementSize = size(bitget(byte5,1));
  cloudmask.visibleTest250m = repmat(0,elementSize*4);

  xStartInds = [1 1 1 1 2 2 2 2];
  yStartInds = [1 2 3 4 1 2 3 4];

  %% insert each element into the array of NaNs.
  for j = 1:8
    %allbits(j,:,:) = bitget(byte5,j);
    cloudmask.visibleTest250m([xStartInds(j):4:elementSize(1)*4], ...
              [yStartInds(j):4:elementSize(2)*4]) = bitget(byte5,j);
  end

  clear byte5

%% BYTE 6

  byteInd = find(6 == cloudMaskDataByteList);
  byte6 = flipud(rot90(squeeze(cloudMaskData(:,:,byteInd)) ));
  clear byteInd

  % find negative integers and remap them
  ind = find(byte6 < 0);
  byte6(ind) = 256 + byte6(ind);
  clear ind

  byte6bits = [9:16];
  xStartInds = [3 3 3 3 4 4 4 4];
  yStartInds = [1 2 3 4 1 2 3 4];

  %% insert each element into the array of NaNs.
  for j = 1:8
```

```
        %allbits(byte6bits(j),:,:) = bitget(byte6,j);
        cloudmask.visibleTest250m([xStartInds(j):4:elementSize(1)*4], ...
            [yStartInds(j):4:elementSize(2)*4]) = bitget(byte6,j);

      end
      clear byte6

      %cloudmask.sumVisibleTest250m = squeeze(sum(allbits,1));

    end  %% byte 5,6

    clear cloudMaskData

  %%%%%%%%%%%%%%%%%%%%%%%%%%%%%%%%%%%%%%%%%%%%%%%%%%%%%%%%%%%%%%%%%%%%%%%%%
  % QA: Open cloud mask file and read QA data, dimensions, and attributes
  %
  % NOTE: It is repetitive to do QA separately after all of the 'Cloud_Mask'
  %       data, however it would take too much memory to keep
  %       'Quality_Assurance' and 'Cloud_Mask' (qaData and cloudMaskData)
  %       arrays around simultaneously
  %%%%%%%%%%%%%%%%%%%%%%%%%%%%%%%%%%%%%%%%%%%%%%%%%%%%%%%%%%%%%%%%%%%%%%%%%

   SD_id = hdfsd( 'start', maskFilename, 'read' );
   if (SD_id < 0)
     error(['HDF file' maskFilename ' was not opened.']);
   end

  % data we want is 'Quality_Assurance'
   mask_ex = hdfsd('nametoindex', SD_id, 'Quality_Assurance');
   mask_id = hdfsd('select',SD_id, mask_ex);
   [name,rank,dimsizes,data_type,nattrs,status(1)] = hdfsd('getinfo',mask_id );

  %  npixels_along = dimsizes(1);
  %  npixels_across = dimsizes(2);
  %  nbytes = dimsizes(3);
    start = [0 ; 0 ; minBytes-1];
    count = [1 ; 1 ; 1];
  %
  %  if maxBytes <= nbytes
  %    edge = [npixels_along; npixels_across; maxBytes-minBytes+1];
  %  else
  %    error(['maxBytes cannot be greater than the number of bytes in the file']);
  %  end
```

```
 edge = [npixels_across ;  npixels_along; maxBytes-minBytes+1];

 if (nargin == 3)
    start(1) = min( [max([area(1) 0]) (npixels_across - 1)] );
    start(2) = min( [max([area(2) 0]) (npixels_along - 1)] );
    edge(1) = min( [max([area(3) 0]) (npixels_across - start(2))] );
    edge(2) = min( [max([area(4) 0]) (npixels_along - start(3))] );
end

 [qaData,status(2)] = hdfsd('readdata',mask_id,start,count,edge);

 qaData  = double(qaData);

 attr_ex = hdfsd('findattr', mask_id, 'scale_factor');
 [qascale, status(3)] = hdfsd('readattr', mask_id,attr_ex) ;

 attr_ex = hdfsd('findattr', mask_id, 'long_name');
 [qalongname, status(4)] = hdfsd('readattr', mask_id,attr_ex) ;

 attr_ex = hdfsd('findattr', mask_id, 'Cell_Along_Swath_Sampling');
 [qasampling, status(5)] = hdfsd('readattr', mask_id,attr_ex) ;

 attr_ex = hdfsd('findattr', mask_id, 'add_offset');
 [qaoffset, status(6)] = hdfsd('readattr', mask_id,attr_ex) ;
 if qaoffset ~= 0 | qascale ~= 1
    error(['Quality_Assurance offset ~= 0 or slope ~= 1']);
 end

% stop accessing data
 status(7) = hdfsd('endaccess',mask_id);

 if any(status == -1)
   error('Trouble reading Quality_Assurance data, dimensions, or attributes');
 end

 clear status

% close HDF file
 status = hdfsd('end', SD_id);
 if (status < 0)
    warning(['HDF file' maskFilename ' was not closed.']);
 end

 if any(byteList == 1)
```

```
%%%%%%%%%%%%%%%%%%%%%%%%%%%%%%%%%%%%%%%%%%%%%%%%%%%%%%
%%%%%%%%%
        %% 'Quality_Assurance': BYTE 1

%%%%%%%%%%%%%%%%%%%%%%%%%%%%%%%%%%%%%%%%%%%%%%%%%%%%%%
%%%%%%%%%
        byteInd = find(1 == cloudMaskDataByteList);
        qabyte1 = flipud(rot90(squeeze(qaData(byteInd,:,:)) ));
        % find negative integers and remap them
        ind = find(qabyte1 < 0);
        qabyte1(ind) = 256 + qabyte1(ind);
        clear ind

        %% BIT 0 - Cloud Mask QA
        %% 0 = not useful    1 = useful
        %% Assign all not useful values to -1 byte1 fields
        notUsefulInds = find(~bitget(qabyte1,1));
        cloudmask.byte1.mask(notUsefulInds) = -1;

        if onlyBits1and2 == 0
          cloudmask.byte1.dayOrNight(notUsefulInds) = -1;
          cloudmask.byte1.sunglint(notUsefulInds) = -1;
          cloudmask.byte1.snowIce(notUsefulInds) = -1;
          cloudmask.byte1.landWater(notUsefulInds) = -1;

          %% BITS 1,2,3 - Cloud Mask Confidence
          bit2 = bitget(qabyte1,2);
          bit3 = bitget(qabyte1,3);
          bit4 = bitget(qabyte1,4);
          ind0 = find(~bit4 & ~bit3 & ~bit2);
          ind1 = find(~bit4 & ~bit3 & bit2);
          ind2 = find(~bit4 & bit3 & ~bit2);
          ind3 = find(~bit4 & bit3  & bit2);
          ind4 = find(bit4 & ~bit3 & ~bit2);
          ind5 = find(bit4 & ~bit3 & bit2);
          ind6 = find(bit4 & bit3 & ~bit2);
          ind7 = find(bit4 & bit3 & bit2);
          clear bit2 bit3 bit4

          cloudmask.byte1.confidenceQA = NaN * ones(size(qabyte1));
          cloudmask.byte1.confidenceQA(ind0) = 0;
          cloudmask.byte1.confidenceQA(ind1) = 1;
          cloudmask.byte1.confidenceQA(ind2) = 2;
          cloudmask.byte1.confidenceQA(ind3) = 3;
          cloudmask.byte1.confidenceQA(ind4) = 4;
          cloudmask.byte1.confidenceQA(ind5) = 5;
```

```
      cloudmask.byte1.confidenceQA(ind6) = 6;
      cloudmask.byte1.confidenceQA(ind7) = 7;

      clear ind0 ind1 ind2 ind3 ind4 ind5 ind6 ind7
    end
    clear qabyte1 notUsefulInds

  end  %% qa byte 1

  if any(byteList == 2 | byteList == 3 | byteList == 4)


%%%%%%%%%%%%%%%%%%%%%%%%%%%%%%%%%%%%%%%%%%%%%%%%%%%%%%
%%%%%%%%
     %% Quality_Assurance: BYTES 2-4
     %%
     %% 0 = Not Applied   1 = Applied

%%%%%%%%%%%%%%%%%%%%%%%%%%%%%%%%%%%%%%%%%%%%%%%%%%%%%%
%%%%%%%%

     indBytes234 = find(byteList == 2 | byteList == 3 | byteList == 4);
     for j = 1:length(indBytes234)

       qaByteInd = find(byteList(indBytes234(j)) == cloudMaskDataByteList);
       qaByteData = flipud(rot90(squeeze(qaData(qaByteInd,:,:)) ));
     clear qaByteInd

       % find negative integers and remap them
       ind = find(qaByteData < 0);
       qaByteData(ind) = 256 + qaByteData(ind);
       clear ind

       if byteList(indBytes234(j)) < 4
         %% 8 qa bits (0-7) in qa bytes 2 and 3
         numBits = 8;
       else
         %% 5 qa bits (0-4) in qa byte 4
         numBits = 5;
       end

       %% For QA "not applied", set corresponding value in
       %% cloudmask.byte#.bit# to -1
       for k = 1:numBits
         eval(['cloudmask.byte' num2str(byteList(indBytes234(j))) ...
           '.bit' num2str(k-1) '(find(~bitget(qaByteData,k))) = -1;']);
```

```
      end % for k

      clear qaByteData

    end %% for j
  end  %% bytes 2, 3, 4


%%%%%%%%%%%%%%%%%%%%%%%%%%%%%%%%%%%%%%%%%%%%%%%%%%%%%%%%%%%%%%%%
%%%%%%%%%%%%%%%%%%%%%
  %% Quality_Assurance: BYTES 5 & 6: 250-m Cloud Flag, Visible Tests
  %%   0 = Not Applied     1 = Applied

%%%%%%%%%%%%%%%%%%%%%%%%%%%%%%%%%%%%%%%%%%%%%%%%%%%%%%%%%%%%%%%%
%%%%%%%%%%%%%%%%%%%%%
  if any(byteList == 5) | any(byteList == 6)

  save tempCMdata
  keep2 cloudMaskDataByteList qaData
  clear cloudmask

  %% BYTE 5

    qaByteInd = find(5 == cloudMaskDataByteList);
    qaByteData = flipud(rot90(squeeze(qaData(qaByteInd,:,:)) ));
    clear qaByteInd

    % find negative integers and remap them
    ind = find(qaByteData < 0);
    qaByteData(ind) = 256 + qaByteData(ind);
    clear ind

    %% create an array of all NaNs 4x the size of one element
    %% repmat is faster than ones*NaN
    elementSize = size(bitget(qaByteData,1));
    temporaryQA = repmat(0,elementSize*4);

    xStartInds = [1 1 1 1 2 2 2 2];
    yStartInds = [1 2 3 4 1 2 3 4];

    %% insert each element into the array of NaNs.
    for j = 1:8
      temporaryQA([xStartInds(j):4:elementSize(1)*4], ...
              [yStartInds(j):4:elementSize(2)*4]) = bitget(qaByteData,j);
    end
```

```
   clear qaByteData

%% BYTE 6

   qaByteInd = find(6 == cloudMaskDataByteList);
   qaByteData = flipud(rot90(squeeze(qaData(qaByteInd,:,:)) ));
   clear qaByteInd

   % find negative integers and remap them
   ind = find(qaByteData < 0);
   qaByteData(ind) = 256 + qaByteData(ind);
   clear ind

   xStartInds = [3 3 3 3 4 4 4 4];
   yStartInds = [1 2 3 4 1 2 3 4];

   %% insert each element into the array of NaNs.
   for j = 1:8
     temporaryQA([xStartInds(j):4:elementSize(1)*4], ...
               [yStartInds(j):4:elementSize(2)*4]) = bitget(qaByteData,j);
   end

   clear qaByteData qaData

   notAppliedInds = find(~temporaryQA);

   load tempCMdata
   cloudmask.visibleTest250m(notAppliedInds) = -1;

   clear notAppliedInds temporaryQA

end  %% byte 5,6
```

Appendix B. Acronyms

ACARS	ARINC (Aeronautical Radio Inc.) Communications, Addressing and Reporting System
AERI	Atmospheric Emitted Radiation Interferometer
AEROCE	Aerosol/Ocean Chemistry Experiment
AERONET	Aerosol Robotic Network
AirMISR	Airborne MISR
AIRS	Atmospheric Infrared Sounder
AMSU	Advanced Microwave Sounding Unit
APOLLO	AVHRR (Advanced Very High Resolution Radiometer) Processing scheme Over cLoud Land and Ocean
ARM	Atmospheric Radiation Measurement Program
ARMCAS	Arctic Radiation Measurements in Column Atmosphere-surface System (Beaufort Sea, Alaska, June 1995)
ASTEX	Atlantic Stratocumulus Transition Experiment (Azores, June 1992)
ASTER	Advanced Spaceborne Thermal Emission and Reflection radiometer
AVHRR	Advanced Very High Resolution Radiometer
AVIRIS	Airborne Visible/Infrared Imaging Spectrometer
BRDF	Bi-directional Reflectance Distribution Function
CAR	Cloud Absorption Radiometer
CALIOP	Cloud-Aerosol Lidar with Orthogonal Polarization
CAIPSO	Cloud-Aerosol Lidar and Infrared Pathfinder Satellite Observation
CART	Clouds and Radiation Testbed
CEPEX	Central Equatorial Pacific Experiment (Fiji, February-March 1993)
CERES	Clouds and the Earth's Radiant Energy System
CHAPS	Collocated HIRS/2 and AVHRR Processing Scheme
CLAVR	Cloud Advanced Very High Resolution Radiometer

CLS	Cloud Lidar System
COARE	Coupled Ocean-Atmosphere Response Experiment
DAO	Data Assimilation Office (Goddard Space Flight Center)
EOS	Earth Observing System
EOSDIS	EOS Data and Information System
FIRE	First ISCCP Regional Experiment (California, June-July 1987, Beaufort Sea, Alaska, April-June, August 1998)
FOV	Field of View
GAC	Global Area Coverage
GLAS	Geoscience Laser Altimeter System
GLI	Global Imager
GOES	Geostationary Operational Environmental Satellite
HIS	High-spectral resolution Interferometer Sounder
HIRS	High Resolution Infrared Radiation Sounder
HSB	Humidity Sounder from Brazil
ILAS	Improved Limb Atmospheric Spectrometer
ISCCP	International Satellite Cloud Climatology Project
LASE	Lidar Atmospheric Sensing Experiment
LBA	Large Scale Biosphere-Atmosphere Experiment in Amazonia
M-AERI	Marine-Atmospheric Emitted Radiation Interferometer
MAS	MODIS Airborne Simulator
MAST	Monterey Area Ship Tracks Experiment (Monterey and nearby Pacific Ocean, June 1994)
McIDAS	Man-computer Interactive Data Access System
MISR	Multi-angle Imaging Spectro-Radiometer
MOBY	Marine Optical Buoy
MODIS	Moderate Resolution Imaging Spectroradiometer

NAST	NPOESS Aircraft Sounding Testbed
NCAR	National Center for Atmospheric Research
NDSI	Normalized Difference Snow Index
NDVI	Normalized Difference Vegetation Index
NPOESS	National Polar Orbiting Environmental Satellite System
NSA	North Slope of Alaska
POLDER	Polarization and Directionality of Earth's Reflectances
RAMS	Radiation Measurement System (NASA Ames Research Center and Scripps Institution of Oceanography)
SCAR-A	Sulfate, Clouds and Radiation–Atlantic (Delmarva Peninsula and near-by Atlantic Ocean, July 1993)
SCAR-B	Smoke, Clouds and Radiation–Brazil (Brazil, August-September 1995)
SCAR-C	Smoke, Clouds and Radiation–California (Pacific Northwest, September 1994)
SCF	Science Computing Facility
SeaWiFS	Sea-viewing Wide Field-of-view Sensor
SGP	Southern Great Plains
SHEBA	Surface Heat Budget of the Arctic Ocean
SSFR	Spectral Solar Flux Radiometer (NASA Ames Research Center)
SST	Sea Surface Temperature
SUCCESS	Subsonic Aircraft Contrail and Cloud Effects Special Study (April-May 1996)
TARFOX	Tropospheric Aerosol Radiative Forcing Observational Experiment (Delmarva Peninsula and near-by Atlantic Ocean, July 1996)
TIROS	Television and Infrared Observation Satellite
TLCF	Team Leader Computing Facility
TM	Thematic Mapper
TOGA	Tropical Ocean Global Atmosphere

TOMS	Total Ozone Mapping Spectrometer
TOVS	TIROS-N Operational Vertical Sounder
WINCE	Winter Cloud Experiment
WMO	World Meteorological Organization